

The optimization, evaluation, and design of a side-feed wood-burning cookstove with fan-driven secondary air injection.

Devin John Udesen

A thesis submitted in partial fulfillment of the requirements for the degree

Master of Science in Mechanical Engineering

University of Washington

2019

Committee:

Jonathan Posner, Co-Chair

John Kramlich, Co-Chair

Paul Means

Program Authorized to Offer Degree:

Department of Mechanical Engineering

©Copyright 2019
Devin John Udesen

University of Washington

Abstract

The optimization, evaluation, and design of a side-feed wood-burning cookstove with fan-driven secondary air injection.

Devin John Udesen

Chairs of the Supervisory Committee:

Professor Jonathan Posner

Professor John Kramlich

Department of Mechanical Engineering

3 billion people still rely on open-fires and/or traditional cookstoves that burn unprocessed biomass fuels to cook and provide heat for their homes. These traditional cooking practices require large amounts of fuel and emit high-levels of harmful pollutants that have long lasting health, social, economic, and environmental impacts. The emissions from traditional cooking practices is the leading cause of household air pollution (HAP), which is the world's single greatest environmental health risk to the human population, causing 3.8 million premature deaths each year and sickening many more. Improved cookstoves that burn locally available unprocessed biomass fuels (e.g., wood, charcoal, dung, and agricultural-waste), referred to as intermediate cookstoves, can provide significant reductions in household $PM_{2.5}$ and CO concentrations, alleviating health risks. These stoves can also reduce the amount of fuel a household needs to procure on a daily-basis, saving households time and money. The design of intermediate cookstoves that effectively reduce in-home emissions and household fuel-consumption requires sophisticated knowledge of solid-fuel combustion and cookstove thermodynamics. Secondary air injection is often used in cookstoves to improve fuel-to-air mixing to achieve comprehensive

reductions in emissions. The design of secondary air injection systems requires complex and time intensive experimental investigation to optimize numerous jet design parameters. In this thesis, the development of a secondary air injection system design tool for fan-driven systems in side-feed wood-burning cookstoves (i.e., rocket-stoves) is detailed. We find that jet configurations where jet radial penetration lengths approach the mid-line of a cylindrical cross-flow result in a maximum reduction in $PM_{2.5}$ emissions and provide a good compromise between jet injection energy (representative of operational cost), quality of cross-flow mixing characteristics, and thermal-efficiency; supporting the results of previous investigations into secondary air injection optimization in furnace and gas turbine combustion chambers. The design tool is applied to the development of a solar-powered fan-driven secondary air injection system for the Kuniokoa™, a natural-draft, side-feed, wood-burning cookstove, manufactured and sold in East-Africa by BURN Manufacturing. The resulting system was integrated into a prototype stove, referred to as the Kuniokoa-Turbo™. Laboratory performance testing of this prototype was performed at operating conditions typical of in-home use in rural-Kenya. Testing results suggest the Kuniokoa-Turbo™ reduces $PM_{2.5}$ emissions by 97% compared to measured household-kitchen $PM_{2.5}$ concentrations in households in rural-Kenya using traditional three-stone-fires. Compared to the natural-draft Kuniokoa™, we find that the Kuniokoa-Turbo™ significantly reduces $PM_{2.5}$ emissions at a stove firepower greater than 3kW and is effective in reducing $PM_{2.5}$ emissions throughout a wide range of fuel-types and burn-rates, corresponding to Tier 3 emissions performance for a stove firepower between 0.75kW-5.5kW.

Table of Contents

Abstract.....	3
Table of Contents.....	5
List of Figures	8
List of Tables	10
Acknowledgements.....	11
CHAPTER 1: SIGNIFICANCE AND BACKGROUND	12
1.1 Significance	12
1.2 ISO/IWA Cookstove Performance Metrics	23
1.3 University of Washington Clean Cookstoves Laboratory (UWCCL)	26
1.4 A Natural-Draft Side-Feed Wood-Burning Cookstove for East-Africa	27
1.4.1 <i>Natural-Draft Rocket-Stove Design Overview</i>	28
1.4.2 <i>The Kuniokoa™</i>	29
1.4.3 <i>Kuniokoa™ Laboratory Performance</i>	35
1.4.4 <i>Summary</i>	42
1.5 PM _{2.5} Emissions	44
1.5.1 <i>Design Challenges and Performance Limitations in Reducing PM_{2.5} Emissions of Natural-Draft Rocket-Stoves</i>	44
1.5.2 <i>Design Strategies to Reduce PM_{2.5} Emissions</i>	48
1.7 Objectives.....	50
1.8 Summary	51
CHAPTER 2: AN ANALYTICAL MODEL FOR SECONDARY AIR INJECTION OPTIMIZATION IN A SIDE-FEED WOOD-BURNING COOKSTOVE.....	52
2.1 Analytical Model Description.....	52
2.2 Cross-Flow Parameters	59
2.3 Jet Parameters	62
2.4 Cross-Flow Mixedness Optimization Parameters.....	64

2.5 System Impedance	67
2.6 Fan Performance Curve and System Operating Point	69
CHAPTER 3: COOKSTOVE PERFORMANCE TESTING SYSTEM AND TESTING	
METHODOLOGIES	73
3.1 Cookstove Performance Testing System	73
3.2 Cookstove Performance Testing Methodologies	74
3.2.1 Water-Boil-Test (WBT)	75
3.2.2 Firepower-Sweep-Test (FPS).....	76
3.2.3 Excess-Air.....	79
CHAPTER 4: ANALYTICAL MODEL EXPERIMENTAL EVALUATION AND VALIDATION.....	
4.1 Jet Configurations.....	83
4.2 Experimental Apparatus	85
4.2.1 Three-Dimensional Computational Fluid Dynamic Model of the Kuniokoa™ with Secondary Air Injection	85
4.2.2 Kuniokoa™ with Modular Secondary Air Injection	88
4.3 Experimental Results.....	90
4.3.1 Cross-Flow Temperature Contours and Uniformity.....	90
4.3.2 Cross-Flow Fuel Scalar Uniformity	94
4.3.3 Flame Behavior.....	95
4.3.4 Cross-Flow Velocity Contours	97
4.3.5 PM _{2.5} Emissions	98
4.3.6 Inlet Air Flow Ratio	100
4.3.7 Thermal-Efficiency	102
4.3.8 System Impedance	103
4.4 Summary.....	105
CHAPTER 5: A SOLAR-POWERED FAN-DRIVEN SECONDARY AIR INJECTION SOLUTION FOR THE KUNIOKOA™	
5.1 Kuniokoa-Turbo™.....	107

5.1.1 <i>Project Goals and Design Parameters</i>	109
5.1.2 <i>Fan-Driven Secondary Air Injection System Design</i>	110
5.2 Kuniokoa-Turbo™ Laboratory Performance.....	115
5.3 Summary	119
CHAPTER 6: CONCLUSIONS AND FUTURE WORK	123
References	125
Appendix.....	132
A1: Analytical Model Code.....	132
A2: Kuniokoa™ Modular Air Injection Prototype Diagram	136

List of Figures

Figure 1: Rocket-stove cross section	28
Figure 2: SFR, Tall-Boy, and SFR 35B natural-draft rocket stove prototypes	30
Figure 3: High-power WBT ISO performance tier laboratory results for the SFR, Tall-Boy, SFR 35B, and Kunioko TM	33
Figure 4: Moisture-content (MC) of fuel-feedstocks found in rural-Kenya	36
Figure 5: Distribution of in-home fuel burn-rates (i.e., firepower)	37
Figure 6: Kunioko TM FPS PM _{2.5} emissions behavior.....	38
Figure 7: Kunioko TM high-power WBT ISO performance tiers	38
Figure 8: Kunioko TM optimum WBT ISO performance tier results	41
Figure 9: PM _{2.5} emissions and flame-height behavior of the Kunioko TM	47
Figure 10: Radial jets in cross-flow diagram.....	53
Figure 11: Momentum flux ratio vs. cross-flow mixedness	66
Figure 12: Air-injection system diagram.	67
Figure 13: Fan performance curve for a typical 12V computer fan.	71
Figure 14: Example definition of the system operating point for a fan-driven system.....	72
Figure 15: Cookstove emissions and performance testing system	74
Figure 16: Aluminum 5L flat-bottomed pot used for WBT performance testing.....	76
Figure 17: Example FPS CO ₂ data.....	77
Figure 18: Example FPS PM _{2.5} and instantaneous firepower data	78
Figure 19: Example PM _{2.5} emission rate vs. stove firepower curve.	79
Figure 20: Illustration of the excess-air sampling rake and sample location.	81
Figure 21: Example excess-air CO ₂ concentration data.....	81
Figure 22: CFD model cookstove domain (geometry/flow-path).	86
Figure 23: Modular Kunioko TM secondary air injection experimental apparatus.	89
Figure 24: Riser temperature contours	91
Figure 25: Riser cross-flow temperature uniformity index.....	92
Figure 26: Riser cross-flow fuel scalar uniformity index.....	95
Figure 27: Stoichiometric flame surfaces.....	96
Figure 28: Riser velocity contours	98
Figure 29: PM _{2.5} emission rate (mg/min) as a function of momentum-flux ratio	99
Figure 30: Primary to secondary air mass-flow ratio as a function of momentum-flux ratio.....	100
Figure 31: Primary to secondary air mass-flow ratio as a function of momentum-flux ratio.....	101

Figure 32: Primary to secondary air mass-flow ratio as a function of riser outlet temperature.	102
Figure 33: Thermal-efficiency (%) as a function of momentum-flux ratio	103
Figure 34: Jet system impedance comparison	104
Figure 35: Model corrected jet system impedance	104
Figure 36: Kuniokoa-Turbo™ isometric and top view.	111
Figure 37: External duct, fan, fan nozzle, and control board assembly.....	112
Figure 38: Kuniokoa-Turbo™ assembly cross-section and air injection system.....	112
Figure 39: Kuniokoa-Turbo™ air injection system impedance	114
Figure 40: Kuniokoa-Turbo™ FPS results	117
Figure 41: Kuniokoa-Turbo™ high-power WBT ISO performance tiers.....	118
Figure 42: Kuniokoa-Turbo™ user focus-group image 1.	121
Figure 43: Kuniokoa-Turbo™ user focus-group image 2	121
Figure 44: Kuniokoa-Turbo™ user focus-group image 3	122

List of Tables

Table 1: <i>ISO/IWA Tiers for emissions</i>	23
Table 2: <i>ISO/IWA Tiers for thermal-efficiency/fuel-use and indoor emissions</i>	24
Table 3: Kenya TSF baseline values and Kuniokoa™ high-power WBT ISO performance values for small-dry, large-dry, and large-wet feedstocks. Simulated field-typical performance metrics are averaged across all fuel-types and shown for comparison.	39
Table 4: Kuniokoa™ WBT ISO performance values	42
Table 5: High-power WBT tiered performance summary for the Kuniokoa™	44
Table 6: Secondary air jet optimization analytical model user-defined design parameters and system characteristics (i.e., independent variables).	55
Table 7: Example analytical model optimum jet configuration outputs.....	58
Table 8: Ultimate analysis of Douglas Fir from Kobayashi et al.	61
Table 9: Secondary air jet optimization analytical model user-defined design parameters and system characteristics for the Kuniokoa-Turbo™	84
Table 10: Kuniokoa-Turbo™ optimum jet configurations and corresponding jet characteristics .84	84
Table 11: Jet configurations used in the evaluation of the analytical model.....	85
Table 12: Four step global mechanism	87
Table 13: Mass fractions of species in wood volatile mix.....	87
Table 14: Corrected jet characteristics for the jet configurations evaluated	106
Table 15: Kenya TSF baseline values and Kuniokoa-Turbo™ high-power WBT ISO performance values	118
Table 16: High-power WBT tiered performance summary for the Kuniokoa-Turbo™.....	119

Acknowledgements

This research was funded by Intellectual Ventures, through their Global Good Fund, and supported by the University of Washington College of Engineering.

In the 4 ½ years I have been a part of the University of Washington Clean Cookstoves Lab and in the last year over which much of this work was performed I was supported by numerous mentors, colleagues, friends, and family. It is my pleasure to acknowledge them and their contributions.

First, I would like to acknowledge and thank my two advisors, Prof. Jonathan Posner and Prof. John Kramlich for their support and guidance throughout my undergraduate and graduate career at the University of Washington. I believe that my skill as an engineer, researcher, and communicator are a direct reflection of the advice and lesson's I have learned from you and through the projects we have been a part of together.

I would like to thank Paul Means, his organization BURN Design Lab, and the many people who I have worked with through the organization for their support, mentorship, and collaboration. Without your contributions much of the work presented here and all of our previous work together that lead up to this point would not have been made possible.

I would also like to thank my labmates at the University of Washington Clean Cookstoves Lab. I appreciate the countless hours we spent together advancing improved cooking technology. My experience would not have been the same without Anamol Pundle, Benjamin Sullivan, Garrett Allawatt, Jackson McFall, Emily Lore, Casey Tackman, and Erin Graf. Thank you all for your continued support.

Finally, I dedicate this thesis to my parents, Sekou and Alicia Kone, and my grandparents, John and Patricia Straub, who instilled on me a curiosity of the natural world, inspired my passion for humanitarian focused technology, and drove me to pursue my goals.

CHAPTER 1: SIGNIFICANCE AND BACKGROUND

This chapter describes the motivation behind the work presented in this thesis. This in large part focuses on the need for continued development of innovative design tools and strategies to guide the development of fuel-efficient, clean-burning biomass cooking technology for the developing world. The impacts of traditional cooking practices and household solid biomass fuel use are reviewed, and the current status of clean and efficient cooking technology is discussed in the context of global statistics, field-observations, and the previous development and analysis of an improved cooking solution for Sub-Saharan Africa in the form of an unvented, natural-draft, side-feed wood-burning cookstove. The performance limitations of current unvented, natural-draft, side-feed wood-burning cookstove technology is detailed and an overview of past investigations focused on overcoming these limitations is presented. Finally, an innovative solution and design strategy is introduced in pursuit of solving the current performance limitations of unvented, natural-draft, side-feed wood-burning cookstove technology.

1.1 Significance

There are 9 million premature deaths each year due to disease, illness, or injury caused by global environmental pollution; this is roughly 16% of all global deaths annually .¹ This makes pollution the world's largest cause of disease and premature death, killing three-times as many people as AIDS, tuberculosis, and malaria combined, or fifteen-times as many people that are killed due to war and all other forms of violence .¹ Low-to-middle income countries take the brunt of the impacts of pollution, with premature deaths from this cause accounting for 92% of the 9 million people killed each year .¹ The world economy spends 6.2% of the global economic output (4.6 trillion USD) on welfare programs focused on preventing premature deaths by treating public-health crises caused by environmental pollution .¹ These efforts are, by and large, solutions focused on treating the side-effects of pollution, not the actual cause. Without intervention into the leading

causes of environmental pollution, these global health crises will continue and/or worsen for the foreseeable future.

The leading cause of environmental pollution related deaths is air-pollution, killing an estimated 8 million people each year, accounting for approximately 90% of all environmental pollution caused premature deaths .² This is a direct consequence of the fact that 91% of the world's population lives in a place where air quality exceeds World Health Organization (WHO) guideline limits .² The WHO defines air quality based upon the concentrations of six key airborne pollutants; particulate-matter (PM), black-carbon (BC), ground-level ozone (O₃), nitrogen-dioxide (NO₂), sulphur-dioxide (SO₂), and carbon-monoxide (CO). Many of these pollutants are present in both ambient air pollution (AAP) and indoor, or household air pollution (HAP). The widespread overexposure to these pollutants, via both AAP and HAP, among populations around the world leads to an estimated 4.2 million premature deaths each year caused by AAP and an estimated 3.8 million premature deaths each year due to HAP .²

The leading source of HAP is the burning of solid biomass fuels, such as wood, charcoal, dung, and agricultural-waste, for household cooking and heating needs .³ Many of these fuels are burned indoors using traditional cooking practices such as unvented open-fires and/or traditional cookstoves .⁴ Currently, 3 billion people rely on these traditional cooking practices to cook and provide heat for their homes .³ Almost all these people live in low-to-middle income countries in Asia, Africa, and Latin America, where access to cleaner household energy sources, like electricity or liquified petroleum gas (LPG), is either non-existent, unreliable, or too expensive .^{5,3} The continued reliance on traditional cooking practices that burn biomass fuels, combined with lack of access to cleaner household energy sources among billions of people around the globe makes HAP the world's single greatest environmental health risk to the human population, according to the WHO .³

The primary pollutants that are of concern when solid biomass fuels are burned in a household setting are methane (CH₄), carbon-monoxide (CO), particulate-matter (PM), polyaromatic-hydrocarbons (PAH), and volatile-organic-compounds (VOC) .³ PM, PAH, and VOC's are the main components of the smoke emitted by an open-fire and traditional cookstove. The PM in this smoke is of especially great concern due to the well-defined correlation between increases in exposure and increased health risks. Particles with a diameter less than 10 microns (PM₁₀), including fine particles with diameters less than 2.5 microns (PM_{2.5}) pose the greatest risks to health, due to their ability to penetrate deep in the lungs and enter the bloodstream .⁶ The PM_{2.5} emission rate of most open-fires and traditional cookstoves is over 174 times the WHO HAP guideline of 35 µg/m³ .³ Exposure to PM_{2.5} concentrations greater than this guideline can lead to acute lower respiratory infections, chronic obstructive pulmonary disease, lung cancer, ischemic heart disease, stroke, pregnancy complications, and even cataracts .⁶ These health risks disproportionately impact women and children with 59% of indoor air pollution caused deaths being women and 56% being children under 5 years of age .⁶ The widespread exposure to PM_{2.5} in a household setting greater than what is recommended by the WHO causes 50% of all deaths from pneumonia in children under 5 years of age; pneumonia being the leading cause of child mortality worldwide .⁷

In addition, PM_{2.5} emissions have a strong impact on global climate change. Black carbon (BC), a primary constituent of PM_{2.5} emitted from the burning of solid biomass, accounts for 25% of all anthropogenic BC released into the atmosphere .⁸ The release of BC into the atmosphere greatly influences the radiative-forcing of the earth's atmosphere; one of the main components of the greenhouse-effect. On a per-mass basis, BC contributes 2,200 times more to climate change than CO₂, due to the increased absorption of solar radiation of BC particles compared to CO₂ .⁹ BC may contribute more to climate change than CO₂ by mass, but compared to CO₂, BC has a relatively short atmospheric lifespan, only remaining in the atmosphere for one to four weeks. This

means BC climate effects are strongly regional and would dissipate quickly if BC emissions were reduced, thus benefiting most directly the countries or communities that invest in policies and/or technologies to reduce BC emissions .¹⁰

Emissions are not the only distinguishing characteristic associated with the local and global impacts of traditional solid biomass fuel use. The fuel-consumption rate of traditional cooking technologies has associated environmental, health, and economic implications as well. Traditional open-fires, commonly referred to as three-stone-fires (TSF), named due to the practice of using three large stones to balance a cooking implement over an open-fire, typically have thermal-efficiencies of 14-15% and most traditional cookstoves struggle to operate at thermal-efficiencies greater than 25% .¹¹ Due to this low thermal-efficiency, 75% or more of the fuel-energy is not actively used for cooking and/or heating (i.e., wasted) meaning the amount of fuel needed to complete basic daily cooking and/or heating tasks is much greater than what is required. This poses a significant challenge for households relying on solid biomass fuels because this increases the amount of fuel that must be procured.

For households in rural areas solid biomass fuels are predominantly gathered. The time required to collect enough fuel to meet their cooking and heating needs demands hours each week, depending on the scarcity of locally available fuel. The time-intensive task of gathering fuel falls on the shoulders of women and children, which has been found to increase their risk of sexual violence, increase their risk of physical injuries from carrying heavy loads of fuel, and decrease time available to spend focused on education, employment opportunities, and/or leisure activities .¹² Further, the act of fuel collection is not a regulated activity, so the impact of household fuel-collection on the surrounding ecosystem is often left unchecked, contributing to 5% of global deforestation .²⁴

Households in urban regions must purchase solid biomass fuels, which are often the only household energy sources with a reliable distribution network and affordable cost. Households

purchasing solid biomass fuels spend, on average, less than 10% of their monthly income on fuel, highlighting the affordability of traditional fuels, even when burned inefficiently, providing key insight into why so many people still rely on and use them.²³ These fuels could become even more affordable than they already are if the fuel-consumption of traditional cooking practices was reduced, with the potential to significantly reduce household fuel demand and reduce the environmental and social impacts of solid biomass fuel use.

In general, the share of traditional solid biomass fuels in household energy demand varies widely across countries and regions, primarily reflecting their resource endowments, but also their levels of economic development and urbanization.¹³ As households become poorer and/or more rural their household energy options become more limited, with traditional biomass fuels often being the only energy source that remains accessible to households regardless of their economic standing or geographical location. Unfortunately, the traditional practices that are used to burn solid biomass fuels pose great risk to an individual's health, financial-stability, and their surrounding environment, due to the inefficiency and high-level of harmful emissions associated with these traditional practices. This highlights the inequity associated with household energy access. As household, or per capita income, decreases, so does the availability of affordable household energy solutions²⁵, meaning households become more reliant on solid biomass fuels and traditional cooking practices; increasing the rate of illness, disease, and death in low-income households compared to households in higher income brackets.

Millions of households around the globe are faced with this inequity every day and remain solely reliant on traditional solid biomass fuel sources to feed their families and provide heat for their homes, adding to the many barriers that they already struggle to overcome on a daily basis to maintain their health, financial-stability, and quality of life. Without increased investment into providing these households with clean-burning, fuel-efficient, and affordable household energy solutions, this inequity will remain an ongoing and growing problem.

In 2010, the UN Foundation formed the Global Alliance for Clean Cookstoves (a.k.a Clean Cooking Alliance or Alliance) kickstarting a global initiative to provide clean-burning, efficient, and affordable cooking technology and fuels for the 3 billion people reliant on the burning of biomass in open-fires and/or traditional cookstoves. The Alliance supports a multi-disciplinary coalition of private and public entities that are focused on the development, sale, distribution, and consistent use of improved cooking solutions that transform lives by improving health, protecting the environment, creating jobs and income opportunities, and helping consumers save time and money.¹⁴ The Alliance defines improved-cookstoves and/or fuels as technology that provides a 70% reduction in fuel-consumption and an 80% reduction in PM_{2.5} and CO emissions when compared to traditional cooking practices and fuels.²¹ The original target was to convert 100 million households to solutions that meet these targets by the year 2020.¹⁴

Much of this work is focused in Sub-Saharan Africa, the region of the world with the highest density of countries that have populations that are more than 95% reliant on solid biomass fuels.³ The vast majority (81%) of all African households rely on wood-based biomass as a household energy source; this will be an estimated 1 billion people by the year 2030.¹⁵ This high demand means that 89% of all wood harvested in Africa ends up being burned as household fuel.¹⁵ The emissions from the use of solid biomass fuels in open-fires and traditional cookstoves in Africa leads to 680,000 premature deaths per year and the total impact of these deaths on Africa's economy is greater than \$232 billion USD annually.¹⁶ Africa has a lot to gain from investment in clean and efficient cooking technologies, especially considering Sub-Saharan Africa is the only region in the world where the use of solid biomass fuels is expected to grow in coming decades.¹⁵

So far, much of the current work in Sub-Saharan Africa has focused on the development and implementation of improved cookstoves that burn traditional unprocessed solid biomass fuel supplies (e.g., wood, charcoal, dung, agricultural waste, etc.), but burn these fuels in a clean and efficient manner. From herein after these types of technologies will be referred to as intermediate

cookstoves or technologies. Intermediate cookstoves are notoriously difficult to design so that they burn clean, are fuel-efficient, meet a household's daily cooking needs, and that are affordable to either distribute or sell to local cooks, who are among populations that are some of the poorest in the world. Most intermediate solutions sacrifice one or more of these design traits, which has led to poor adoption rates, negligible reductions in household air pollution, and limited reductions in household fuel-demand.¹⁷ Additional investment into projects focused on developing advanced biomass cookstoves that burn or use non-traditional processed fuels or energy sources, like wood-pellets, biogas, solar, and liquid petroleum gas (LPG), have been plagued with similar issues to intermediate solutions, but with the added difficulty of having to create the markets and build the infrastructure necessary to make these new fuel sources and cooking technologies available and affordable to their respective target populations.

Despite the difficulties in developing improved cooking technology there are currently 40 industrial and semi-industrial improved cookstove enterprises doing business in Sub-Saharan Africa who have distributed an estimated 8 million intermediate improved cookstove solutions and 100,000 advanced biomass cookstoves as of 2014.¹⁸ There are a lot more households in Sub-Saharan Africa that have access to clean cooking technology than in the past, but the current progress has only led to one out of every six households in the region transitioning to the use of improved cooking technology for most cooking tasks.¹⁸ Even for the households who have made the transition to improved cooking technology and fuels, the impact that these technologies have on their day-to-day lives is difficult to quantify and is generally unknown. Health impact studies of clean cooking technology have found mixed results and the meaning of these results to the viability of clean cooking solutions in reducing the risks of illness, disease, or death, and in alleviating household fuel-demand is often debated among the improved cooking technology community. Currently, there is no clear-cut conclusion on if the implementation of improved household cooking technologies that meet the current performance targets defined by the Alliance

result in significant reductions/improvements in health risks, household fuel-demand, social inequities, and/or environmental damage.

A study completed in 2016 assessed the daily use of a mixture of six different intermediate and advanced biomass cookstove products currently on the market in Sub-Saharan Africa in 45 households in Kenya. The study found that the median reduction in PM_{2.5} household-kitchen concentrations was 38.8%, with a median concentration of 409 µg/m³. While this reduction is significant, the post implementation median household-kitchen concentration is still almost 12 times the WHO air-quality guideline of 35 µg/m³ and it is far from the 80% reduction that the Alliance uses to define a clean-burning solution.¹⁹ The same study did find personal exposure levels of CO to be consistently lower than the WHO guideline and that average fuel-consumption was reduced by 30%, so there does seem to be some confirmation of the potential benefits of the use of improved cookstoves for households that adopt clean cooking technology.¹⁹ But the reality is that these products still fall short of the minimum performance targets set forth by the Alliance used to define efficient and clean cooking solutions.

One of the main lessons learned from this study -- and what is becoming more apparent with each additional health study conducted -- is that stove-stacking, defined to be the use of improved cookstoves in addition to traditional cookstoves and open-fires, is usually responsible for the limited impact of improved-cookstove implementations.¹⁹ Another study completed in 2012 found that households only exclusively used an improved cookstove 25% of the days the study was performed, and stove-stacking visibly occurred over 40% of the time.²⁰ The high-emissions and relatively high fuel-demand of traditional cooking practices can minimize the benefits of improved cooking solutions if traditional practices are not eliminated from use.

When asked why people tended to continue using traditional cooking practices, most cooks said that factors such as ease of use, cooking speed, the inability to cook for large groups, the inability to cook some local dishes, and unfamiliarity with the improved cookstove meant that cooks

gravitated toward using their traditional techniques over the improved cooking solutions .¹⁹ Put simply, these households were provided cooking technology that they did not fully understand how to use, did not meet their needs, and that, in general, lacked the incentives needed to encourage the complete transition to the new technology. There should be some expected level of stove-stacking during a transition period while households adjust to new cooking technology or fuels, but the widespread stove-stacking found in these studies suggests that the success of clean and efficient cooking technology is heavily dependent on developing solutions that are well suited to local cooking culture and cuisine.

One possible outcome is that the majority of clean-burning and/or fuel-efficient solutions used in these studies are not well suited for their target communities. Specifically, this includes meeting the expectations of local cooks, their cooking needs, and providing enough incentive to transition away from traditional cooking practices. This emphasizes the importance of taking into consideration local cultures, cuisines, consumer preferences, and consumer education when developing and implementing improved biomass cooking technologies and fuels. Without consideration of these factors even the most clean-burning, fuel-efficient, and affordable improved cookstoves can result in low-impact if households do not use them exclusively.

Currently, there are nearly 500 improved cookstove designs listed on the Clean Cooking Alliance's website as of 2018 and an estimated 116 million individual improved cookstoves and/or fuels deployed in households worldwide as of 2016, with 200 million predicted to be distributed by 2020.²¹ Millions of households are becoming more aware of the clean cooking initiative and of the dangers associated with their traditional cooking techniques. Developing clean and efficient products that also have high adoption rates have, however, remained a challenge. Of the 116 million improved cookstoves and/or fuels being used by households around the globe, only 70 million meet the Clean Cooking Alliance's definition of efficient and only 44 million meet the definition of clean-burning, with adoption rates often remaining unknown.²¹

Currently, very few solutions are clean-burning and fuel-efficient, with LPG being one of the only technologies satisfying the Alliance's performance targets as well as resulting in high-adoption rates. This fact drives investment towards LPG technologies, which is apparent in the distribution of improved cooking technology with LPG technology accounting for 68% of all in-home deployments worldwide.²¹ The successful distribution of LPG technologies has primarily been driven by government funded programs that give LPG the benefit of economies of scale. India is one such country with government-backed clean cooking initiatives; here, the success of these LPG focused programs accounts for approximately 50% of all in-home clean cooking products.²¹ But this is only one region of the world that has made significant progress in transitioning households in their region to improved cooking technology.

In many regions around the world, such as in Sub-Saharan Africa, government-backed LPG initiatives like that are found in India are still developing or non-existent. Without government or consortia led initiatives, most markets suffer from price fluctuations and supply issues that are all-to-common in the petroleum industry in developing countries. In addition, LPG stove technology and fuel canisters are relatively expensive for many households. All these contributing factors reduce the likelihood of complete transition to LPG without significant investment from government or private organizations, meaning households still must rely on solid biomass fuels and stove-stacking to meet their household energy needs if their region lacks investment into LPG access and technology. This is where clean-burning, fuel-efficient, and affordable intermediate technologies that burn existing low-cost and reliably available unprocessed solid biomass fuels could act, at the very least, as an interim solution until household electricity access and/or access to LPG technology and fuel is improved to a point that they become a viable household energy option and competitor of traditional solid biomass fuels.

Unfortunately, the current state of intermediate improved cooking technologies does not compete with the performance and utility of electricity or LPG technology. Intermediate cooking

technologies are competitive in cost, fuel affordability/availability, and in their similarity to traditional cooking practices, but the marginal reduction in HAP and poor thermal-efficiency of current intermediate technologies proves to be a persistent barrier to the successful deployment of low-cost, clean-burning, and fuel-efficient stoves and/or fuels. Globally, only 25% of all in-home technologies burn traditional solid biomass fuel supplies and very few of these products meet the Alliance's clean-burning and fuel-efficiency targets, with even less achieving high adoption rates.²¹ Designing improved cooking technology has proven to be a seemingly insurmountable task. Challenges include (1) burning locally available traditional biomass fuel supplies, (2) reducing household emissions, (3) increasing fuel-efficiency to meet the performance targets set by the Alliance, (4) reducing manufacturing cost to a sustainable level, and (5) meeting the needs of local cooks. Meeting these challenges are necessary to achieve high adoption rates and complete transition to the new technology.

Innovative intermediate cookstove design tools and strategies are needed to help define, understand, and overcome the technical issues preventing the successful development and implementation of clean-burning and fuel-efficient intermediate improved cookstoves that bridge the gap between products that meet the performance targets set by the Alliance and products that meet the needs of local cooks. Bridging this gap would increase the incentives for households to transition to improved cooking technologies that burn locally available fuels, that are clean-burning and fuel-efficient, that result in meaningful improvements in personal health, quality of life, and financial-stability, and that result in meaningful reductions in environmental damage. The risk of not developing such design tools and design strategies would result in the continuation of the greatest environmental health risk to the human population, leaving billions of people worldwide without a suitable clean-burning and fuel-efficient household energy option until major investment has been made in increasing access to sustainable household electricity and/or LPG household energy solutions.

1.2 ISO/IWA Cookstove Performance Metrics

In pursuit of facilitating the development of cookstove design tools/strategies and the sharing of knowledge of improved cooking technology the Alliance, in partnership with the International Organization for Standardization (ISO) and the US Environmental Protection Agency (EPA), developed a set of performance metrics for quantitative cookstove evaluation. These are detailed in ISO/IWA 11:2012 “Guidelines for evaluating cookstove performance” .²⁶ The metrics are separated into three groupings: cookstove emissions, thermal-efficiency, fuel-consumption, and indoor emissions. While the cookstove emissions and indoor emissions categories are very similar, the two groupings use different units to describe emissions rates, providing unique information about stove performance. Each metric has five tiers (0-4, with Tier 4 being the most stringent). Stoves and/or fuels that meet Tier 4 satisfy all WHO HAP guidelines. The Alliance’s definition of clean and efficient cooking technologies correspond to a 70% reduction in fuel-consumption and an 80% reduction in PM_{2.5} and CO emissions, equating to Tier 2 and Tier 3 performance levels, respectively. The full classification of the metrics and tiers are listed in Table 1 and Table 2.

Table 1: ISO/IWA Tiers for emissions

	High Power CO (g/MJd)	Low Power CO (g/min/L)	High Power PM2.5 (mg/(MJd))	Low Power PM2.5 (mg/min/L)
Tier 0	> 16	> 0.2	> 979	> 8
Tier 1	≤ 16	≤ 0.2	≤ 979	≤ 8
Tier 2	≤ 11	≤ 0.13	≤ 386	≤ 4
Tier 3	≤ 9	≤ 0.10	≤ 168	≤ 2
Tier 4	≤ 8	≤ 0.09	≤ 41	≤ 1

Note: MJd denotes the energy delivered to the water in the pot.

Table 2: ISO/IWA Tiers for thermal-efficiency/fuel-use and indoor emissions

	High Power Thermal Efficiency (%)	Low Power Specific Consumption (MJ/min/L)	Indoor Emissions CO (g/min)	Indoor Emissions PM2.5 (mg/min)
Tier 0	< 15	> 0.050	> 0.97	> 40
Tier 1	≥ 15	≤ 0.050	≤ 0.97	≤ 40
Tier 2	≥ 25	≤ 0.039	≤ 0.62	≤ 17
Tier 3	≥ 35	≤ 0.028	≤ 0.49	≤ 8
Tier 4	≥ 45	≤ 0.017	≤ 0.42	≤ 2

The ISO/IWA performance tiers are designed to operate using the Water Boil Test (WBT) 4.2.3²⁷, which is detailed in Chapter 3 Section 3.2.1. The high-power and low-power metrics are designed to characterize stove performance as the user transitions from a rapid cooking mode, i.e., heating food/water as fast as possible, to a simmer mode, in which the user is only trying to maintain the food/water temperature. The characterization of stove performance under a high-power and low-power condition is believed to provide the necessary information to make informed cookstove design decisions and quantify how a stove may perform in the field under similar conditions. Field testing and user focus-groups are still highly recommended to evaluate stove performance and evaluate if a stove meets the needs of local cooks before implementation to ensure maximum impact on fuel-consumption, HAP, and ensure high adoption rates.

The WBT provides a standardized testing procedure, but it is largely up to the stove designer and testing center to determine the context in which the tests are run, i.e., what is high-power, what is low-power, what species of fuel, what size of fuel, what fuel moisture-content, what fire-tending and/or fuel burn-rate characteristics, and what cooking implements best match what would be expected upon implementation in the field? All these metrics can change the performance of a stove significantly, so it is of utmost importance to understand the region and population the stove

is intended for and how the stove will be used in the field in order to most accurately predict the performance of the stove upon implementation among households in this region.

The cookstove community has found that the carbon monoxide metrics are relatively easy to meet for most wood-burning stoves, while the thermal-efficiency/fuel-consumption and PM_{2.5} emissions metrics present the biggest challenge, especially at the high-power operating condition. Most cookstove development projects focus on the high-power performance metrics. In general, the cookstove community has been found that if a stove meets the intended performance targets at high-power, or under a more “stressed” fueling condition, it will also meet these targets at the low-power operating condition. Cookstove performance results that are reported only for the high-power operating condition, or boil phase of the WBT, are often referred to as rapid-WBT, or high-power-WBT results.

The PM_{2.5} and CO indoor emissions metrics are included for straightforward comparison against the World Health Organization’s (WHO) intermediate household combustion emissions rate targets of 1.75 mg/min and 0.35 g/min for PM and CO, respectively.³ The WHO encourages the use of their most stringent emissions rate targets of 0.23 mg/min (PM) and 0.16 g/min (CO) to encourage the use of healthier technology and ensure the repair or replacement of non-compliant devices.³

Note: The ISO has recently released new cookstove testing standards and performance targets with ISO/TR 19867-1:2018 and ISO/TR 19867-3:2018.^{28,29} Future investigations should adhere to the protocols and performance metrics outlined in these current standards documents, or any subsequent updates to the standards. The work presented in this paper was completed prior to the release of the new standards, the ISO/IWA 11:2012 standards were followed and used for reporting herein.

1.3 University of Washington Clean Cookstoves Laboratory (UWCCL)

In 2012, the US Department of Energy (DOE), one of the founding partners of the Alliance, announced a funding opportunity made available for applied research and development to advance clean and efficient biomass cookstove technologies.³⁰ The goal of the DOE was to facilitate an initiative powered by the combined expertise of private and public entities, within the US, with the necessary technical expertise needed to define, understand, and overcome the leading technical and performance issues preventing the successful development, widespread implementation, and adoption of clean and efficient cooking technologies that burn locally available unprocessed solid biomass fuels (i.e., intermediate solutions). This DOE backed initiative primarily focused on remedying the lack of in-depth knowledge of how solid-fuel combustion, cookstove thermodynamics, and cookstove mechanical design characteristics interact and contribute to cookstove performance.

In early 2013, the University of Washington received a grant from the DOE as part of this initiative, which established the University of Washington Clean Cookstoves Laboratory (UWCCL); a research laboratory focused specifically on understanding all aspects of cookstove design and performance. The mission of the UWCCL is to help bring viable intermediate cookstove products to market, via providing the knowledge, tools, and design innovations needed to produce intermediate cookstove products that eliminate harmful cookstove emissions, optimize thermal-performance, and that meet the needs of local-cooks. The UWCCL develops cookstove design tools/strategies and testing protocols in partnership with cookstove designers and manufacturers which are then made available to the entire cookstove development community. The goal of the design tools/strategies and testing protocols that the UWCCL develops is to make it easier for stove designers and manufacturers to assess the performance of their designs, understand how to interpret performance results, and make strategic and informed improvements to their products,

increasing their effectiveness of making a positive impact upon implementation in their target communities.

1.4 A Natural-Draft Side-Feed Wood-Burning Cookstove for East-Africa

The DOE grant the UWCCL received in 2013 (grant number DE - EE0006284.0000), in partnership with BURN Manufacturing (BURN) and BURN Design Laboratory (BDL), funded a three-year project focused on assisting BURN and BDL in the development and design of an unvented, natural-draft, side-feed, wood-burning cookstove for rural regions of East-Africa, with an initial target market in rural-Kenya. An unvented, natural-draft, side-feed, wood-burning cookstove was selected for this region because of the fuel-flexibility, ease of use, and relative simplicity of stoves in this design category (i.e., inexpensive). An unvented design requires no modification to a household to install a chimney, saves on cost, and keeps the stove mobile. Natural-draft stoves, or in other words, stoves that do not use electric fans or components to augment the cookstoves flow-characteristics or to control fuel input, provide significant cost savings over designs that incorporate electronic components. Side-feed, wood-burning stoves allow for the flexibility required to burn the highly-variable unprocessed wood fuels that are found and used in rural-Kenya and are relatively easy to operate and control while cooking, with the process being very similar to the open-fires and traditional cookstoves that households in rural-Kenya are already accustomed to using. The final stove design needed to culminate in a product that was capable of being locally manufactured in Kenya, sold at a retail cost <\$40 USD, meet a target product lifespan of +2.5 years, meet the needs and design requirements of local cooks, and meet all ISO/IWA Tier 4 performance standards during in-home use.

1.4.1 Natural-Draft Rocket-Stove Design Overview

Side-feed, wood-burning stoves are referred to as rocket-stoves, or rocket-elbow stoves, which are wood-burning stoves that use a simple side-feed combustion chamber containing a short insulated vertical chimney, or riser, that are configured into an “L”, or elbow-shaped assembly.

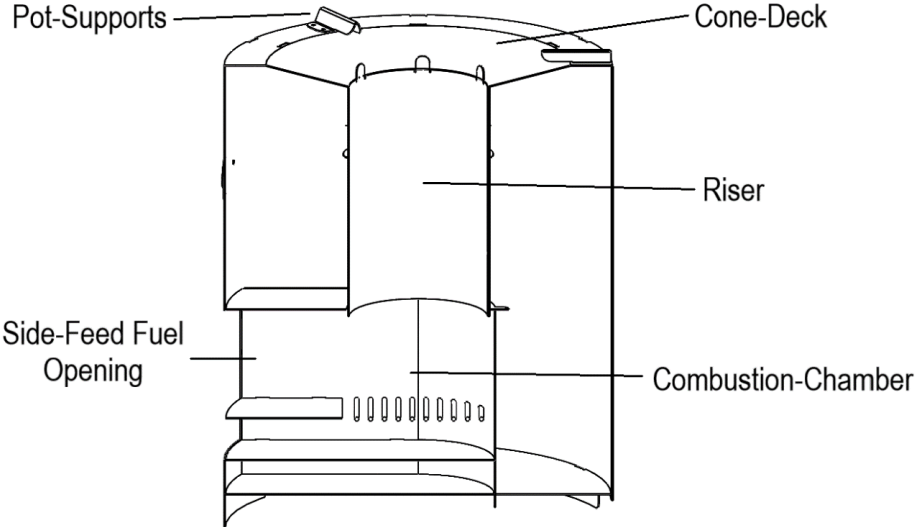


Figure 1: Rocket-stove cross section detailing the components and geometry of a typical natural-draft design.

The user feeds wood through the fuel-opening in the side of the stove, leading to the combustion chamber, where the fuel is burned. Fuel burn-rates, or the amount of fuel used, or burned per unit of time are determined by the user. Rocket-stoves have no active way of controlling fueling characteristics (type, size, species, moisture-content, quantity, etc.) beyond modifying the size of the combustion-chamber or fuel inlet to physically limit the total amount of fuel that can be inserted into the stove and burned at the one time. Cooking is done on the top of the stove where a cooking implement, such as a pot or pan, is placed on pot supports directly above the outlet of the riser where the hot combustion products exit the stove. The hot combustion gases exiting the riser, flow through a gap between the bottom of the cooking implement and what is referred to as the

cone deck, which is essentially the top of the stove. Cooking temperature and speed is controlled by how aggressively fuel is fed into the combustion chamber by the user.

1.4.2 The Kuniokoa™

The DOE funded project, a partnership between the UWCCL, BURN, and BDL, resulted in the launch of the Kuniokoa™, an unvented, natural-draft, side-feed, wood-burning cookstove manufactured and sold by BURN in Kenya. The Kuniokoa™ was developed using a three-pronged approach consisting of computational and analytical modeling, experimental testing of conceptual prototypes, and extensive field and user research.

At the beginning of the project, BURN had an existing unvented natural-draft rocket-stove prototype, referred to as the Stick-Fed-Rocket, or SFR (Figure 2) that they had developed for initial design and performance optimization investigations, but had limited success in improving performance. The SFR, in its original form, was a sub-Tier 3 performing stove when tested under laboratory conditions (Figure 3). In the early stages of the DOE project, the UWCCL used the SFR as a test-bed for initial investigations into the thermodynamics and combustion behavior that dictates natural-draft rocket-stove performance. The UWCCL used a combination of computational-fluid-dynamic modeling (CFD), analytical models, laboratory experiments, and practical prototype development to build off the baseline SFR design, eventually designing a stove prototype that met the Tier 4 performance targets under laboratory testing conditions; this prototype was referred to as the Tall-Boy (Figure 2).

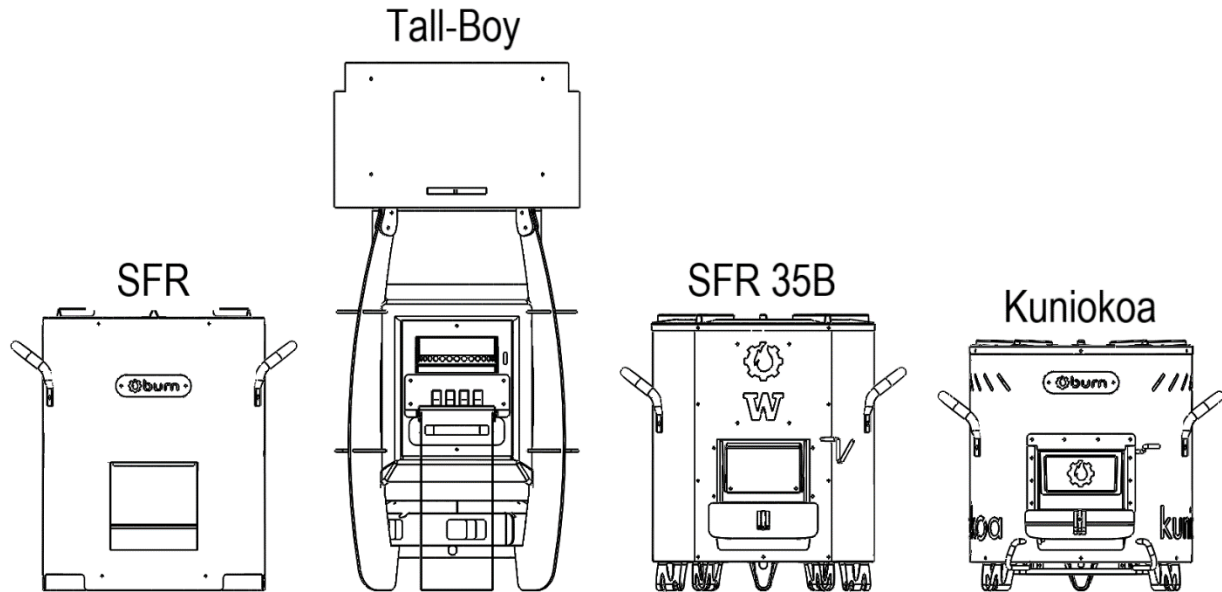


Figure 2: Illustration of the SFR, Tall-Boy, and SFR 35B natural-draft rocket stove prototypes that lead to the development of the Kunioko™.

The Tall-Boy incorporated many novel innovations in natural-draft rocket stove design that were developed in pursuit of Tier 4 performance. The strategy used in developing the Tall-Boy revolved around performing a thermodynamic energy availability analysis of the SFR. By first understanding where the energy produced by combustion was distributed throughout the baseline cookstove assembly, design strategies could be developed to eliminate energy pathways that were not contributing to cooking, in effect, maximizing the energy available (i.e., availability) to be used for cooking, resulting in Tier 4 thermal-efficiency. The primary energy pathways of concern were convective, conductive, and radiative heat-transfer mechanisms that were responsible for heat-loss from the cookstove assembly to the surrounding environment. Two specific strategies led to the largest impact. The first was the elimination of conduction pathways connecting the combustion chamber to the cone deck and the exterior. This was achieved by using low conductivity connections. Second, the use of low thermal inertia insulation (e.g., radiation shields as opposed to heavier refractory insulation) reduced the amount of heat absorbed by the stove

during a cold start. In addition, by understanding where and why PM_{2.5} emissions are produced in a wood-burning cookstove we were able to strategically modify the Tall-Boy design to reduce PM_{2.5} emissions to within the Tier 4 performance targets (Tier 4 CO emissions were easily achieved even in the original SFR). The design strategies used in the Tall-Boy that were necessary to reach this level of performance in an unvented, natural-draft, side-feed, wood-burning cookstove are summarized below and the corresponding high-power WBT performance tiers for the Tall-Boy are shown in Figure 3:

- Minimize thermal-mass, or heat capacitance, of the stove assembly.
- Use of low-thermal mass insulation and heat-shield material.
- Use of a multi-layered insulation technique using an air-gap between internal stove components (combustion chamber, riser, etc.) and glass-fiber insulation and/or heat-shield assemblies.
- Thermal-isolation, with respect to convection, conduction, and radiation, of stove components that are directly exposed to the fuel-bed and/or combustion gases.
- Precise control of primary, over-fire, and under-fire air injection location, flow-rates, and velocities.
- Precise control of fuel-size, moisture-content, species, feed-rate, and fuel-position in the combustion-chamber.
- Use of specialized stove lighting techniques optimized to produce minimal start-up emissions.
- Multi-stage combustion chamber, providing separate regions for primary combustion, secondary charcoal combustion, a low-oxygen region for wood-gasification, and a secondary combustion zone for over-fire wood-gas re-burn.
- Use of static-mixers to increase mixing between unburnt fuel and air, also used to increase the effectiveness of various natural-draft air injection techniques.

- Increased stove height to increase draft, or flow-potential, through the stove and to reduce flame-impingement on the bottom surface of the cooking surface (pot).
- Use of an insulated pot-skirt and finned-bottom pot to increase the surface area and time available for heat-transfer between combustion products exiting the top of the stove and the cooking surface (pot).
- Optimization of the internal flow pathway geometry to maximize heat-transfer to the cooking surface (pot).

Note: These design strategies are detailed in the following conference proceedings^{31, 32, 33, 34, 35, 53}.

When limited to natural-draft, all the strategies outlined above were required to meet the Tier 4 performance targets under laboratory testing conditions. Unfortunately, some of these strategies are not compatible with producing a product that was inexpensive, manufacturable, durable, easy-to-use, and that met the needs of local cooks. To mitigate these issues many of the novel cookstove design strategies and characteristics that were developed through the process of designing the Tall-Boy were incorporated into a more cost-effective and manufacturable design, in the form of the SFR 35B; a Tier 3 performing stove under laboratory testing conditions (Figure 3). In 2016, ten of the SFR 35B prototypes were built in Kenya and underwent home-placement in various rural-regions of Kenya to assess the design's impact on household fuel-consumption and HAP. While placed with these household's, Berkeley Air Monitoring Group (BAMG) observed the in-home use of the SFR 35B and collected data on fuel-consumption and HAP for both the SFR 35B and the traditional TSF that the households were currently using for cooking.

BAMG found that the SFR 35B reduced fuel-consumption by 43% and PM_{2.5} emissions by 66% when compared to the traditional TSF used by the households in the study, corresponding to Tier 2 and Tier 0 performance respectively. Unsurprisingly, the field data collected by BAMG suggests that the stove performance predicted under laboratory testing conditions and by laboratory testing protocols did not correspond to equivalent performance when the stove was used by local cooks

in the field. Laboratory tests do show the same reduction in fuel-consumption (43%) and PM_{2.5} emissions (66%) between the lab-based TSF and the SFR 35B, but the performance testing protocols and procedures used in the laboratory did not produce accurate predictions of the absolute value of fuel-consumption or PM_{2.5} emissions when compared to what was measured in the field. Our experiments suggest that the discrepancies between laboratory and field performance results stem from differences in fuel characteristics (e.g., fuel-size, moisture-content) and stove operation (e.g., burn-rate). Subsequent changes were made to how lab-based performance analysis is performed to better match in-home operation and were used in characterizing the performance of the projects final cookstove design; the KuniokoTM.

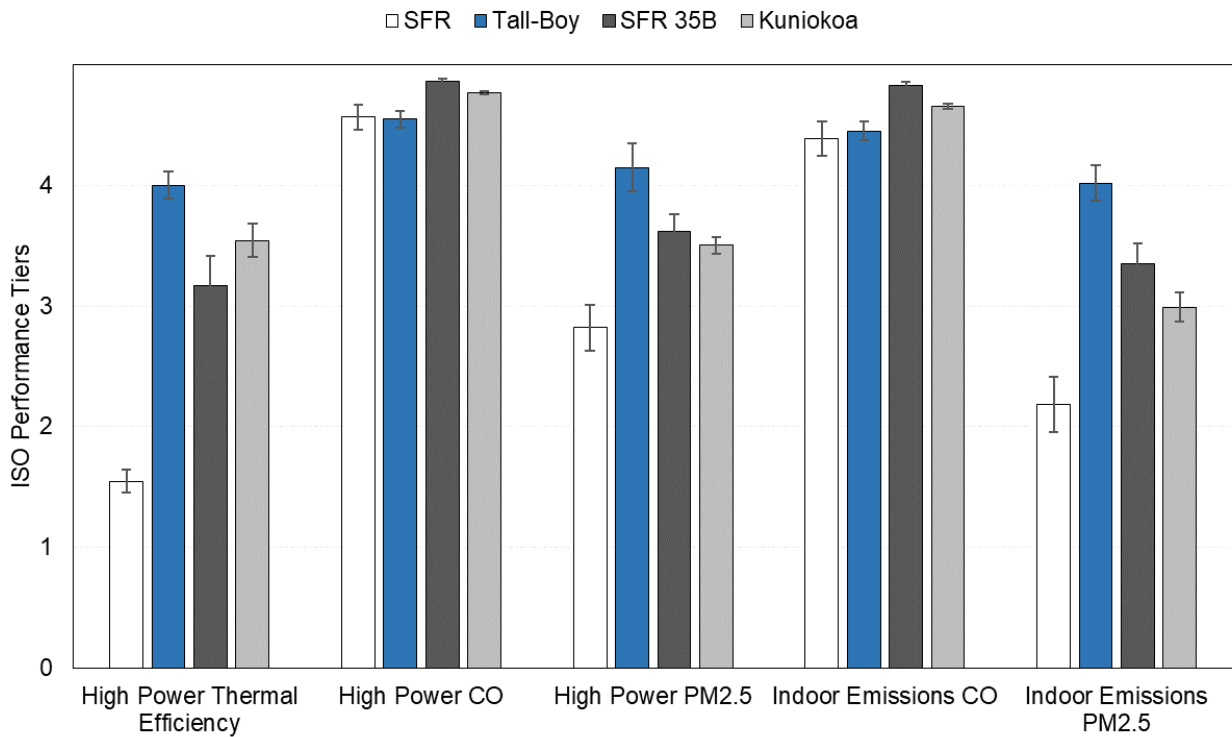


Figure 3: Comparison of the high-power WBT ISO performance tier laboratory results for the SFR, Tall-Boy, SFR 35B, and KuniokoTM. Note: error bars represent a 90% CI.

The SFR 35B may not have met the Tier 4 performance goals of the project, in the laboratory or in the field, but the performance of the SFR 35B was a significant improvement over BURN's existing SFR design and the traditional TSF. BURN decided these performance increases would still provide an immediate and significant benefit to households. At the time of the SFR 35B field-study there was not an unvented, natural-draft, side-feed, wood-burning cooking product available in Kenya that matched the thermal-efficiency and emissions performance of the SFR 35B, suggesting that significant progress had been made in advancing the performance of wood-burning stove technology among what was currently available in East-Africa, even if the performance was short of the original Tier 4 target.

In the final stages of the project, BURN and BDL used the SFR 35B design, the design strategies the UWCCCL developed as part of the Tall-Boy and SFR 35B design process, and user feedback data from an extensive series of product focus-groups conducted in Kenya, to create a manufacturable product that BURN could produce in their cookstove factory outside of Nairobi, Kenya. BURN's natural-draft, side-feed, wood-burning rocket-stove, marketed under the product name Kuniokoa™, is the culmination of the work completed by the UWCCCL, BURN, and BDL, made possible by the US DOE. The Kuniokoa™ meets nearly all the original project goals, it is locally manufactured in Kenya, sold at a retail cost <\$40 USD, has a proven lifespan of +4 years when subjected to daily in-home use, and meets the needs and design requirements of local cooks. The Kuniokoa™ did not satisfy the original Tier 4 performance targets set at the onset of the project, but at the time of launch the Kuniokoa™ was the most fuel-efficient and clean-burning natural-draft cookstove available in Sub-Saharan Africa that burns locally available unprocessed wood-fuel.

1.4.3 Kuniokoa™ Laboratory Performance

The UWCCL subjected the Kuniokoa™ to a series of laboratory performance tests including WBT's and Firepower-Sweep-Test's (FPS, detailed in Chapter 3 Section 3.2.2) as part of the final design analysis for the DOE project and to provide BURN and BDL with a comprehensive laboratory performance analysis of the Kuniokoa™ when subject to field typical use. The purpose of this testing was to characterize the fuel-consumption and emissions behavior of the Kuniokoa™ over a wide-range of operating conditions (e.g., fuel-sizes, moisture-content, and burn-rates) typical of in-home use in rural-Kenya and to also define the optimum operating condition(s) and corresponding performance. The datum were then provided to BURN as an official performance analysis of the Kuniokoa™ and for comparison for future design development.

BURN and BDL provided field data characterizing the size and moisture-content of the unprocessed wood-fuel most commonly used by households in rural-Kenya, which is shown in Figure 4. Using these data, small-dry, large-dry, and large-wet wood feedstocks were selected for testing, acting as a representative sample of the unprocessed wood-fuel found in rural-Kenya. All the feedstocks were the same species of fuel (Douglas Fir) but had varying size and moisture-content. The small-dry and large-dry feedstocks had an average moisture content of 10% on a dry-basis and were 2cm x 2cm and 4cm x 4cm in cross-sectional dimension respectively. The large-wet feedstock consisted of freshly cut Douglas Fir that was cut to an average equivalent diameter of 4.3cm and kiln dried to within 25-40% moisture content on a dry-basis, matching BURN and BDL's field estimate of the moisture-content typical of wet-wood used during the wet-season in rural-Kenya (Figure 4).

BAMG measured fuel burn-rate, or firepower, during the in-home study for the SFR 35B, which was used to estimate the burn-rate associated with in-home use. The Kuniokoa™ and SFR 35B have the same size combustion-chamber and fuel-inlet, so fuel burn-rates should remain within the same range for both designs during in-home use. Of the 20 cooking events that were included

in the SFR 35B field study, the median firepower was 3.5kW and most cooking events resulted in fuel burn-rates between 2.5kW to 4.5kW, shown in Figure 5. Based upon the fuel and burn-rate characteristics measured by BURN, BDL, and BAMG, we configured and performed an FPS to characterize the PM_{2.5} performance of the Kuniokoa™ for small-dry and large-dry feedstocks covering a range of fuel burn-rates similar to what was measured in the field. The results from the FPS are shown in Figure 6.

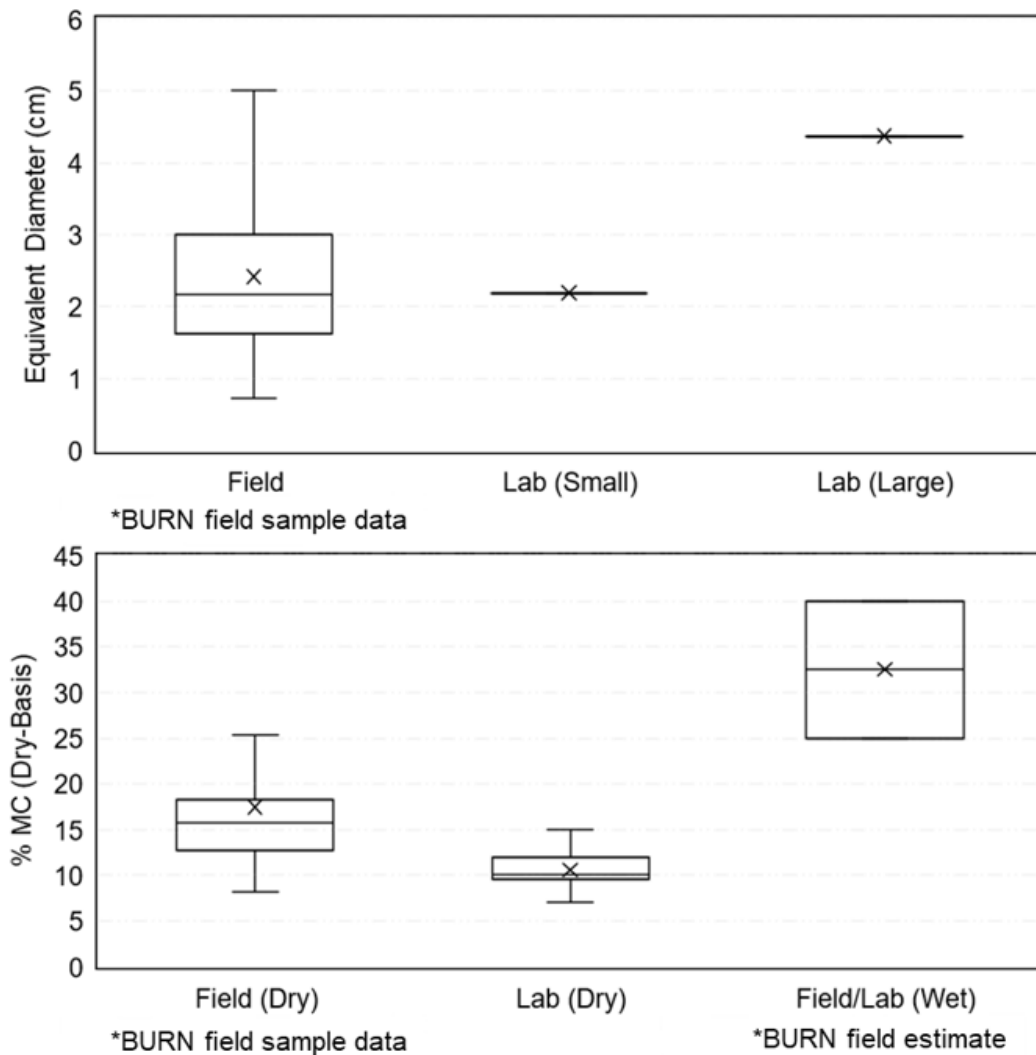


Figure 4: Comparison of the moisture-content (MC) of fuel-feedstocks found in rural-Kenya, based from data and estimates collected by BURN and BDL, to the fuel-feedstocks used by UWCCL for performance testing of the Kuniokoa™.

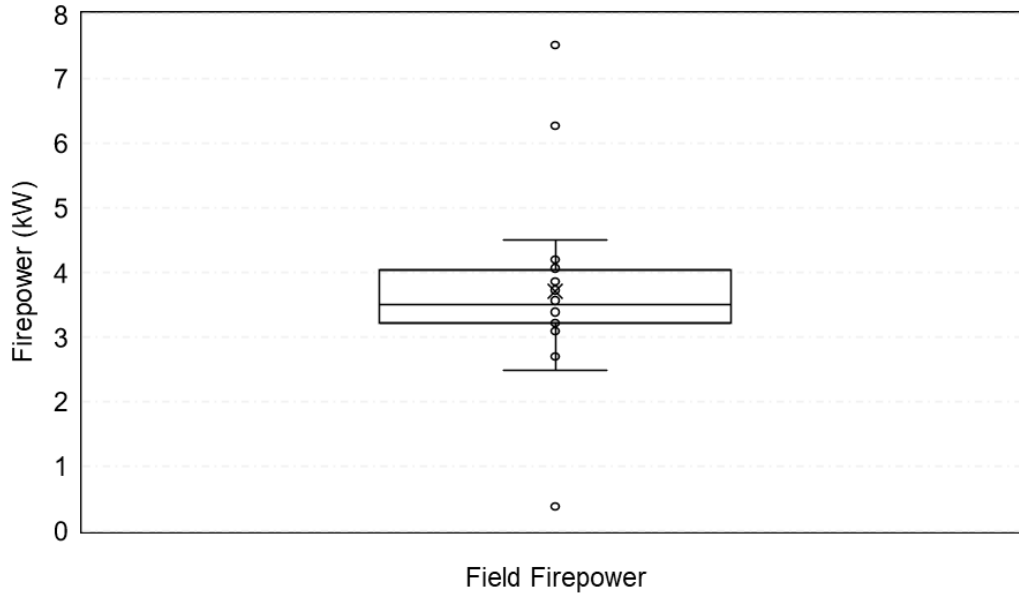


Figure 5: Distribution of fuel burn-rates (i.e., firepower) measured during the 20 cooking events included in the SFR 35B field-study conducted by BAMG.

The FPS results show that the PM_{2.5} emission rate remains under or near Tier 3 (8 mg/min) for small-dry and large-dry fuel burn-rates of 3kW or less. As the fuel burn-rate increases past 3kW, there is an inflection in the PM_{2.5} emission rate behavior, where a small increase in burn-rate corresponds to a large increase in PM_{2.5} emissions. In the range of burn-rates between 1kW and 3kW the relationship between the PM_{2.5} emission rate and fuel burn-rate can be described by a linear relationship of 6.2 mg/min per kW increase in burn-rate. Above 3kW this relationship is 21.3 mg/min per kW increase in burn-rate; 3.5 times more than the relationship below 3kW. This suggests that the Kuniokoa™ is incapable of meeting the Alliance’s definition of clean-burning for burn-rates more than approximately 3kW for small-dry and large-dry feedstocks.

We performed high-power WBT’s using the small-dry, large-dry, and large-wet feedstocks at the highest burn-rates achievable for each respective fuel-type. The corresponding tiered performance metrics and values for the Kuniokoa™ are shown in Figure 7 and Table 3.

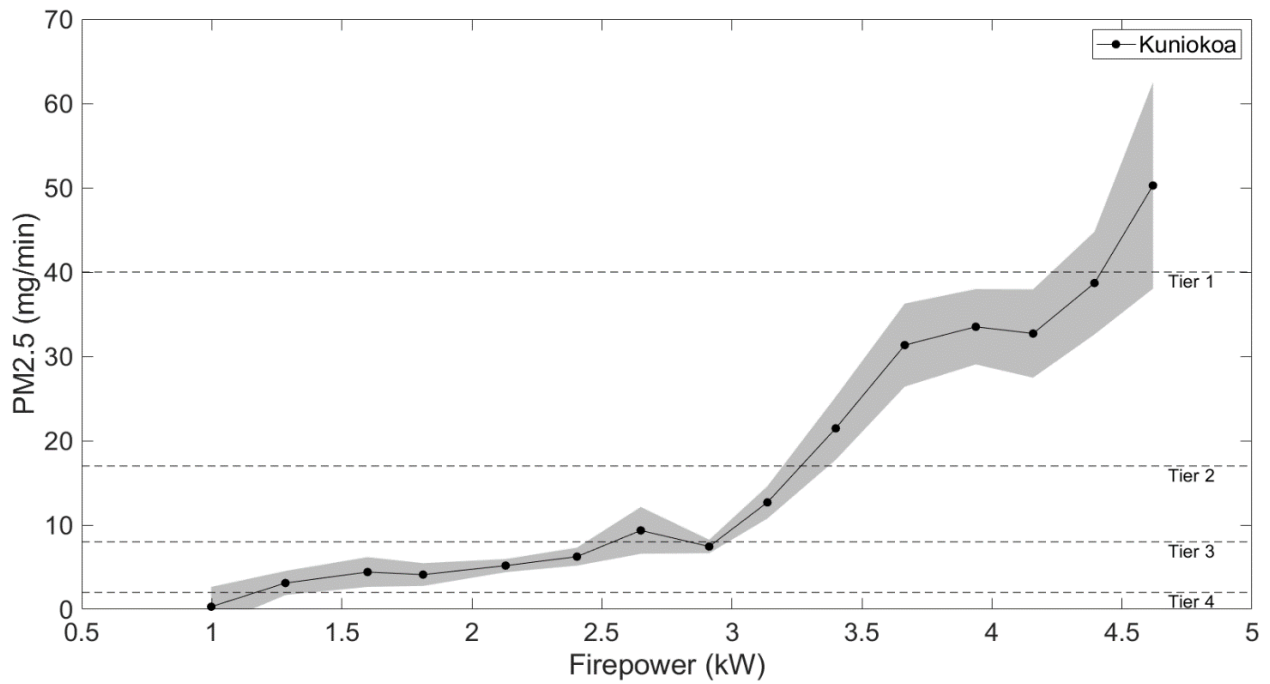


Figure 6: Kuniokoa™ FPS PM_{2.5} emissions behavior for small-dry and large-dry feedstocks for burn-rates from 1kW to 4.75kW. Note: the shaded region represents a 90% CI.

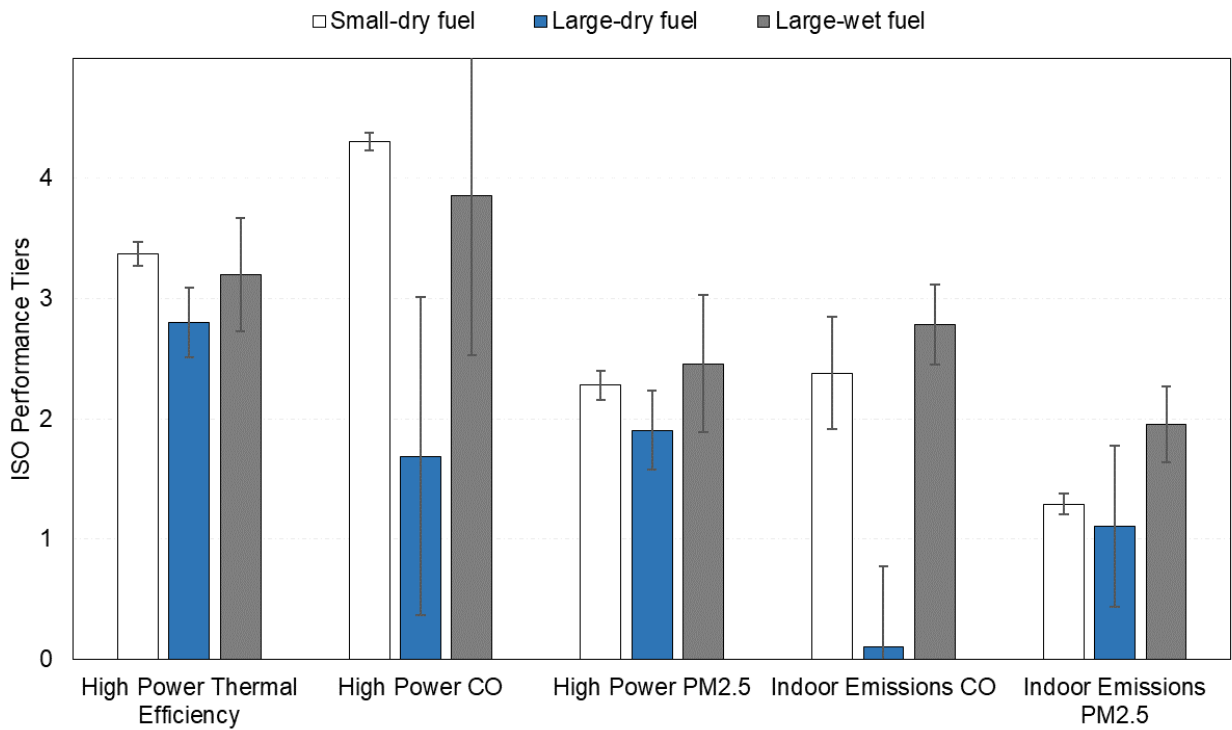


Figure 7: Kuniokoa™ high-power WBT ISO performance tiers for small-dry, large-dry, and large-wet feedstocks. Note: error bars represent a 90% CI.

Table 3: Kenya TSF baseline values and Kuniokoa™ high-power WBT ISO performance values for small-dry, large-dry, and large-wet feedstocks. Simulated field-typical performance metrics are averaged across all fuel-types and shown for comparison.

	Firepower (kW)	Time-to-Boil (min)	High Power Thermal-Efficiency (%)	High Power CO (g/MJd)	High Power PM _{2.5} (mg/MJd)	Indoor Emissions CO (g/min)	Indoor Emissions PM _{2.5} (mg/min)
Kenyan TSF	7.1 ± 2	N/A	N/A	4.2 ± 1.7	542 ± 212	1.7 ± 0.7	217.9 ± 71
Small-dry fuel (n = 6)	4.4 ± 0.3	17.8 ± 1.4	38.7 ± 1.2	5.6 ± 0.7	325 ± 32	0.57 ± 0.07	33.3 ± 2.5
Large-dry fuel (n = 6)	4.4 ± 0.1	24.7 ± 4.3	33 ± 3.5	12.6 ± 4	442 ± 136	1.1 ± 0.2	37.6 ± 8.1
Large-wet fuel (n = 3)	2.5 ± 0.1	35.5 ± 4	37 ± 8.2	8.1 ± 1.3	286 ± 74	0.52 ± 0.03	18.1 ± 2.8
Simulated Field-Typical	3.8 ± 1	26 ± 8.9	36 ± 3	8.7 ± 3.5	351 ± 81	0.72 ± 0.3	29.6 ± 10.3

Note: variabilities represent one standard-deviation.

The high-power WBT performance results suggest that the performance of the Kuniokoa™ is dependent on fuel size and moisture-content, in addition to fuel burn-rate. The small-dry fuel provided a significantly faster cooking time of 17.8 minutes when compared to both the large-dry and wet-dry feedstock results, which is also represented by the thermal-efficiency trend across all fuel-types with small-dry fuel having the highest thermal-efficiency. At an equivalent burn-rate to small-dry fuel, using large-dry fuel in the Kuniokoa™ results in an average thermal-efficiency of 33% (15% less than the result for small-dry fuel), a 40% increase in the time-to-boil, a 125% increase in CO emissions (g/MJd), a 36% increase in PM_{2.5} emissions (mg/MJd), and a 93% and

13% increase in CO and PM_{2.5} indoor emission rates, respectively, when compared to the small-dry feedstock performance results.

Both the large-dry and large-wet fuel performance results had higher variability in performance compared to the small-dry fuel even though the variability in fuel burn-rate across all tests was not significantly different than the small-dry fuel. This suggests variability in burn-rate is not the only factor responsible for the higher performance variabilities when using large-dry and large-wet feedstocks.

The large-wet feedstock performance results suggest that the Kuniokoa™ is limited in its ability to burn large-wet wood with the highest fuel burn-rate achievable being 43% less than the small-dry and large-dry feedstocks. The ability of the stove to burn high moisture content wood is vital for local cooks during the wet-season when dry wood can be hard to procure. In addition, the PM_{2.5} emission rate of the large-wet wood results suggest that the PM_{2.5} emission rate increases for higher moisture-content fuel when compared to the results at an equivalent fuel burn-rate for the small-dry and large-dry feedstocks.

Averaging the tiered performance results across all the fuel-types is used as a simulated representation of field-typical performance. The simulated field-typical performance across all fuel-types is on average Tier 3 for high-power thermal-efficiency, Tier 3 for high-power CO, Tier 2 for high-power PM_{2.5}, Tier 1 for indoor emissions CO, and Tier 1 for indoor emissions PM_{2.5}. If this performance is compared to the Kenyan TSF emissions data measured by BAMG during the SFR 35B field-study (Table 3), the Kuniokoa™ corresponds to a 66% increase in high-power CO emissions, a 47% decrease in high-power PM_{2.5} emissions, a 67% decrease in the indoor CO emission rate, and an 89% decrease in the indoor PM_{2.5} emission rate.

Reviewing the high-power WBT results suggests that the wood feedstock that the Kuniokoa™ is best suited to burn, resulting in the best compromise between cooking-time, thermal-efficiency,

and emissions performance, is the small-dry fuel-type. This fuel-type and a fuel burn-rate of 3kW (the maximum fuel burn-rate that corresponds to Tier 3 PM_{2.5} emissions) was used to define the operating conditions that correspond to the Kuniokoa's™ optimum performance, or performance under ideal conditions. When these conditions are met the Kuniokoa™ meets both the Alliance's definition of fuel-efficient and clean-burning, resulting in an average performance of Tier 3 with respect to all WBT performance metrics except for low-power specific-consumption, which is Tier 2, and a time-to-boil of 27.6 minutes. This corresponds to a 55% reduction in high-power CO emissions, an 81% reduction in high-power PM_{2.5} emissions, a 91% reduction in the indoor CO emission rate, and a 96% reduction in the indoor PM_{2.5} emission rate when compared to the Kenyan TSF data collected by BAMG. The WBT performance results corresponding to these ideal conditions are shown in Figure 8 and Table 4.

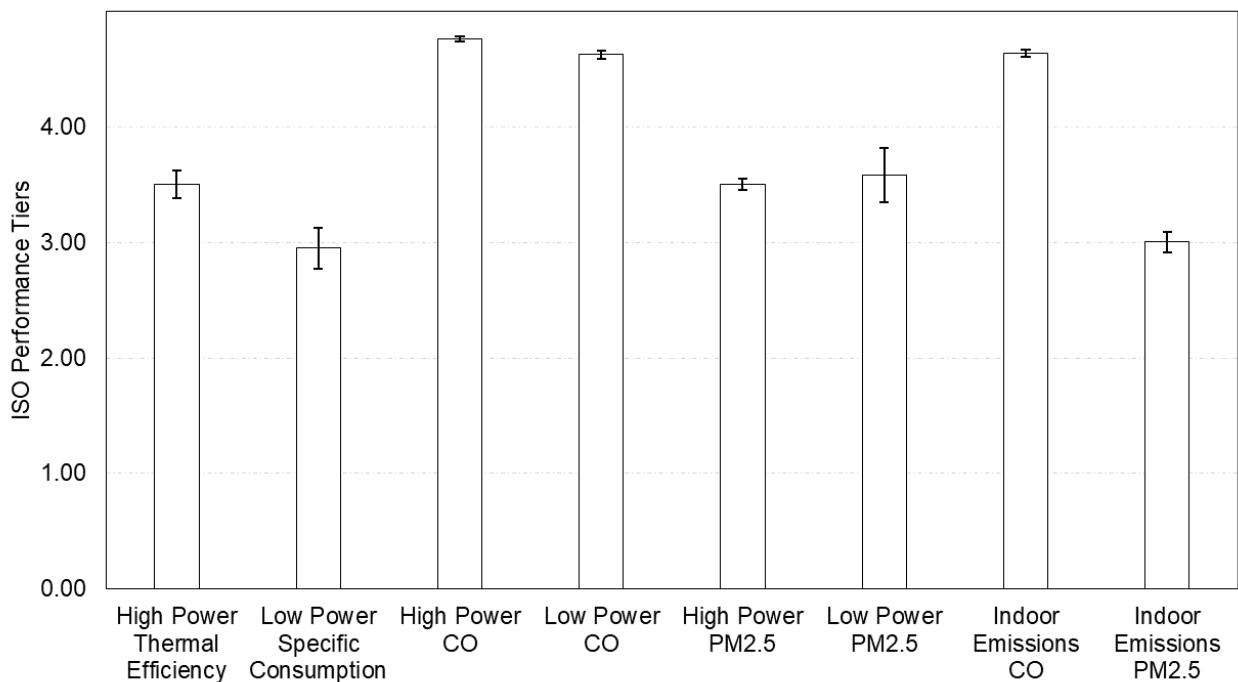


Figure 8: WBT ISO performance tier results when the Kuniokoa™ is used with small-dry wood and a fuel burn-rate of 3kW. Note: error bars represent a 90% CI.

Table 4: KuniokoTM WBT ISO performance values for small-dry wood and a fuel burn-rate of 3kW.

	Firepower (kW)	Time-to-Boil (min)	High Power Thermal- Efficiency (%)	High Power CO (g/MJd)	High Power PM _{2.5} (mg/MJd)
Small- dry fuel (n = 5)	3.2 ± 0.04	28 ± 0.7	40 ± 1.3	1.9 ± 0.2	104 ± 6.7
	Indoor Emissions CO (g/min)	Indoor Emissions PM _{2.5} (mg/min)	Low Power Specific Consumption (MJ/min/L)	Low Power CO (g/min/L)	Low Power PM _{2.5} (mg/min/L)
Small- dry fuel (n = 5)	0.15 ± 0.01	8 ± 0.7	0.03	0.03	1.42 ± 0.14

Note: variabilities represent one standard-deviation.

1.4.4 Summary

BURN Manufacturing’s KuniokoTM is a market leading unvented, natural-draft, side-feed, wood-burning cookstove for East-Africa. The KuniokoTM is a locally manufactured product that provides job and income opportunities for the Kenyan people with a renowned brand and company behind it that is trusted throughout the region for their quality of service and modern cooking products that burn locally available biomass fuels.

The KuniokoTM is the culmination of years of development driven by laboratory research and development completed by the UWCCCL, and extensive field-based user-feedback studies, in-home impact studies, and durability analysis completed by BURN, BDL, and BAMG. This work has culminated in an affordable improved cooking product that is sold for <\$40 USD, has an in-home lifespan of +4 years, and that meets the Alliance’s definition of a fuel-efficient and clean-burning cookstove product under ideal laboratory testing conditions. At the time of launch this

performance placed the Kuniokoa™ as the most fuel-efficient, natural-draft, wood-burning cookstove product on the market and one of the leading natural-draft stoves in terms of emissions reductions.

The Kuniokoa™ does have its limitations, with thermal-efficiency and emissions performance remaining highly-sensitive to operating conditions such as fuel-size, fuel moisture-content, and fuel burn-rates typical of in-home use. The performance sensitivity of the Kuniokoa™ to these factors suggests that the optimum or ideal performance of the Kuniokoa™ is unlikely to be experienced during in-home use unless the user strictly limits burn-rates to below 3kW and uses only small-dry wood. Both operating conditions need to be met to see the reductions in fuel-consumption and emissions during in-home use consistent with the Kuniokoa's™ optimum performance. For field-typical operating conditions the average performance of the Kuniokoa™ is Tier 3 for thermal-efficiency and high-power CO emissions, but Tier 2 or less for all other high-power WBT performance metrics. A summary of the optimum and simulated field-typical high-power WBT performance tiers for the Kuniokoa™ are shown in Table 5.

The Kuniokoa™ remains a market leading clean-burning, fuel-efficient, user-friendly, and affordable wood-burning household cooking product in East-Africa, but there still exists room for improvement. The field-typical performance of the Kuniokoa™ is unlikely to provide a significant decrease in HAP and the limited usability of the stove outside a narrow range of fuel and operating characteristics is likely to contribute to poor adoption rates and/or stove-stacking. Further investigation is needed to understand the cause of these design and performance limitations to develop superior designs that eliminate these issues ensuring the best performance and user-experience during in-home use. Overcoming the Kuniokoa's™ current limitations will encourage increased adoption resulting in the largest impact on HAP and household fuel consumption.

Table 5: High-power WBT tiered performance summary for the Kuniokoa™ comparing optimum performance to simulated field-typical performance.

	Firepower (kW)	Time-to-Boil (min)	High Power Thermal-Efficiency	High Power CO	High Power PM _{2.5}	Indoor Emissions CO	Indoor Emissions PM _{2.5}
Optimum	3.2 ± 0.04	28 ± 0.7	3	4	3	4	3
Simulated Field-Typical	3.8 ± 1	26 ± 8.9	3	3	2	1	1

Note: variabilities represent one standard-deviation.

1.5 PM_{2.5} Emissions

Reducing the PM_{2.5} emissions of natural-draft cookstoves that burn solid biomass fuel is one of the most challenging problems in developing natural-draft cooking technology. One of the principal performance issues of the Kuniokoa™ is the high-variability in PM_{2.5} emissions when subjected to field-typical operating conditions. Without understanding the mechanisms and causes behind the formation of PM_{2.5}, or other incomplete combustion products in stoves like the Kuniokoa™, it is difficult to design a stove that minimizes emissions. The success of any improved cooking technology will largely be judged by its ability to reduce PM_{2.5}.

1.5.1 Design Challenges and Performance Limitations in Reducing PM_{2.5} Emissions of Natural-Draft Rocket-Stoves

Natural-draft solid-fuel combustion systems require special design considerations to burn solid fuels while producing minimal PM_{2.5} emissions, or soot. Solid-fuel combustion relies on thermal-decomposition, or pyrolysis to process raw-fuel into volatile-gases (i.e., pyrolysis products) and char. These pyrolysis products then mix with air and burn, releasing heat. A portion of this heat feeds the endothermic wood pyrolysis reaction. Soot is generated by the pyrolysis of fuel gas under oxygen-deficient conditions. Normally, soot is oxidized when mixed with O₂ under high-temperature conditions. Soot emissions normally result when either (1) the soot-containing gases

are thermally quenched before soot oxidation is complete (e.g., impingement of the flame on the relatively cool cooking pot), or (2) poor mixing prevents the soot from contacting O_2 needed for oxidation. In both cases, achieving adequate mixing within the space provided by the cookstove is critical. The difficulty in designing a natural-draft wood-burning rocket-stove is satisfying the conditions required for complete combustion of $PM_{2.5}$ when limited to natural-draft and when balancing cost, user, and fuel-efficiency requirements.

One of the primary reasons providing a combustion environment that results in minimal $PM_{2.5}$ emissions is difficult is because of the type of flame and flow-characteristics of a natural-draft wood-burning cookstove. Wood-flames are non-premixed diffusion-flames, meaning that the fuel and oxidizer are not mixed prior to reaction relying on molecular-diffusion and mixing due to natural-convection that are typically disturbed laminar flows. The Reynolds-number of the flow through the combustion-chamber and riser of most unvented, natural-draft, rocket-stoves falls within the laminar-to-transitional region ($Re < 2900$), which results in minimal flow-turbulence and/or turbulent kinetic-energy that can be used to aide in mixing fuel and air and reduce the length scales of molecular-diffusion. Therefore, unvented natural-draft rocket-stoves must rely only on the relatively slow mixing mechanisms of molecular-diffusion and natural-convection, which severely limits the ability of oxygen to mix and react with fuel. This results in insufficient residence time in a high-temperature and oxidizer-rich region necessary to completely burn-off soot particles and other products of incomplete combustion.

A direct consequence of the relatively slow characteristics of molecular-diffusion and natural-convective mixing is that, in non-premixed flames, flame-height is strongly dependent on the volumetric flow-rate of fuel and the diffusivity of fuel into air. The ratio of the volumetric flow-rate of fuel and the diffusivity of fuel into air is proportional to flame-height for laminar/transitional non-premixed diffusion-flames, like that are found in natural-draft rocket-stoves. For a constant diameter non-premixed fuel-jet, if diffusivity remains the same and the volumetric flow-rate of fuel

increases, so will flame-height. The inverse is also true, if diffusivity increases, flame-height will decrease, if the volumetric flow-rate of fuel remains constant. This proportionality is described using Roper's definition for laminar/transitional diffusion-flames³⁶, where y_f is flame-height, Q is the volumetric flow-rate of fuel, and D is the diffusivity of fuel into air, given as,

$$y_f \sim \frac{Q}{\pi D} \quad \text{Eq. 1}$$

This behavior is observed in the operation of natural-draft rocket-stoves, as can be seen in the flame-height images observed during an FPS performed on the Kuniokoa™ overlaid on the PM_{2.5} emissions behavior, shown in Figure 9. As fuel burn-rate (i.e., firepower) increases, so does flame-height, apparent from the degree of impingement of the flame on the bottom surface of the pot being used on top of the stove. The impingement of the flame on the bottom surface of the pot, which is a relatively cold surface, acts as a combustion quenching mechanism, dropping the temperature necessary for combustion reactions to proceed through completion, producing incomplete combustion products like PM_{2.5}.³⁵ Looking at the trends of flame-height and PM_{2.5} emissions for the Kuniokoa™ in Figure 9 suggests that flame-height, or fuel burn-rate, and the degree to which the flame impinges on the bottom surface of the pot, or the degree of quenching, is strongly correlated to the PM_{2.5} emission rate of the stove, aligned with the results of a previous study into the impact and relation of flame-height, stove-height, and PM_{2.5} emissions.³⁵

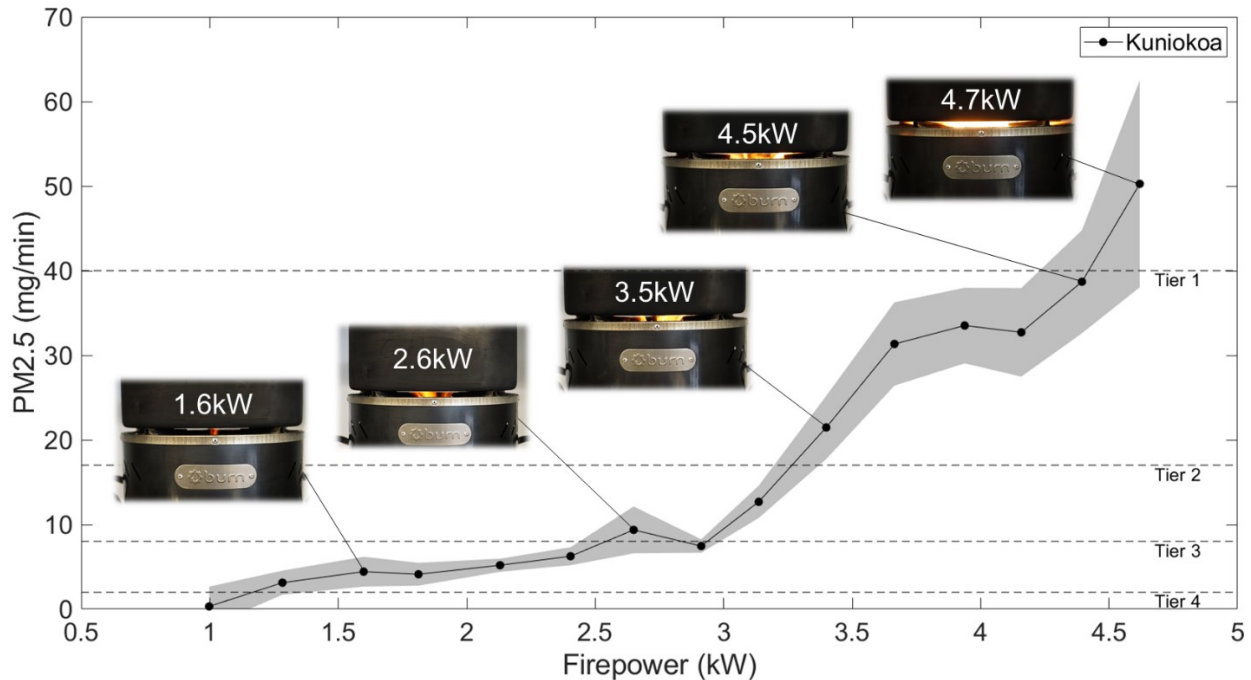


Figure 9: PM_{2.5} emissions and flame-height behavior of the Kuniokoa™, illustrating the correlation between flame-height, or degree of impingement of the flame on the bottom of the pot, and PM_{2.5} emission rate.

When designing a natural-draft, wood-burning cookstove it is important to limit the interaction of the flame with quenching surfaces, like the bottom of a pot, and increase fuel-to-air mixing, to control flame-height, if PM_{2.5} emissions are to remain low. Careful consideration should be made to understand the relationship between fuel burn-rate, diffusivity, flame-height, and PM_{2.5} emissions during the stove development process so that appropriate design strategies can be developed and implemented to provide the necessary conditions for complete combustion, avoiding the emission of harmful incomplete combustion products, like PM_{2.5}.

In the Kuniokoa™ it is likely that the relatively short height of the stove, combined with the wide range of fuel burn-rates the stove is capable of, results in flame-to-pot interaction that significantly increases PM_{2.5} emissions at burn rates higher than 3kW. To solve this issue, design strategies need to be studied, developed, and implemented that effectively control the mechanisms

responsible for non-premixed diffusion flame behavior in laminar/transitional flow and that can be packaged into a product that still meets all other product requirements.

1.5.2 Design Strategies to Reduce $PM_{2.5}$ Emissions

The main design strategies that can and have been used to control $PM_{2.5}$ emissions in natural-draft, wood-burning cookstoves are increasing stove-height to limit flame-to-pot interaction, limiting the volumetric flow-rate of fuel by reducing combustion-chamber size and/or fuel-inlet size, and increasing the flow mixing in the combustion chamber and riser by using static-mixers, natural-draft air injection, and/or chimneys.

Unfortunately, many of these design strategies have trade-offs and any potential reduction in $PM_{2.5}$ emissions seen from the implementation of such strategies can be outweighed by the unintended impacts of these strategies on other aspects of the stoves design and its performance. Increasing stove-height increases material cost and has the potential to reduce thermal-efficiency, making the stove more expensive and reducing fuel-consumption benefits. Reducing combustion-chamber size and/or the fuel-inlet size can severely limit the type or amount of fuel that can be used with the stove, decrease heat-output, increase cooking time, and make the stove more difficult to operate due to the increased sensitivity of sustaining a smaller fire. Static-mixers and natural-draft air injection are limited in their effectiveness due to the relatively high-pressure drops needed to make these types of strategies effective in increasing turbulence and diffusivity when compared to what typical rocket-stove natural-draft flow can provide. Chimneys can help overcome this issue by increasing the pressure-drop through a stove, increasing natural-draft and the effectiveness of static-mixers and natural-draft air injection, but add cost and can limit the utility of a stove.

In many applications of solid-fuel combustion, such as boilers, heaters, and cookstoves, an effective method of increasing turbulent-mixing resulting in a reduction in flame-height and $PM_{2.5}$

emissions is forced secondary (i.e., overfire) air injection, or air injection in the combustion-chamber (or riser) above the fuel-bed that is driven by a fan, blower, or compressed-air source .³⁷⁻

⁴¹ By using a flow-source independent of natural-draft, air injection is no longer limited to the characteristics and limited capabilities inherent of natural-draft air injection techniques. Forced air injection expands the range of jet configurations, air injection locations, air flow-rates, and jet velocities that can be used to optimize the mixing traits within the combustion zone (i.e. combustion-chamber and riser) to reduce unwanted emissions and control flame-height for all fuel-characteristics and/or burn-rates expected during in-home use.

Achieving comprehensive reductions of harmful emissions using secondary air injection requires many design parameters to be optimized. A careful balance needs to be found between the promotion of sufficient turbulent-mixing to reduce harmful emissions, secondary air-flow rates that do not lower combustion zone temperatures excessively (reducing thermal-efficiency and increasing quenching), air injection systems that can be driven by inexpensive fans, and air injection systems that can be manufactured at low cost. Past studies have investigated the optimization of some air injection traits and evaluated their impact on stove performance, but most of these investigations only demonstrate the importance of secondary air injection optimization for advanced biomass cookstoves that utilize processed fuels, with the most popular application being wood-pellet gasifier cookstoves .^{37,38,43,44,47} Only one published study, conducted by a research group at the University of California, Berkeley and Lawrence Berkeley National Laboratory, investigated the optimization of secondary air injection in a side-feed wood-burning rocket-stove ⁴⁸, acting as the sole source of guidance for air injection design optimization for cookstoves that burn unprocessed fuel (i.e., intermediate solutions). The study found that cookstove PM_{2.5} emissions are highly sensitive to secondary air injection flow-rate and velocity with the most significant reductions in PM_{2.5} emissions seen for low flow-rate and high velocity jet configurations. ⁴⁸

Despite the findings demonstrated in previous studies, secondary air injection optimization remains dependent on optimizing numerous variables that can require complex and time intensive experimental investigation to determine optimum design characteristics. These studies also do not provide guidance on how to optimize air injection within the context of cookstove design parameters like fan-performance, power-consumption, and total system cost requirements. A comprehensive air injection optimization design tool that defines the relationship between effective turbulent-mixing, stove performance (thermal-efficiency and emissions behavior), jet-characteristics (size, number, flow-rate, pressure, velocity, etc.), fan-performance (pressure, flow-rate, power, cost), and total system cost is not readily available. Such a design tool could help improve the capabilities of stove designers to produce effective and inexpensive air injection systems that can be used to overcome the performance limitations of natural-draft and existing forced-draft intermediate and advanced cookstove technologies that are unable to effectively reduce harmful emissions during in-home use.

1.7 Objectives

The objectives of the work reported in this thesis are to develop and evaluate a design tool that guides the optimization and design of fan-driven secondary air injection systems for wood-burning cookstoves that are effective in reducing $PM_{2.5}$ emissions during in-home use and that are within the context of a cookstove project's design parameters and cost targets. Specific objectives include evaluating the application of known jet-in-cross flow mixedness optimization parameters to the optimization of flow mixing in the combustion-chamber and riser of a cookstove to effectively control flame-height behavior and emissions; constructing an analytical model that calculates optimum secondary air jet configurations within a range of user-defined fan design parameters (fan flow-rate and pressure); evaluating the impact of secondary air jet characteristics on cookstove flow-characteristics and performance; and applying the analytical model and lessons

learned to the development of a solar-powered fan-driven secondary air injection system for the Kuniokoa™ to improve in-home emissions performance.

1.8 Summary

3 billion people still rely on open-fires and/or traditional cookstoves that burn unprocessed biomass fuels to cook and provide heat for their homes. These traditional cooking practices require large amounts of fuel and emit high-levels of harmful pollutants that have long lasting health, social, economic, and environmental impacts. The emissions from traditional cooking practices is the leading cause of HAP, which is the world's single greatest environmental health risk to the human population, causing 3.8 million premature deaths each year and sickening many more. In 2010, a global initiative was kickstarted to provide households around the globe with clean and efficient cooking technology and/or fuels. Since the launch of this initiative, there is an estimated 116 million improved cooking products being used by households that previously had no other viable household energy option to meet their cooking and/or heating needs, beyond an open-fire or traditional cookstove. Progress is being made in developing clean and efficient cooking technology and fuels, but many improved cooking solutions on the market suffer from design and performance limitations that are not thoroughly investigated, difficult to overcome, and that have contributed to the limited impacts and unsuccessful implementations of many previous technologies. There still exists a need for innovative cookstove design strategies to help improve current technology and guide the development of future cookstoves and/or fuels that are more effective in reducing HAP, reducing household fuel-consumption, and meeting household cooking and/or heating needs; all contributing to the successful adoption of clean-burning and fuel-efficient cooking products that have the potential to save lives, save the environment, and improve the livelihoods of billions of people around the globe.

CHAPTER 2: AN ANALYTICAL MODEL FOR SECONDARY AIR INJECTION OPTIMIZATION IN A SIDE-FEED WOOD-BURNING COOKSTOVE

This chapter details the analytical method developed for the optimization of secondary air injection in side-feed wood-burning cookstoves to reduce flame-height and $PM_{2.5}$ emissions. We discuss the extension of jet in cross-flow mixedness optimization parameters maximum radial jet penetration length, Y_{max} , and jet-to-cross flow momentum-flux ratio, J , originally developed during early investigations into the impact of air jet characteristics on cross-flow mixedness for gas turbine and furnace applications, to secondary air injection in the riser of a side-feed wood-burning cookstove. The functionality of the analytical model/design tool and the methods used to calculate secondary air jet configurations that require minimum jet injection energies, E_j , to achieve optimum cross-flow mixedness, controlling the characteristic flame-height and $PM_{2.5}$ emissions behavior of a cookstove design, are detailed. We also present the methods used to determine jet configurations that are within the context of fan-driven systems for side-feed wood-burning cookstoves with specified fan design requirements (e.g., type, size, power, etc.) that define fan flow-rate and pressure limitations, ensuring that all model predicted jet configurations can be driven by fans meeting these requirements and within these performance limitations.

2.1 Analytical Model Description

The analytical model/design tool presented optimizes the mixing characteristics of a single-row of equal-diameter circular air jets located symmetrically around the perimeter of a cylindrical cross-flow (i.e., the cylindrical riser of a cookstove), as illustrated in Figure 10. The behavior of jets in cross-flow and the impact of jet and cross-flow characteristics on cross-flow mixedness has been thoroughly characterized by earlier work on secondary air injection into cylindrical furnace combustion chambers, gas turbine combustors, and gas turbine dilution zones. A detailed overview of previous investigations and the design tools that were developed from these

investigations, some of which have been incorporated into the analytical model presented here, can be found in A. H. Lefebvre and D. R. Ballal, and in J. Vanormelingen and E. Van Den Bulck.^{49,52}

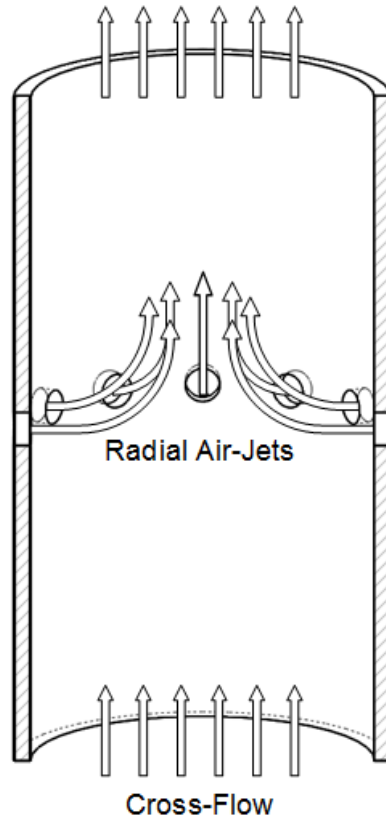


Figure 10: Radial jets in cross-flow diagram.

Previous investigations have focused on defining jet characteristics that result in optimum cross-flow mixedness defined by a maximum increase in cross-flow mixedness and/or temperature uniformity in a minimum downstream distance, while minimizing jet injection energy, E_j . Past work has shown that in systems using a single-row of jets in a cylindrical cross-flow, optimum cross-flow mixedness corresponds to maximum radial jet penetration lengths (i.e., the maximum radial distance jets penetrate into the cross-flow, or riser) that approach the centerline of the cross-flow in the range of $Y_{max} = [0.4D_{xf} \dots 0.5D_{xf}]$ ^{49,52} and have suggested that an increase in the number of jets results in an increase in the quality of mixing due to an increase in localized mixing

regions .⁵² Jets that penetrate the cross-flow within the range of Y_{max} have also been found to result in the minimum jet injection energy (likely corresponding to the lowest operational cost) required to achieve the most beneficial cross-flow mixing patterns to improve fuel and air mixing and reduce emissions.⁵² The model uses Y_{max} to predict secondary air jet configurations that provide optimum cross-flow mixing characteristics for a stove design and user-defined project parameters. These jet configurations are likely to result in a maximum reduction in PM_{2.5} emissions and minimal negative impacts on thermal-efficiency.

The user defined design parameters (i.e., independent variables) necessary for the model to predict optimum jet configurations within the context of a cookstove design project are listed in Table 6. The variables are a mixture of fan design parameters, cookstove dimensions, and fuel and riser-flow properties. For the model to work most efficiently stove designers should have previously established the minimum/maximum number and diameter of jets (n_{min} , n_{max} , D_{min} , D_{max}) that will work with their design, or within their manufacturing techniques. Stove designers should also establish the maximum secondary-air volumetric flow-rate, Q_{max} , the stove-design can handle without detrimental effects on stove performance or utility; this will guide fan selection and act as the model's upper-limit for jet flow-rate. Finally, stove designers should have defined the maximum static-pressure, ΔP_{max} , that fans within their type, size, and power requirements can deliver. This information is typically provided in fan specification sheets. Knowing these parameters will ensure that the model outputs optimum jet configurations that are within the context and design parameters of a specific cookstove design project.

Table 6: Secondary air jet optimization analytical model user-defined design parameters and system characteristics (i.e., independent variables).

User-defined design parameters and system characteristics	
Number of jets	$\mathbf{n}_j = [n_{min} \dots n_{max}]$
Jet diameter	$\mathbf{D}_j = [D_{min} \dots D_{max}]$
Fan volumetric flow-rate	$\mathbf{Q} = [Q_{min} \dots Q_{max}]$
Max fan static pressure	ΔP_{max}
System head-loss	ΔH_L
Jet Discharge Coefficient	C_d
Cross-flow diameter	D_{xf}
Cross-flow temperature	T_{xf}
Cross-flow pressure	P_{xf}
Secondary air pre-heat temperature	T_j
Secondary air duct (i.e., plenum) pressure	P_j
Stove firepower	FP
Fuel species concentrations (i.e., ultimate analysis values)	$C(x), H(y), O(z)$
Fuel lower heating value	LHV
Excess-air	$(\varphi - 1)$

The model uses the design parameters listed in Table 6 to calculate the dependent variable optimum jet-to-cross flow momentum flux ratio, J , for user-defined values of number of jets, \mathbf{n}_j , system flow-rates, \mathbf{Q} , and cookstove system characteristics that are used to characterize the flow through the riser of the cookstove (i.e., the cross-flow). The optimum jet-to-cross flow momentum flux ratio is then used to calculate the dependent variable optimum jet diameter, \mathbf{d}_j , for corresponding values of \mathbf{n}_j and \mathbf{Q} that satisfy Y_{max} , fully defining the jet configurations with optimum mixing characteristics for each user-defined value of n_j and Q . The model then selects

all configurations with the maximum number of jets for each user-defined Q and removes any configurations that do not satisfy the user-defined design parameters D_j and ΔP_{max} . The optimum configurations are defined by jet configurations that have maximum radial jet penetrations lengths $Y_{max} = [0.4D_{xf} \dots 0.5D_{xf}]$, have a maximum number of jets, and that fall within the user-defined parameters n_j , Q , D_j , ΔP_{max} .

An overview of the model's calculations and optimization methods are shown below. For detailed information on each user-defined variable and model derived variable, optimization methods, assumptions made, relevant calculations, and general information with regards to fan-driven air injection system design the reader is directed to subsequent sections of this chapter.

The model begins calculating optimum jet configurations by first calculating the jet-to-cross flow momentum flux ratios, J , that correspond to values in the range defined by Y_{max} , for all user-defined n_j and Q using Equation 2⁵², where K is the ratio of total jet mass flow-rate and total cross-flow mass flow-rate for all values of Q .

$$J = \left[0.8 \frac{Y_{max}}{D_{xf}} \sqrt{n_j} \left(\frac{\rho_j}{\rho_{xf}} \right)^{1/4} \frac{1+K}{\sqrt{K}} \right]^4, \quad K = \frac{\rho_j Q}{\dot{m}_{xf}} \quad \text{Eq. 2}$$

Once J is defined, the jet diameters, d_j , corresponding to J , n_j , and Q , can be calculated using Equation 3, where V_j is jet velocity. Any jet configurations with jet diameters that fall outside the range of the user-defined D_j are removed.

$$d_j = \sqrt{\frac{4Q}{\pi n_j V_j}} \quad \text{Eq. 3}$$

The system pressure-drop, or the system static-pressure, Δp_{static} , can then be predicted for corresponding values of n_j , d_j , and Q , using Equation 4. Any jet configurations with a predicted system static-pressure greater than the user-defined ΔP_{max} are removed.

$$\Delta p_{static} = \frac{1}{2} Q^2 \rho_j \left(1 - \left(\frac{\sqrt{n_j} d_j}{D_{xf}} \right)^8 \right) \left(\frac{4}{n_j \pi C_d d_j^2} \right)^2 + \Delta H_L \quad \text{Eq. 4}$$

In general, at this point there will be multiple jet configurations for each value of Q that satisfy the cross-flow mixedness design parameter, Y_{max} , and the user-defined design parameters n_j , D_j , Q , and ΔP_{max} . The model finds the optimum jet configurations (n_j, d_j) , among all the configurations calculated for each value of Q , by finding the configurations that have the maximum number of jets, which a previous study suggests will increase the uniformity of the cross-flow mixing characteristics, resulting in a higher quality of mixing.⁵² If there are multiple jet configurations sharing this same maximum value for a single value of Q the model takes the mean of the jet parameters for these configurations and defines the resulting configuration as the optimum. The resulting matrix of jet configurations represents the optimum configurations for maximizing cross-flow mixedness that are possible within the user-defined design parameters and system characteristics listed in Table 6. In general, these jet configurations will have the highest system static-pressures among all the configurations calculated for each value of Q , so to provide additional design flexibility, with respect to fan static-pressure requirements, all the other jet configurations are provided in the final model outputs. It should be noted that although these configurations may have decreased fan static-pressure requirements compared to the optimum jet configurations, their mixing characteristics may be less-ideal than the predicted optimum configurations, since they do not satisfy all the mixedness design parameters, so when possible, only the optimum configurations should be used.

This model was used in the development of the Kuniokoa-Turbo™ detailed in Chapter 5 and an example of the optimum jet configurations predicted by the model, within the projects specific design parameters and system characteristics, are shown in Table 7.

Table 7: Example analytical model optimum jet configuration outputs.

Optimum Jet Configurations											
Q (cfm)	1	1.2	1.4	1.6	1.8	2	2.2	2.4	2.6	2.8	3
n_j	6	8	8	8	10	10	10	12	12	12	12
d_j (mm)	3.4	3.1	3.5	3.8	3.4	3.7	3.9	3.6	3.8	3.9	4.1
V_j (m/s)	8.7	9.3	8.8	8.5	9.3	9	8.8	9.4	9.1	9.1	9.1
J	134	151	137	129	151	142	136	156	146	145	145.16
Δp_{static} (in-H ₂ O)	0.50	0.56	0.51	0.48	0.57	0.53	0.51	0.58	0.55	0.54	0.54
Y_{max}/D_{xf}	0.42	0.40	0.41	0.42	0.41	0.41	0.42	0.40	0.40	0.41	0.41

In addition to predicting optimum jet configurations, the model can determine if a specific fan can drive a secondary air injection system that uses any of the optimum configurations. If the fan performance curves (fan volumetric flow-rate vs. fan static-pressure) of various fans that are being considered for a specific cookstove design project are known, these can be appended to the model. With the fan performance curves defined, the model then compares the Q and Δp_{static} values for each optimum configuration to the fan performance curves to determine if the system operating point ($Q, \Delta p_{static}$) for a given configuration corresponds to a point on any of the fan performance curves. If it is found that a fan can deliver the volumetric flow-rate at the static-pressure corresponding to Q and Δp_{static} , respectively, then the model appends a list of the user-defined fans that can be used to operate a secondary air injection system using this particular optimum jet configuration.

This only works for secondary air injection systems that are perfectly sealed, meaning all the flow produced by the fan exits the system through the secondary air jets and none is lost through system leakage. If the system is not perfectly sealed the total system leakage area needs to be

known in order to approximate how much of the fans flow is lost through system leakage and the impact this leakage has on the system static-pressure, or system impedance. A change in system impedance will impact the system operating point necessary to provide the appropriate flow through the secondary air jets to achieve the optimum jet mixing characteristics calculated by the model. If performance information on specific fan models that are within a projects size, power, and cost requirements are unknown the Q and Δp_{static} values of the optimum jet configurations can be provided to fan manufacturers to help guide fan selection.

It should be emphasized that the model does not provide guidance in determining the optimum location of secondary air injection within the riser of the cookstove or in determining the jet flow-rate that best works with a stove design. The model only predicts the optimum number and diameter of jets for the user-defined flow-rates, Q , that will result in optimum cross-flow mixing and accomplish this with the least amount of operational energy. Cookstove designers still must rely on experimental data to determine what secondary air injection flow-rates will result in minimal impacts on thermal-efficiency and other important cookstove performance metrics. In addition, the cross-flow mixedness optimization parameters are only intended for application to the optimization of a single-row of equal-diameter circular air jets located symmetrically around the perimeter of a cylindrical cross-flow. Furthermore, the model only applies to jets that are perpendicular to the cross-flow, or in other words not angled upstream, downstream, or in a swirl pattern. Previous studies have investigated the impact of these additional jet design parameters and more information about the impact of these parameters on cross-flow mixedness can be found here ^{49,52}.

2.2 Cross-Flow Parameters

The optimization parameters used in the analytical model require the geometry, mass-flow, and density of the cross-flow, or flow through the riser of the stove to be known to a good approximation in order to calculate optimum jet configurations. This section details the required

user-defined cross-flow parameters and method for approximating the flow through the riser of the cookstove for secondary air jet optimization purposes.

The analytical model approximates the cross-flow, or the reacting flow of combustion gases through the riser of the cookstove, as a non-reacting flow of air. The cross-flow cross-sectional area, temperature, density, mass-flow rate, and velocity are needed to fully define the cross-flow. The cross-sectional area of a cylindrical riser can be calculated using Equation 5, where D_{xf} is the diameter of the riser and A_{xf} is the cross-sectional area of the riser.

$$A_{xf} = \frac{\pi}{4} D_{xf}^2 \quad \text{Eq. 5}$$

The temperature of the cross-flow can be measured and approximated experimentally using a thermocouple. A previous study has shown that rocket-stove riser temperatures typically fall between the range of approximately 500-950K depending on fuel burn-rate, or firepower⁵⁰. Once the cross-flow temperature is known the density can be calculated using Equation 6, assuming the cross-flow is air and can be represented as an ideal-gas, where P_{xf} is the mean cross-flow pressure (approximated as 1 atm for most cookstoves), R_{xf} is the ideal-gas constant of air, T_{xf} is the mean cross-flow temperature, and ρ_{xf} is the cross-flow density.

$$\rho_{xf} = \frac{P_{xf}}{R_{xf}T_{xf}} \quad \text{Eq. 6}$$

The cross-flow mass flow-rate is calculated by taking the sum of the mass-flow rate of fuel, the stoichiometric air mass-flow rate, and the mass-flow rate of excess-air. The mass-flow rate of fuel is chosen to correspond to a burn-rate within the range of firepower's the stove is designed for, or that is expected during in-home use. Equation 7 can be used to convert firepower (kW) to mass-flow (kg – fuel/s) using the lower heating value (LHV) of wood (19,314 kJ/kg for Douglas Fir²⁷), where FP is firepower and \dot{m}_f is the mass-flow rate of fuel.

$$\dot{m}_f = \frac{FP}{LHV} \quad \text{Eq. 7}$$

The stoichiometric air mass-flow rate is calculated from the stoichiometric air-to-fuel equivalence ratio and the mass-flow rate of fuel from Equation 7. The stoichiometric air-to-fuel equivalence ratio can be calculated using Equation 8, where x , y , and z are the concentrations of carbon, hydrogen, and oxygen in the fuel species, respectively, and θ is the stoichiometric air-to-fuel ratio in kilograms of air per kilograms of fuel.

$$\theta = \frac{138.25\left(x + \frac{y}{4} - \frac{z}{2}\right)}{12.01x + 1.01y + 15.99z} \quad \text{Eq. 8}$$

The fuel species used in the development of this model and in the experimental evaluation and validation of the model was Douglas Fir and the results from an ultimate analysis of Douglas Fir performed by Kobayashi et al. is shown in Table 8.⁵¹

Table 8: Ultimate analysis of Douglas Fir from Kobayashi et al.

Species	Moles per gram of wood
C (x)	0.0419
H (y)	0.0635
O (z)	0.0269

Once θ is known Equation 9 can be used to calculate the stoichiometric air mass-flow rate, where \dot{m}_f is the mass flow-rate of fuel from Equation 7 and \dot{m}_{sa} is the stoichiometric air mass-flow-rate.

$$\dot{m}_{sa} = \theta * \dot{m}_f \quad \text{Eq. 9}$$

A previous study found the percentage of excess-air in a typical rocket-stove to vary significantly over a wide range of firepower's and for different fueling characteristics (i.e., how much fuel is used at one time), ranging from 100-1100% of the stoichiometric air requirement at firepower's between 2-6kW.⁵⁰ It is important to consider the mass flow-rate of excess air when calculating the total cross-flow mass flow-rate. The mass-flow rate of excess-air can be calculated using

Equation 10, where $(\varphi - 1)$ is excess-air, \dot{m}_{sa} is the stoichiometric air mass-flow rate from Equation 9, and \dot{m}_{ea} is the mass flow-rate of excess-air.

$$\dot{m}_{ea} = (\varphi - 1) \dot{m}_{sa} \quad \text{Eq. 10}$$

Finally, the total cross-flow mass-flow rate can be calculated by summing the mass flow-rate of fuel, stoichiometric air mass flow-rate, and the mass flow-rate of excess-air, shown in Equation 11, where \dot{m}_{xf} is the cross-flow mass flow-rate.

$$\dot{m}_{xf} = \dot{m}_f + \dot{m}_{sa} + \dot{m}_{ea} \quad \text{Eq. 11}$$

Using the cross-flow cross-sectional area calculated in Equation 5, the density calculated in Equation 6, and the total mass flow-rate calculated in Equation 11 the cross-flow velocity can be calculated using Equation 12, where V_{xf} is the cross-flow velocity.

$$V_{xf} = \frac{\dot{m}_{xf}}{\rho_{xf} A_{xf}} \quad \text{Eq. 12}$$

With the calculation of cross-flow velocity the cross-flow characterization parameters required by the model are fully defined. It should be emphasized that any change in firepower, FP , and fueling characteristics will likely change the amount of excess-air present, $(\varphi - 1)$, and the cross-flow temperature, T_{xf} , which will impact the cross-flow characteristics changing the models optimum jet configurations predictions, so care should be taken in determining appropriate values of excess-air and cross-flow temperature if using the model to calculate optimum jet configurations at different firepower's and/or for different fueling characteristics.

2.3 Jet Parameters

The analytical model requires the calculation of a few key jet parameters involved in the optimization of cross-flow mixedness using jet penetration length and jet-to-cross flow momentum-flux ratio as optimization parameters. These parameters are also required in

calculating the characteristic system impedance needed to evaluate if jet configurations satisfy the general fan design parameters (Q , ΔP_{max}) and/or if user-defined fans can be used to drive secondary air injection systems that use the optimum jet configurations the model predicts.

The number of jets, n_j , is an independent variable defined by the user and is a vector spanning the range between the user-defined design parameters n_{min} and n_{max} . The total jet flow-rate, or total system volumetric flow-rate, Q , is also a user-defined parameter representing a vector of values spanning the range between the user-defined design parameters Q_{min} and Q_{max} .

The jet injection preheat temperature, T_j , and initial pressure, or plenum (i.e., duct) pressure, P_j , are needed to calculate the initial jet density, ρ_j , and can either be measured experimentally or estimated, but in most cases setting $T_j = 300K$ and $P_j = 1 atm$ is sufficient. With T_j and P_j defined the initial jet density can be calculated using Equation 13, where R_j is the ideal-gas constant of air.

$$\rho_j = \frac{P_j}{R_j T_j} \quad \text{Eq. 13}$$

Using the initial jet density, the total jet mass flow-rate, \dot{m}_j , can be calculated for all values of Q using Equation 14.

$$\dot{m}_j = \rho_j * Q \quad \text{Eq. 14}$$

Since only circular air jets are considered in the model, the area of a single jet, a_j , can be calculated using Equation 15, where d_j is jet diameter.

$$a_j = \frac{\pi}{4} d_j^2 \quad \text{Eq. 15}$$

The total jet area, A_j , or the sum of the area of all jets for all values of n_j , can be calculated using Equation 16.

$$A_j = n_j * a_j \quad \text{Eq. 16}$$

Finally, jet velocity, V_j , can be calculated using Equation 17, assuming Q is split evenly between all jets.

$$V_j = \frac{Q}{A_j} = \frac{\dot{m}_j}{\rho_j A_j} \quad \text{Eq. 17}$$

Jet diameter, d_j , is dependent on the cross-flow mixedness optimization parameters, so the calculation of this remaining jet parameter is discussed in the next section.

2.4 Cross-Flow Mixedness Optimization Parameters

A previous study showed that maximum radial jet penetration length, Y_{max} , or the maximum radial distance a jet penetrates into the cross-flow, and the dimensionless parameter of jet-to-cross flow momentum flux ratio, J , were the dominant jet characteristics influencing cross-flow mixedness in fully-developed turbulent flow through cylindrical combustion chambers with radial overfire air injection.⁵² This study and other previous studies of jet in cross-flow mixing characteristics have suggested that jets that have trajectories that approach the center-line of the cross-flow, corresponding to a maximum jet penetration length within the range of $Y_{max} = [0.4D_{xf} \dots 0.5D_{xf}]$, require a minimum amount of jet injection energy to achieve optimum cross-flow mixedness, or temperature uniformity, at a minimum downstream distance.^{49,52} A previous study has also shown that, in general, as you increase the number of jets, mixing characteristics tend to be more uniform due to an increase in localized mixing regions, which can provide additional advantages in increasing the quality of cross-flow mixedness.⁵²

These cross-flow mixedness design parameters are applied to the optimization of the mixedness of reacting laminar/transitional flow through the riser of a side-feed wood-burning cookstove for the purposes of reducing flame-height and PM_{2.5} emissions. Since the cross-flow mixedness design parameters were originally developed and validated only for fully-developed turbulent cross-flows, the validity of the cross-flow mixedness design parameters (Y_{max}, J), applied to optimizing secondary air injection for laminar/transitional flow in the riser of wood-burning cookstoves to reduce flame-height and PM_{2.5} emissions were investigated; the results to this investigation are detailed in Chapter 4.

J. Vanormelingen and E. Van Den Bulck found that jet configurations that require the least amount of jet injection energy, E_j (representative of the operational cost of a jet configuration, defined by Equation 18), to provide an optimum increase in cross-flow mixedness correspond to jet configurations with a predicted maximum jet penetration length of $Y_{max} = [0.4D_{xf} \dots 0.5D_{xf}]$, where Y_{max} is calculated using Sridhara's equation for calculating the maximum penetration length of multiple circular jets in a cylindrical cross-flow, shown in Equation 19 .⁵²

$$E_j = \frac{\rho_j V_j^2}{2} \quad \text{Eq. 18}$$

$$\frac{Y_{max}}{D_{xf}} = 1.25\sqrt{J} \frac{\dot{m}_{xf}}{\dot{m}_{xf} + \dot{m}_j} \quad \text{Eq. 19}$$

They discovered this optimization parameter by comparing cross-flow mixedness, which they defined as the mixedness variable U_s , for a constant total jet mass flow-rate, but different values of the momentum flux-ratio (defined by Equation 20), at a cross-section of the cross-flow one radius downstream of the plane where the jets are initially injected into the cross-flow. What they found is that cross-flow mixedness increases to an optimum point that corresponds to $Y_{max} = [0.4D_{xf} \dots 0.5D_{xf}]$, once $Y_{max} > 0.5D_{xf}$, or when the jets penetrate past the mid-line of the cross-flow (i.e., over penetrate), cross-flow mixedness becomes worse, with mixedness only

increasing once again if the momentum-flux ratio is increased by a large amount, resulting in higher jet injection energies, corresponding to a much higher operational cost than the original optimum cross-flow mixedness point defined by jets that satisfy $Y_{max} = [0.4D_{xf} \dots 0.5D_{xf}]$. This behavior is demonstrated in J. Vanormelingen and E. Van Den Bulck's plot of the results from this investigation shown in Figure 11.

$$J = \frac{\rho_j V_j^2}{\rho_{xf} V_{xf}^2} \quad \text{Eq. 20}$$

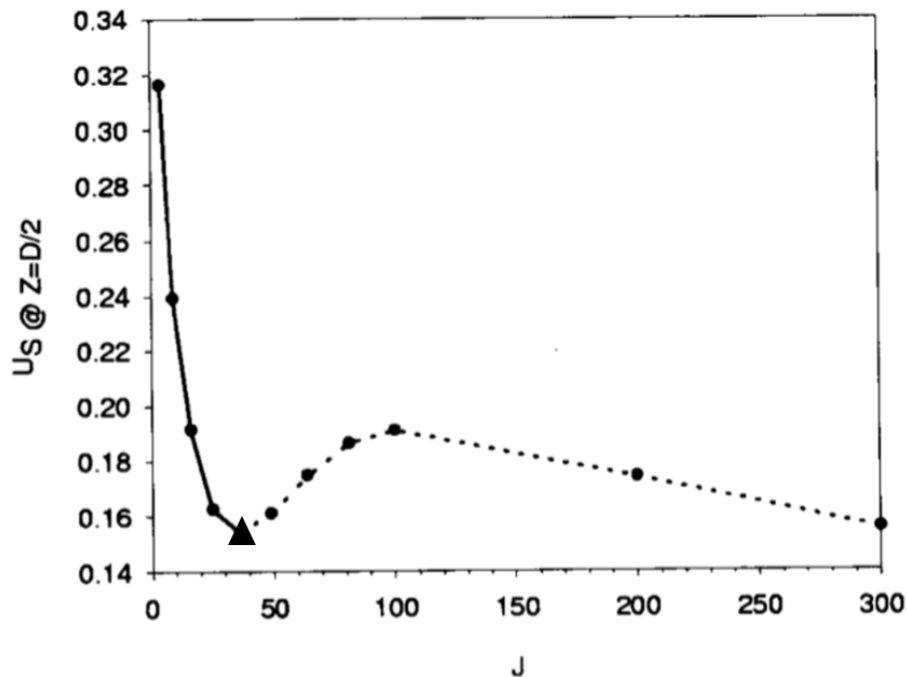


Figure 11: Momentum flux ratio vs. cross-flow mixedness, U_s , at a plane one radius downstream from the jet injection plane, taken from "Optimization of Overfire Air Systems of Cylindrical Combustion Chambers".⁵² As U_s decreases cross-flow mixedness increases. The triangular data point represents the optimum point.

Using Equation 19, Equation 21 defining jet diameter, d_j , and $Y_{max} = [0.4D_{xf} \dots 0.5D_{xf}]$ the momentum flux ratio corresponding to the optimum cross-flow mixedness point, found by Vanormelingen and E. Van Den Bulck, can be predicted for any value of n_j and $\dot{m}_j \sim Q$ using Equation 22, where K is the ratio of total jet mass flow-rate and total cross-flow mass flow-rate.

$$d_j = \left[\frac{KD_{xf}^2}{n_j} \sqrt{\frac{\rho_{xf}}{J\rho_j}} \right]^{1/2}, \quad K = \frac{\dot{m}_j}{\dot{m}_{xf}} \quad \text{Eq. 21}$$

$$J = \left[0.8 \frac{Y_{max}}{D_{xf}} \sqrt{n_j} \left(\frac{\rho_j}{\rho_{xf}} \right)^{1/4} \frac{1+K}{\sqrt{K}} \right]^4 \quad \text{Eq. 22}$$

This provides the basis for the jet optimization calculations used by the model. Once the optimum J is known for all n_j and Q values specified by the user, the corresponding jet velocities, V_j , and jet diameters, d_j , can be calculated using Equation 23 and Equation 24, respectively.

$$V_j = \sqrt{\frac{\rho_{xf} J V_{xf}^2}{\rho_j}} \quad \text{Eq. 23}$$

$$d_j = \sqrt{\frac{4Q}{\pi n_j V_j}} \quad \text{Eq. 24}$$

With jet velocity and jet diameter defined for the corresponding optimum momentum flux values for all n_j and Q values specified by the user, all the necessary optimum jet configuration parameters are defined, and the model can proceed to determine the jet configurations that satisfy the remaining user-defined design parameters and system characteristics.

2.5 System Impedance

System impedance, or resistance, when applied to air injection systems is the characteristic relationship between the volumetric flow through a system and the pressure response, or total pressure-drop between a systems inlet and outlet. In general, as system flow-rate increases so

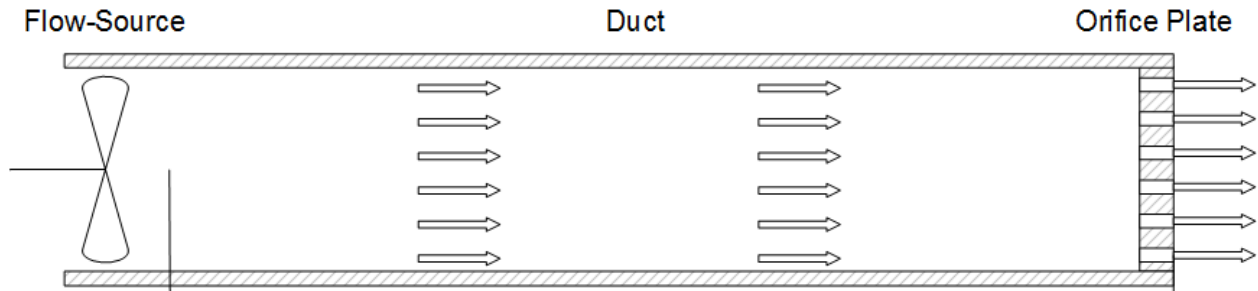


Figure 12: Air-injection system diagram.

does the pressure-drop between the system inlet and outlet, but the degree to which the pressure-drop increases for a given increase in flow-rate depends on the number and size of air jets used in an air injection system. For the purposes of secondary air injection optimization in an unvented side-feed wood-burning cookstove, the system can be described as a constant area duct, with the inlet being a flow-source (i.e., fan/blower/compressed-air source), and the outlet being an orifice plate, i.e., a plate with a matrix of equally-spaced and equal-sized holes/jets, illustrated in Figure 12.

If the flow through this system is assumed to be steady-flow, laminar, and incompressible, and if it is assumed that the orifice plate is the only component in the system restricting the system cross-sectional area of the flow path and all the flow produced by the flow-source passes through the holes in the orifice plate, the Bernoulli equation (Equation 25) can be used to estimate the total pressure-drop through the system, or across the orifice-plate, for a given flow-rate. The system pressure-drop, Δp_{static} , represented by the difference in static-pressure between the flow-source outlet and duct inlet interface (point 1 in Figure 12) and the outlet side of the orifice plate (point 2 in Figure 12) is mainly dependent on the system volumetric flow-rate, Q , fluid-density, ρ_j , the inlet area (total area of orifice plate), A_1 , the outlet area (total area of all jets), A_j or A_2 , the outlet-to-inlet area ratio, $\beta = \frac{A_2}{A_1}$, an orifice discharge-coefficient, C_d , and a head-loss term, ΔH_L .

$$\Delta p_{static} = \frac{1}{2} Q^2 \rho_j (1 - \beta^4) \left(\frac{1}{C_d A_2} \right)^2 + \Delta H_L \quad \text{Eq. 25}$$

For jet systems that use cylindrical risers and circular jets, Equation 25 can be rewritten as Equation 26, where D_{xf} is the diameter of the duct, d_j is the jet diameter, and n_j is the number of jets.

$$\Delta p_{static} = \frac{1}{2} Q^2 \rho_j \left(1 - \left(\frac{\sqrt{n_j} d_j}{D_{xf}} \right)^8 \right) \left(\frac{4}{n \pi C_d d_j^2} \right)^2 + \Delta H_L \quad \text{Eq. 26}$$

Using Equation 26 the system impedance curve, or the relationship between system flow-rate and static-pressure for circular duct and jet systems can be estimated for any jet configuration if an appropriate discharge-coefficient and head-loss term is used and if the system flow is to a good approximation steady, laminar, and incompressible. The analytical model uses Equation 26 to calculate the system static-pressure, or pressure drop across an orifice plate having jet configurations equal to the jet configurations calculated by the model.

If the design of the air injection system is expected to have significant head-loss and/or has other major flow restrictions other than the orifice plate, the cumulative effects of these factors should be well understood and compensated for appropriately when using Equation 26 to calculate the system pressure-drop in order to obtain the most accurate prediction of system impedance for jet optimization purposes.

System impedance can also be measured experimentally using a static-pressure tap placed near the inlet of a system (point 1 in Figure 12) and differential pressure gauge. The system flow-rate is then varied and the corresponding static-pressure measurement is recorded to produce a system impedance curve. This method was used during the jet momentum-flux ratio investigation detailed in Chapter 4 to experimentally validate Equation 26 and its application to secondary air injection system design.

2.6 Fan Performance Curve and System Operating Point

In order to get the most functionality out of the analytical model, it is important to understand the performance characteristics of the fans being considered to deliver flow, or that fall within a projects fan size, power, and cost requirements. The model uses user-defined fan performance curves to determine what optimum jet configurations can be driven by certain fans being

considered. Without the input of user-defined fan performance curves the model outputs all optimum jet configurations that fall within the general fan design parameters defined by the user; Q , ΔP_{max} . In either case, it is important to understand what a fan performance curve is because it is one of the most commonly used metrics to report and compare fan/blower performance.

A fan performance curve is the characteristic relationship between fan static, dynamic, and/or total pressure and volumetric flow-rate for a set fan input voltage (if the fan is driven by an electric motor) or a set RPM. For electric motor driven fans, performance curves corresponding to either the maximum rated input-voltage or nominal input-voltage are usually provided by the fan manufacturer to help guide buyers in determining if a fan will work for their specific application, meeting their pressure and flow requirements. These performance curves are determined using a fan testing apparatus, built in accordance to ANSI/AMCA Standard 210-99, that measures fan pressure and volumetric flow-rate for different system pressures, or impedances, varied by an adjustable damper or venturi of known characteristics. A fan performance curve, typical of a small electronic computer fan, is shown in Figure 13 illustrating the relationship between fan static-pressure and volumetric flow-rate.

In general, as system pressure increases the volumetric flow-rate that the fan can deliver decreases until the system pressure reaches the fans characteristic stall-pressure, or the pressure where the fan is no longer able to deliver flow. The maximum flow-rate of a fan, often listed as the rated flow-rate, corresponds to the open-flow, or zero-pressure condition. The fan performance curve changes if the fan input-voltage is changed. As fan voltage, or RPM decreases the fan performance curve generally shifts downwards and becomes flatter, with a decreased stall pressure and maximum flow-rate.

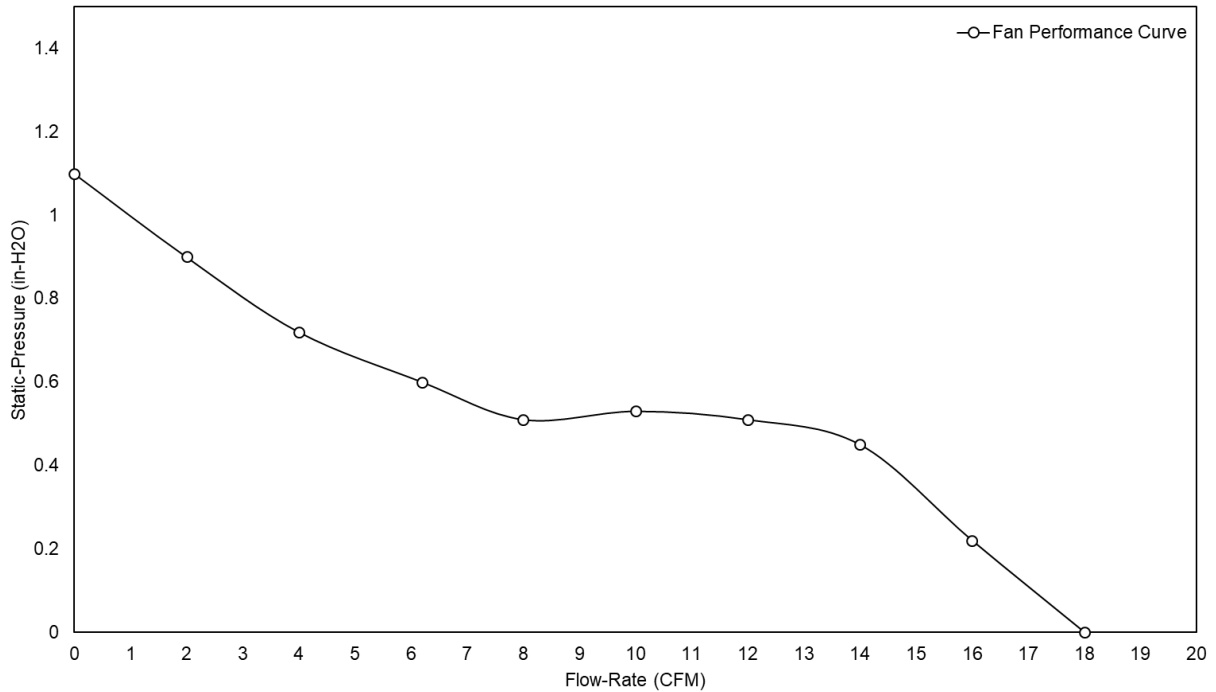


Figure 13: Fan performance curve for a typical 12V computer fan.

The intersection of the system impedance curve and the fan performance curve determines the system operating point, or the maximum volumetric flow-rate the fan can deliver given a systems characteristic impedance behavior. The model does not calculate full system impedance curves because the operating points $(Q, \Delta p_{static})$, corresponding to the optimum jet configurations within the user-defined design parameters and system characteristics, are already defined. With the operating points defined, the model determines if these points correspond to a point on any of the user-defined fan performance curves by calculating if these points satisfy the equations of the polynomial approximations of the fan performance curves. If this condition is satisfied for a particular fan design, then the fan is theoretically capable of delivering the correct volumetric flow-rate corresponding to the operating point $(Q, \Delta p_{static})$ of the optimum jet configuration, meaning it can be used to drive the system. An example of how the operating point for a given fan-system is defined is shown in Figure 14.

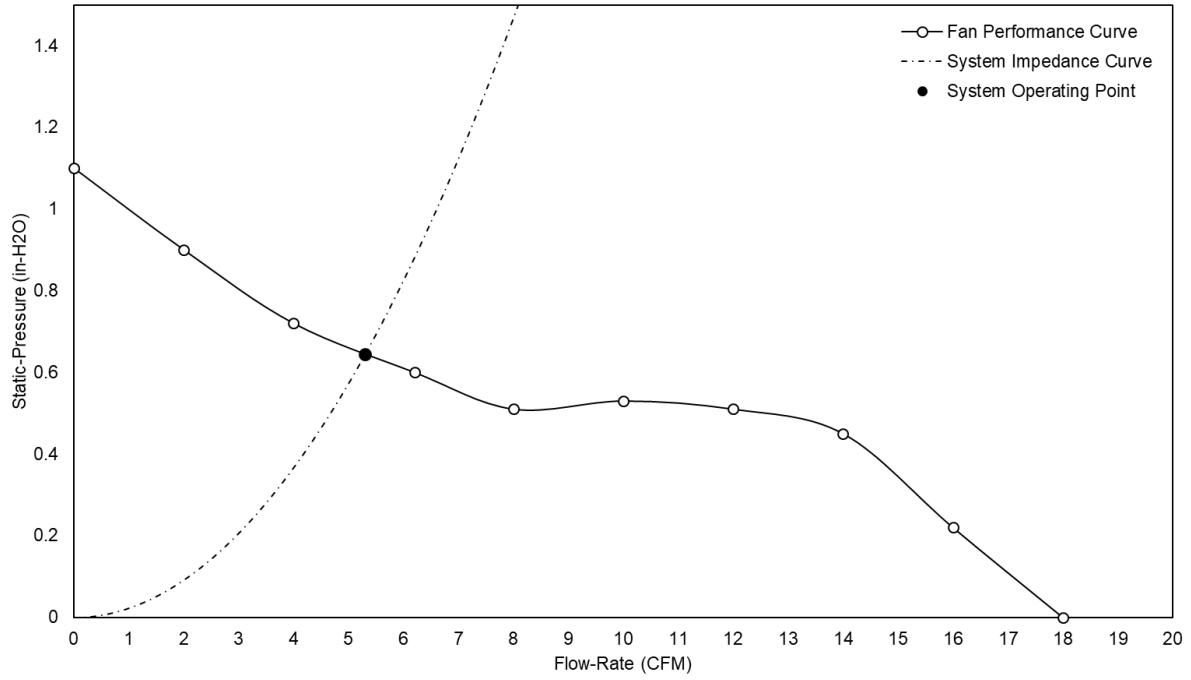


Figure 14: Example definition of the system operating point for a fan-driven system.

CHAPTER 3: COOKSTOVE PERFORMANCE TESTING SYSTEM AND TESTING METHODOLOGIES

This chapter presents the cookstove performance testing system and testing methodologies used in determining the cookstove performance metrics and behaviors presented as part of the investigations of this thesis. A general overview of the UWCCL's cookstove performance testing system is presented and the testing methodologies used in determining ISO/IWA performance metrics, PM_{2.5} emissions behavior, and cookstove excess-air behavior is detailed.

3.1 Cookstove Performance Testing System

The UWCCL's cookstove performance testing system allows for quantitative performance and emissions testing of biomass cookstoves to calculate the ISO/IWA cookstove performance comparison metrics (detailed in Chapter 1 Section 1.2), real-time cookstove PM_{2.5} emissions, and excess-air behavior. The performance testing system uses a fume-hood, digital scale (ABK 70a, Adam Equipment, Danbury, CT), NDIR CO analyzer (VIA-510, Horiba, Kyoto, Japan), NDIR CO₂ analyzer (PIR-2000, Horiba, Kyoto, Japan), a modified PM_{2.5} continuous ambient particulate monitor (TEOM 1405, Thermo Fisher Scientific, MA, USA), and an array of thermocouples, digital differential pressure gauges, flow-meters, and vacuum pumps to provide real-time measurement of cookstove emissions and thermal characteristics necessary for cookstove performance analysis. A schematic of the cookstove emissions and performance testing system is shown in Figure 15. The UWCCL's cookstove performance testing system was originally developed by Ben Sullivan, UW MSME 2016, and the reader is directed to Sullivan's master's thesis, *Development of Cookstove Emissions and Performance Testing Suite with Time-resolved Particulate Matter Analysis and Excess Air Estimation*⁵⁰, for detailed information about the performance testing system. The UWCCL's performance testing system meets the latest cookstove performance testing standards detailed in ISO 19867-1 (2018).^{28,29}

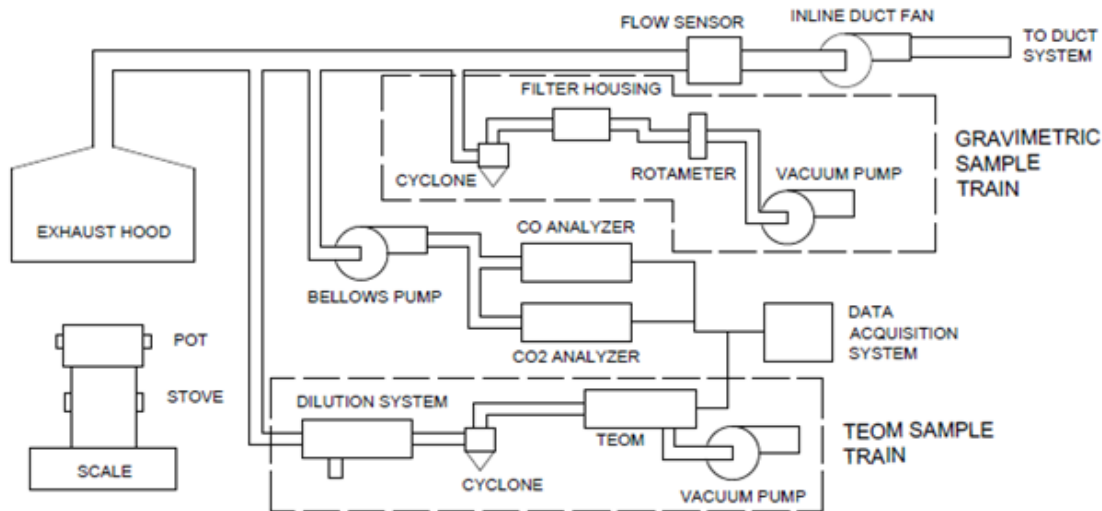


Figure 15: Cookstove emissions and performance testing system. Stove emissions are captured by the hood and drawn through the ducting. Two sampling lines are installed: one for gas (CO/CO₂) analysis and one for particulate matter analysis. Diagram taken from “Development of Cookstove Emissions and Performance Testing Suite with Time-resolved Particulate Matter Analysis and Excess Air Estimation”.⁵⁰

3.2 Cookstove Performance Testing Methodologies

Three different cookstove performance testing methodologies were used to evaluate the cookstove performance metrics and behaviors of the cookstove designs and secondary air injection systems investigated and developed as part of this thesis. The Water-Boil-Test (WBT) was used to evaluate thermal-efficiency and emissions performance in accordance with the ISO/IWA cookstove performance testing standards and to determine all ISO/IWA cookstove performance comparison metrics (detailed in Chapter 1 Section 1.2). The UWCCL’s Fire-Power-Sweep-Test (FPS) was used to characterize and compare the PM_{2.5} emissions behavior of the cookstove designs presented in previous and subsequent chapters. In addition, the UWCCL’s Excess-Air testing methodology was used to analyze cookstove total-flow characteristics. These testing methodologies were also used to experimentally evaluate and validate the analytical model presented in Chapter 2 and investigate the impacts on cookstove performance of

secondary air injection systems with different jet-to-cross flow momentum flux ratio's, presented in Chapter 4.

3.2.1 Water-Boil-Test (WBT)

The Water-Boil-Test (WBT) is the most commonly used cookstove comparison test, developed by Engineers in Technical and Humanitarian Opportunities of Service (ETHOS), the Partnership for Clean Indoor Air (PCIA), and The Global Alliance for Clean Cookstoves. It is a laboratory testing procedure, meant to produce controlled and repeatable results for cookstove evaluation. The test is split into three distinct sections: cold-start, hot-start, and simmer. Hot-start is considered optional. In cold-start, the cookstove starts at room temperature, and 5 liters of water in a typical pot (defined as typical for the region of interest) is heated to the boiling temperature. All stove emissions are captured by an emissions hood, from which CO, CO₂, and PM_{2.5} are extracted for analysis. The mass of the wood required to bring the water to a boil is also recorded. The cold-start section ends once the water reaches the local boiling temperature. The boiling water is then poured out and a fresh 5 liters of water is added to the pot for the hot-start (if hot-start is desired). The process is repeated with all the same metrics recorded. Once the water reaches the boiling temperature after the hot/cold start, the water is kept near the boiling temperature ($\pm 5^{\circ}\text{C}$) for 45 minutes during the simmer phase. Again, the emissions are characterized, and the mass of wood required is recorded. The ISO/IWA tiers detailed in Chapter 1 Section 1.2 are then calculated for universal comparison. The UWCCCL calculates ISO/IWA performance tiers by linear interpolating between each interval bounded by adjacent tiers. This provides the overall tier ranking for each performance metric and allows for a more detailed comparison of the performance of different designs or operating conditions within the corresponding tier. For additional details the reader is directed to *The Water Boiling Test (Version 4.2.3): Cookstove Emissions and Efficiency in a Controlled Laboratory Setting*.²⁷

Most of the experimental investigations and cookstove performance evaluations presented in this thesis use a modified WBT, where only the cold-start section of the WBT is performed, and the simmer section is eliminated. This test is referred to as a rapid-WBT or high-power WBT and only evaluates cookstove performance during the high-power, or boil phase of the WBT. All the WBT test's performed as part of the work presented here were performed using an aluminum 5L flat-bottomed pot typical of what is used in rural-regions of Kenya, detailed in Figure 16.

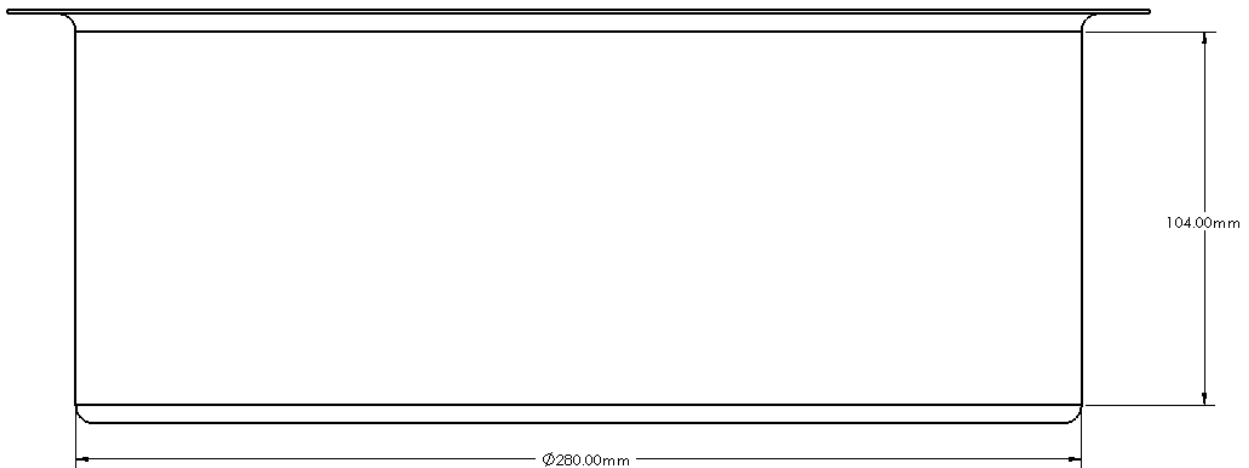


Figure 16: Aluminum 5L flat-bottomed pot used for WBT performance testing.

3.2.2 Firepower-Sweep-Test (FPS)

The Firepower-Sweep-Test (FPS) was originally developed by the UWCCCL to rapidly evaluate cookstove $PM_{2.5}$ emissions behavior, or the characteristic relationship between cookstove $PM_{2.5}$ emission rate and fuel burn-rate (i.e., firepower), by operating the stove at incremental fuel burn-rates throughout a single test. The cookstove is operated at each distinct fuel burn-rate for approximately 15-30 min while CO_2 and $PM_{2.5}$ emissions are measured and logged in real-time. Assuming the combustion efficiency of the cookstove is greater than 90% (most wood-burning cookstoves have combustion efficiencies 95% or greater) the CO_2 emissions data can be used to calculate instantaneous firepower using Equation 27, where Y_{CO_2} is the normalized concentration

of CO₂ (minus ambient) in ppm, Q_D is the sample duct flow rate in moles per second, M_C is the molar mass of carbon in grams per mole, X_C is the carbon ratio of the wood species on a wet basis, LHV is the lower heating value of the wood species in kilojoules per gram, and FP is firepower in kilowatts.

$$FP = \frac{Y_{CO_2} * Q_D * M_C * LHV}{10^6 X_C} \quad \text{Eq. 27}$$

In practice Equation 27 is used to calculate the average firepower for each interval of 20 data points collected. The UWCCCL's testing system has a sampling rate of 0.5Hz, so this corresponds to an average firepower data point for every 40 seconds of run time. An example of the CO₂ data and corresponding instantaneous firepower data, calculated from Equation 27, from a typical FPS test is shown in Figure 17.

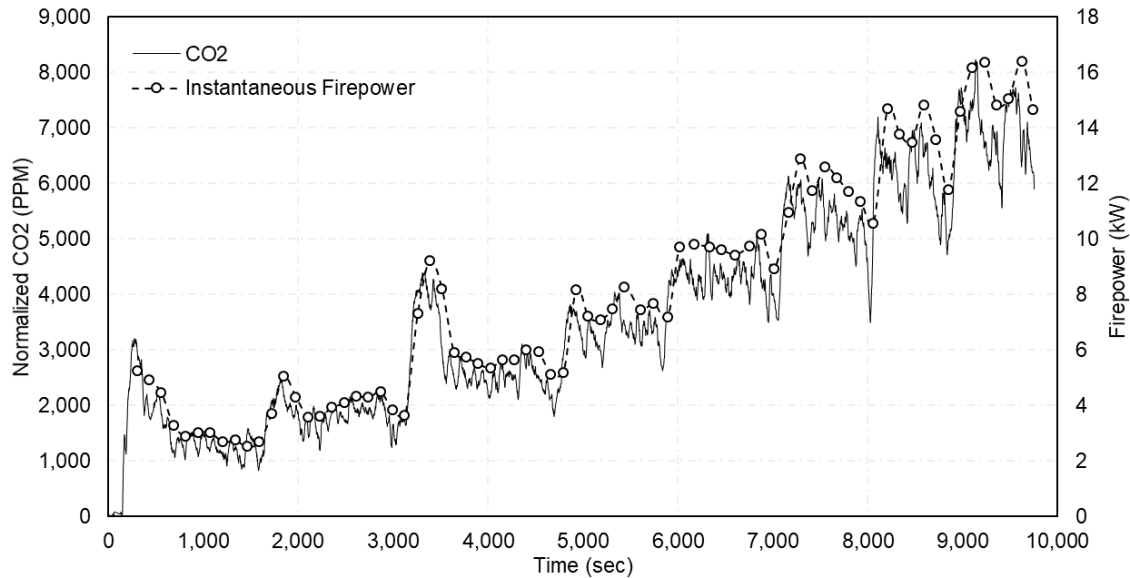


Figure 17: Example FPS data showing normalized CO₂ concentration and the corresponding instantaneous firepower data calculated from Equation 27.

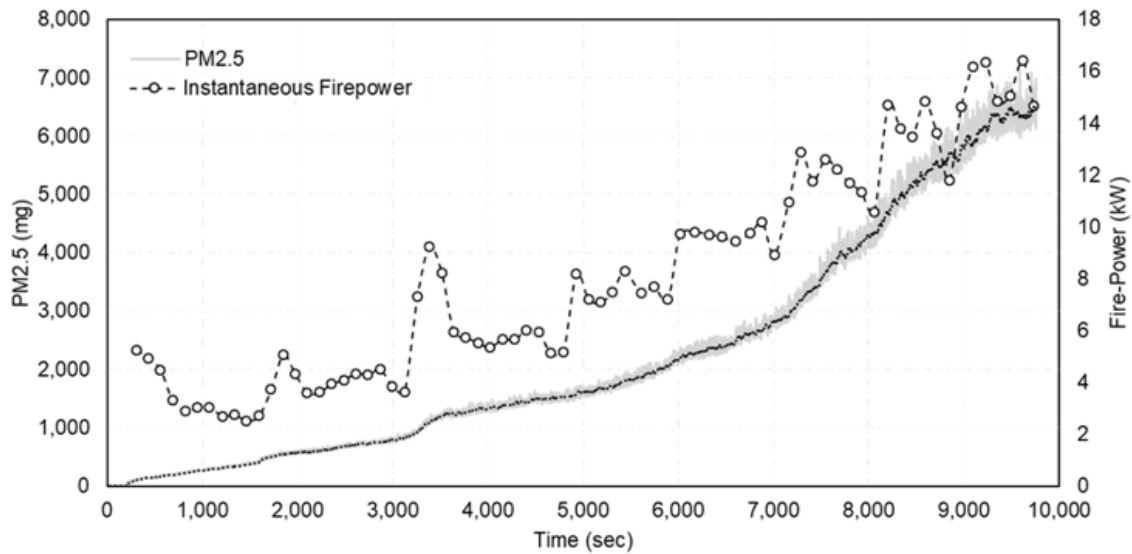


Figure 18: Example FPS data showing total-mass of $PM_{2.5}$ and the corresponding instantaneous firepower data calculated from Equation 27.

Once the average firepower is calculated for each 40 second interval of the test, the corresponding $PM_{2.5}$ emission rate (mg/min) is calculated from the $PM_{2.5}$ total-mass produced data, seen in Figure 18, measured by the $PM_{2.5}$ continuous ambient particulate monitor (TEOM 1405), by calculating the total-mass of $PM_{2.5}$ produced during every 40 second interval of a FPS. The average firepower data and the corresponding $PM_{2.5}$ emission rate data is then sorted by firepower and grouped into bins using an interval of 0.25kW. A statistical analysis is then performed for each bin producing the necessary statistical metrics to characterize the $PM_{2.5}$ emission behavior throughout the range of firepower's tested. The resulting data is then compiled with any additional FPS data and plotted, resulting in the $PM_{2.5}$ emission rate vs. stove firepower curve illustrated in Figure 19.

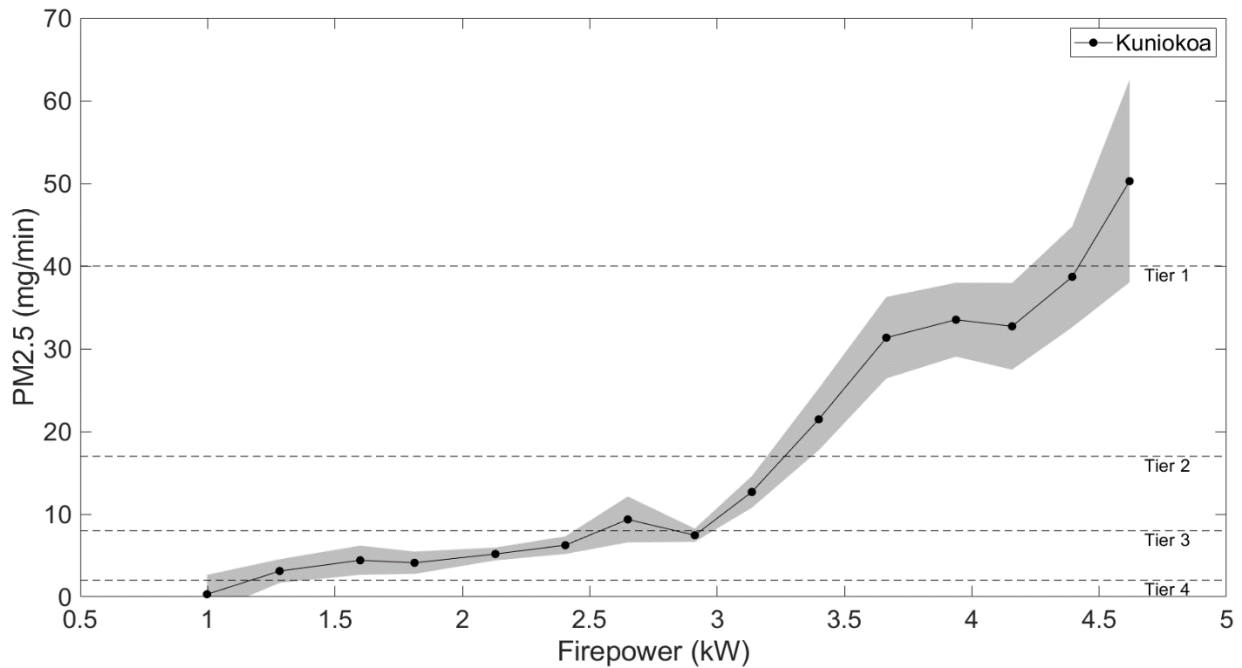


Figure 19: Example PM_{2.5} emission rate vs. stove firepower curve calculated from FPS data for the Kuniokoa™. Note: the shaded region represents a 90% CI.

3.2.3 Excess-Air

The Excess-Air test, originally developed by Ben Sullivan and detailed in his master’s thesis ⁵⁰, is a method for measuring the excess air, or air in excess of the stoichiometric requirement for combustion flowing through a cookstove. Understanding excess air is important for cookstove design, as it is critical to stove performance characteristics including mixing, PM_{2.5} production, as well as heat transfer and thermal efficiency. The Excess-Air test is similar to a FPS test in that the stove is operated at incremental fuel burn-rates throughout a single test, but instead of characterizing PM_{2.5} emissions behavior for each distinct fuel burn-rate the amount of excess-air present is calculated for each burn-rate, effectively evaluating the flow-characteristics of a stove throughout a wide range of burn-rates, which can be used to guide stove design improvements. During the Excess-Air test, CO₂ emissions are sampled directly from the outlet of the stove, or the gap between the cooking implement and the cone-deck of the stove using a four-pronged sampling rake made from 3/16” OD stainless steel tubing and fittings shown in Figure 20. The

sampling rake is connected to ¼" OD PVC tubing and converges into a single sample line. Sampling from this location ensures that only combustion gases, or gases flowing through the combustion-chamber and riser of the stove are measured. Assuming a combustion efficiency greater than 90% and that the sample inlets draw equal flow the amount of excess-air ($\varphi - 1$) can be calculated using Equation 28 where y_{CO_2} is the concentration of CO₂ in the sample gas in ppm and x, y, z are the moles of carbon, hydrogen, and oxygen respectively per gram of wood determined from an ultimate analysis of the wood fuel species.

$$(\varphi - 1) = \frac{\left(\frac{x \cdot 10^6}{y_{CO_2}}\right) - x + \frac{y}{2}}{4.76 \left(x + \frac{y}{4} - \frac{z}{2}\right)} \quad \text{Eq. 28}$$

Using Equation 28, excess-air is calculated for timespan intervals of relatively constant CO₂ output and then compared to corresponding fuel burn-rate data for the same timespan calculated using real-time stove mass measurements and/or pre-weighed fuel batch data. The excess-air data presented as a part of the investigations detailed in Chapter 4 calculated excess-air by pre-weighing three incrementally larger batches of wood that were burned at constant, but incrementally higher burn-rates. The average excess-air was calculated for each batch of wood and the corresponding burn-rate was calculated by dividing the total weight of the batch of wood by the total time it took to burn, an example of the data from these tests is shown in Figure 21. Using Equation 29, excess-air can be converted into the molar flow-rate of air, \dot{n}_{air} , through the stove where \dot{m}_{wood} is fuel burn-rate, or mass-flow rate, and φ is the air-to-fuel equivalence ratio.

$$\dot{n}_{air} = 4.76 * \dot{m}_{wood} * \varphi \left(x + \frac{y}{4} - \frac{z}{2}\right) \quad \text{Eq. 29}$$



Figure 20: Illustration of the excess-air sampling rake and sample location.

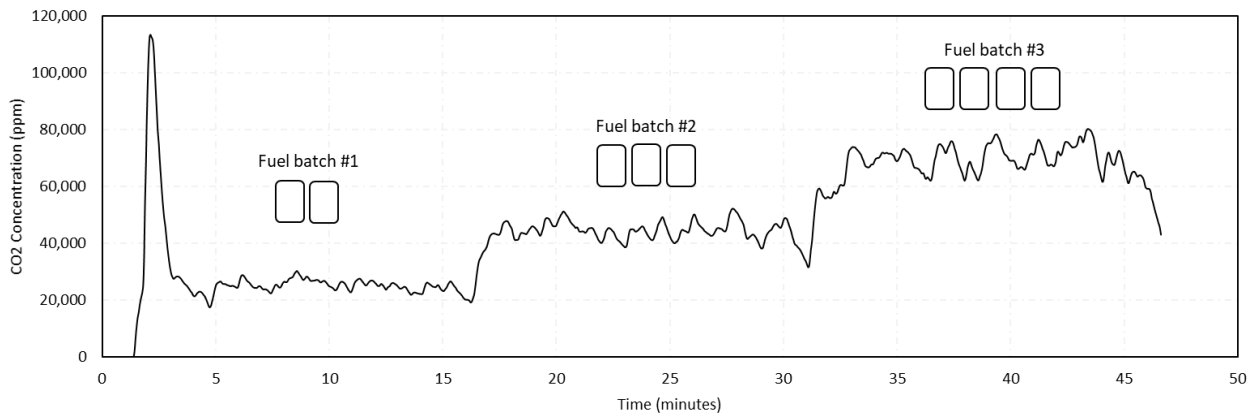


Figure 21: Example excess-air CO₂ concentration data for a test using three incrementally larger fuel batches burned at a constant burn-rate.

CHAPTER 4: ANALYTICAL MODEL EXPERIMENTAL EVALUATION AND VALIDATION

This chapter discusses the experimental evaluation of the analytical model/design tool presented in Chapter 2. A three-dimensional computational fluid dynamic (CFD) model of the Kuniokoa™ with riser secondary air injection and a physical Kuniokoa™ prototype with modular riser secondary air injection were built and configured to investigate the application of maximum jet penetration length and jet-to-cross flow momentum-flux ratio to the optimization and design of secondary air injection systems for side-feed wood-burning cookstoves.

The analytical model was used to predict an optimum secondary air jet configuration using the design parameters and system characteristics that guided the development of the Kuniokoa-Turbo™, detailed in Chapter 5. Three additional non-optimum jet configurations were selected to evaluate the impact of maximum jet penetration and jet-to-cross flow momentum-flux ratio on cookstove riser cross-flow mixing characteristics, flame-height, primary-to-secondary air flow ratio, cookstove emissions, and thermal-efficiency. In addition, the physical air injection systems built for the modular Kuniokoa™ prototype were used to evaluate the analytical model's method of estimating system impedance.

The main objective of this investigation was to develop a comprehensive understanding of how maximum jet penetration and jet-to-cross flow momentum-flux ratio impact cookstove performance, not just cross-flow mixedness, providing a more complete picture of how these jet optimizations parameters influence cookstove combustion, flow, and thermodynamics.

4.1 Jet Configurations

Using the analytical model and the design parameters and system characteristics corresponding to the Kuniokoa-Turbo™ project, listed in Table 9 and detailed in Chapter 5, a list of optimum jet configurations (i.e., configurations satisfying $Y_{max} = [0.4D_{xf} \dots 0.5D_{xf}]$) is predicted for the Kuniokoa™, shown in Table 10. The optimum configuration corresponding to a system flow-rate of 2.8cfm was selected for evaluation, shown in bold in Table 10. This system flow-rate was selected due to its compatibility with the fan and air injection system used in the Kuniokoa-Turbo™ and so to provide a convenient comparison of the results presented in this chapter to the performance of the Kuniokoa-Turbo™, detailed in Chapter 5. The model was then used to select three non-optimum jet configurations, one configuration having what the model predicted as under-penetrating jets ($Y_{max} < 0.4D_{xf}$) and two configurations with over-penetrating jets ($Y_{max} > 0.5D_{xf}$). These non-optimum configurations were used to evaluate the impact of jet penetration and jet-to-cross flow momentum-flux ratio on cookstove performance compared to the baseline natural-draft, or no secondary air injection case, and if the model predicted optimum configuration is in fact the optimal case when considering all aspects of cookstove performance.

System flow-rate (i.e., mass-flow rate), the number of jets, and jet location remained constant for all the selected configurations so to isolate the impacts of jet penetration and jet-to-cross flow momentum-flux ratio on cross-flow mixedness and cookstove performance. The system volumetric flow-rate was 2.8cfm, corresponding to a mass-flow rate of 0.0016 kg/s of air (assuming the secondary air preheat temperature remains constant). A single plane of 12 radially spaced circular air-jets was used, positioned approximately 90mm below the outlet, or top of the riser. The riser measured 100mm in total length (top of the combustion-chamber to riser outlet) and 100mm in diameter, the jet injection plane was positioned 10mm downstream of the riser inlet. All the selected jet configurations are detailed in Table 11.

Table 9: Secondary air jet optimization analytical model user-defined design parameters and system characteristics for the Kuniokoa-Turbo™ project, detailed in Chapter 5.

Kuniokoa-Turbo™ design parameters and system characteristics	
Number of jets	$n_j = [6 \dots 12]$
Jet diameter (mm)	$D_j = [2 \dots 10]$
System volumetric flow-rate (i.e., fan flow-rate) (cfm)	$Q = [1 \dots 3]$
System pressure-drop (i.e., maximum fan static-pressure) (in-H2O)	$\Delta P_{max} = 0.6$
System head-loss	$\Delta H_L = 0$
Jet Discharge Coefficient	$C_d = 0.6$
Cross-flow diameter (mm)	$D_{xf} = 100$
Cross-flow temperature (K)	$T_{xf} = 900$
Cross-flow pressure (atm)	$P_{xf} = 1$
Secondary air pre-heat temperature (K)	$T_j = 300$
Secondary air plenum (i.e., duct) pressure (atm)	$P_j = 1$
Stove firepower (kW)	$FP = 4$
Fuel species concentrations (i.e., ultimate analysis) (mol/g)	See Table 8
Fuel lower heating value (kJ/g)	$LHV = 19.314$
Excess-air	$(\varphi - 1) = 3$

Table 10: Kuniokoa-Turbo™ optimum jet configurations and corresponding jet characteristics calculated by the analytical model.

Kuniokoa-Turbo™ Optimum Jet Configuration and Jet Characteristics											
Q (cfm)	1	1.2	1.4	1.6	1.8	2	2.2	2.4	2.6	2.8	3
n_j	6	8	8	10	10	12	12	12	12	12	12
d_j (mm)	3.44	3.17	3.48	3.22	3.50	3.25	3.46	3.65	3.83	4.04	4.20
V_j (m/s)	8.51	9.00	8.70	9.25	8.82	9.47	9.21	9.02	8.90	8.60	8.55
J	128	143	134	151	137	158	149	143	140	130	129
Δp_{static} (in-H2O)	0.48	0.53	0.50	0.56	0.51	0.59	0.56	0.54	0.52	0.49	0.48
Y_{max}/D_{xf}	0.425	0.405	0.42	0.405	0.41	0.4	0.405	0.41	0.415	0.415	0.42

Table 11: Jet configurations used in the evaluation of the analytical model and the impacts of maximum jet penetration and momentum-flux ratio on cross-flow mixing characteristics and cookstove performance.

Jet Configurations Selected for Evaluation					
	Natural-Draft	Under-Penetrating (12x8mm)	Optimum (12x4mm)	Over-Penetrating (12x3mm)	Over-Penetrating (12x2mm)
Q (cfm)	0	2.8	2.8	2.8	2.8
\dot{m} (kg/s)	0	0.0016	0.0016	0.0016	0.0016
K	0	0.387	0.387	0.387	0.387
n_j	0	12	12	12	12
d_j (mm)	0	8	4	3	2
V_j (m/s)	0	2.2	8.6	15.6	35
J	0	8.4	130	427	2161
E_j (J/m ³)	0	2.8	45	143	725
Δp_{static} (in-H ₂ O)	0	0.03	0.49	1.54	7.8
Y_{max}/D_{xf}	0	0.21	0.42	0.56	0.84

4.2 Experimental Apparatus

The analytical model and the impacts of maximum jet penetration and momentum-flux ratio on riser cross-flow mixing characteristics, flame-behavior, primary-to-secondary air flow ratio, emissions, and thermal-efficiency were evaluated using a combination of three-dimensional CFD modeling of the Kuniokoa™ with secondary air injection and laboratory experiments using a physical Kuniokoa™ prototype with a modular riser secondary air system. System flow-rate, number of jets, and jet location remained constant and were consistent in both the CFD model simulations and the physical prototype experiments. Additional details of both the CFD model and the modular stove prototype can be found in subsequent chapter sections.

4.2.1 Three-Dimensional Computational Fluid Dynamic Model of the Kuniokoa™ with Secondary Air Injection

A three-dimensional CFD model of the Kuniokoa™ was built and configured by Anamol Pundle (PhD candidate, University of Washington, Department of Mechanical Engineering) and Michael Barbour (PhD, Intellectual Ventures Lab) to simulate steady-state combustion, flow, and

thermodynamics of the Kuniokoa™ for each secondary air jet configuration selected for evaluation and to compare to corresponding laboratory experimental results. The model was used to quantify riser cross-flow mixedness through calculation of the fuel scalar uniformity index (Equation 30), temperature uniformity index (Equation 31), average in-plane temperatures, and temperature and velocity contours at various cross-sectional and vertical planes in the riser of the cookstove domain. The model was also used to characterize flame-height behavior through the calculation and visualization of the stoichiometric flame surface, air flow ratio of the primary and secondary air inlets in the model domain, and the thermal-efficiency of the simulated system for each jet configuration evaluated.

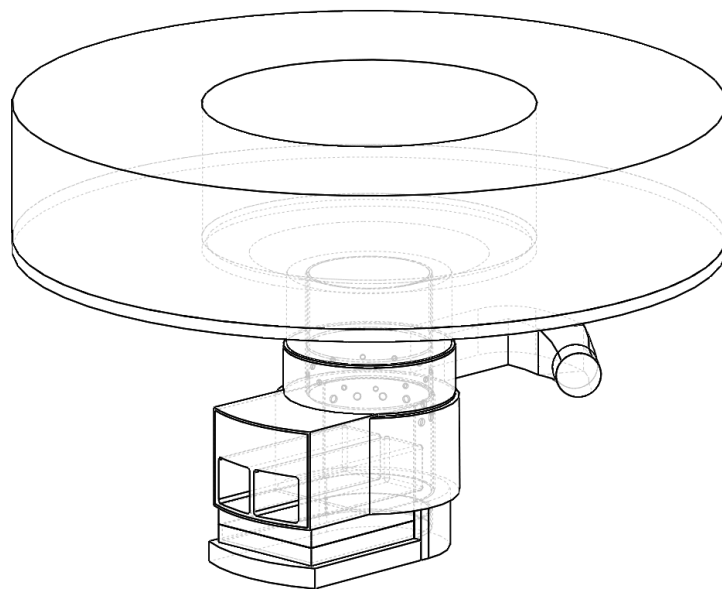


Figure 22: CFD model cookstove domain (geometry/flow-path).

The model domain includes the same geometry of the internal assembly of the Kuniokoa™ (combustion-chamber, riser, cone-deck, heat-shield assembly, etc.), the modular secondary air system used in the experimental prototype, and a pot consistent with what was used in the laboratory experiments. The domain consists of a combined fluid domain and wall, or sheet metal

domain, shown in Figure 22. The fuel, or wood is modeled as 2 – 2cm x 2cm cross-section sticks, which act as the surface from which a wood volatile mixture is released into the system at a specified burn-rate. A boundary condition is defined for the secondary air system inlet that allows for the system flow-rate and/or pressure to be set accordingly.

The model includes turbulent-combustion interaction modeled by the standard Eddy Breakup Model, which assumes that the reaction rate is controlled by turbulent mixing and not chemical kinetics. A simple four-step global reaction mechanism is chosen, which is used to describe all reactions through the combustion and post-combustion zone. The corresponding reaction mechanism is shown in Table 12.

Table 12: Four step global mechanism taken from Glanville, P. “Reducing Particulate Emissions from a Wood-Fired Hydronic Furnace”

Reaction Mechanism
$CO + \frac{1}{2}O_2 \rightarrow CO_2$
$H_2 + \frac{1}{2}O_2 \rightarrow H_2O$
$CH_4 + 2O_2 \rightarrow CO_2 + 2H_2O$
$CO + H_2O \leftrightarrow CO_2 + H_2$

The wood volatiles are approximated as a mixture of CO, CO₂, H₂, H₂O and CH₄. This allows the use of simplified global reaction mechanisms. The mass fractions of each species in the wood volatile mixture are given in Table 13.

Table 13: Mass fractions of species in wood volatile mix, taken from Glanville, P. “Reducing Particulate Emissions from a Wood-Fired Hydronic Furnace”

CO	CO ₂	H ₂	H ₂ O	CH ₄
0.383	0.237	0.006	0.312	0.062

The Reynolds-averaged conservation equations of mass, momentum, energy, and species transport are solved. The model also includes turbulence modeled by the Realizable $k - \varepsilon$ model,

and realistic boundary conditions, including radiation from the gas and the walls (i.e., sheet metal assembly components), as well as heat loss from the sides of the cookstove and heat delivered to the pot. To simulate the presence of soot, the absorption coefficient of the gas is adjusted, which is assumed to be constant throughout the domain. The walls of the domain are treated as made of metal sheet made of stainless steel of constant density. Heat transfer between the fluid domain and domain walls/boundaries is also modeled.

The fuel scalar uniformity index, U_{FS} , is calculated from Equation 30, which is used to represent the mixedness of fuel/combustion-products and air within a specific cross-sectional plane in the riser. Equation 30 calculates U_{FS} by dividing the root-mean-square of the difference between the concentration of all wood volatile and combustion product species, FS , in each cell in a plane and the total planar average of FS by the total planar average of FS . A decrease in U_{FS} represents an increase in fuel/combustion-products and air mixedness, with perfectly mixed flow corresponding to a U_{FS} of zero.

$$U_{FS} = \frac{RMS(FS-avg(FS))}{avg(FS)} \quad \text{Eq. 30}$$

The temperature uniformity index, U_T , was calculated in the same fashion as U_{FS} , but used the average cell temperature in each plane and the total planar temperature average to calculate U_T .

$$U_T = \frac{RMS(T-avg(T))}{avg(T)} \quad \text{Eq. 31}$$

All CFD simulations and data post-processing were performed by A. Pundle and M. Barbour.

4.2.2 Kuniokoa™ with Modular Secondary Air Injection

A stock natural-draft Kuniokoa™ was modified to accept a modular secondary air jet system that allowed for the evaluation of different jet configurations and jet characteristics but kept jet location and position within the cookstove assembly constant and consistent with what was modeled in

the CFD simulations. Three of the modular jet systems were built corresponding to the 12 x 8mm, 12 x 4mm, and 12 x 2mm jet configurations selected for analysis (the 12 x 3mm configuration was not evaluated experimentally). The modular systems were made from 22 gauge 304 stainless-steel and all seams were fully welded, so to provide a completely sealed-system, leaving only the jets and system inlet as flow pathways. A pressure tap was installed near the inlet of each system to measure system static pressure and to measure the system impedance of each system to compare to the model's predictions. Pressure was measured using a Setra 264 Digital Low Differential Pressure Transducer (Setra Systems Inc., Boxborough, MA). Each system was connected to a 100psi compressed air source and system flow-rate was metered using a calibrated Dwyer RMC-104 Flowmeter (Dwyer Instruments Inc., Michigan City, IN). For the baseline natural-draft experiments the 12x8mm modular system was installed and the system inlet was sealed shut to prevent any flow from passing through the system during the test. Figure 23 provides further illustration and details of the modular secondary air system and the complete experimental stove assembly.

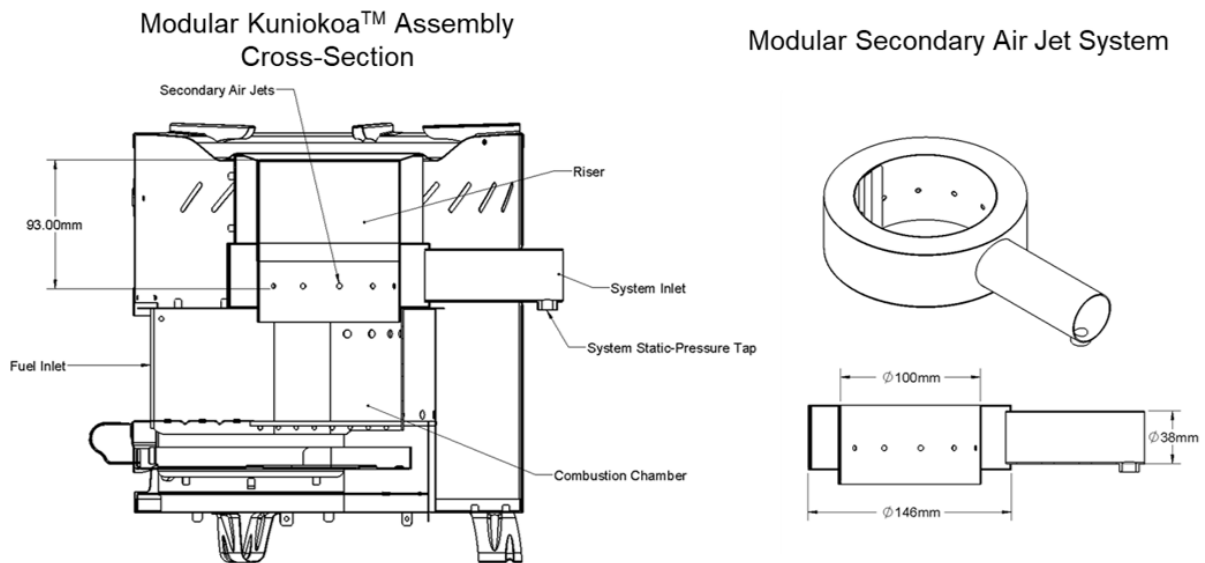


Figure 23: Modular Kuniokoa™ secondary air injection experimental apparatus. Additional dimensions are provided in Appendix A2.

4.3 Experimental Results

The following is a summary of the results from the evaluation of the effects of the cross-flow mixedness optimization parameters used in the analytical model (maximum jet penetration length, Y_{max} , and momentum-flux ratio, J) on cookstove performance and mixing characteristics. A combination of CFD simulation and laboratory experimental results are presented to characterize the impact of varying degrees of J , which is a function of Y_{max} , on riser cross-flow mixing characteristics, system flow behavior, thermal-efficiency, and emissions. The results of this investigation were used to evaluate the validity of the analytical model's predicted optimum jet configuration and define additional design criteria necessary to develop optimized secondary air injection systems for side-feed wood-burning cookstoves.

4.3.1 Cross-Flow Temperature Contours and Uniformity

Contour plots of the riser temperature from the simulation are shown in Figure 24. These plots show the temperature contours at three planes: the injection plane, a plane one radius downstream, and a plane corresponding to the outlet of the riser. These plots, generated for a stove firepower of 4kW, were used to provide an initial assessment and comparison of the system behavior of the natural-draft and secondary air jet configurations. The general behavior observed in Figure 24 suggests that as J increases so does the uniformity of the temperature contours when comparing the natural-draft, 12 x 8mm, and 12 x 4mm contours. This behavior is most prominently seen one radius downstream and at the outlet of the riser, corresponding to the second and third row of Figure 24, respectively, where there appears to be less planar temperature gradients as J increases.

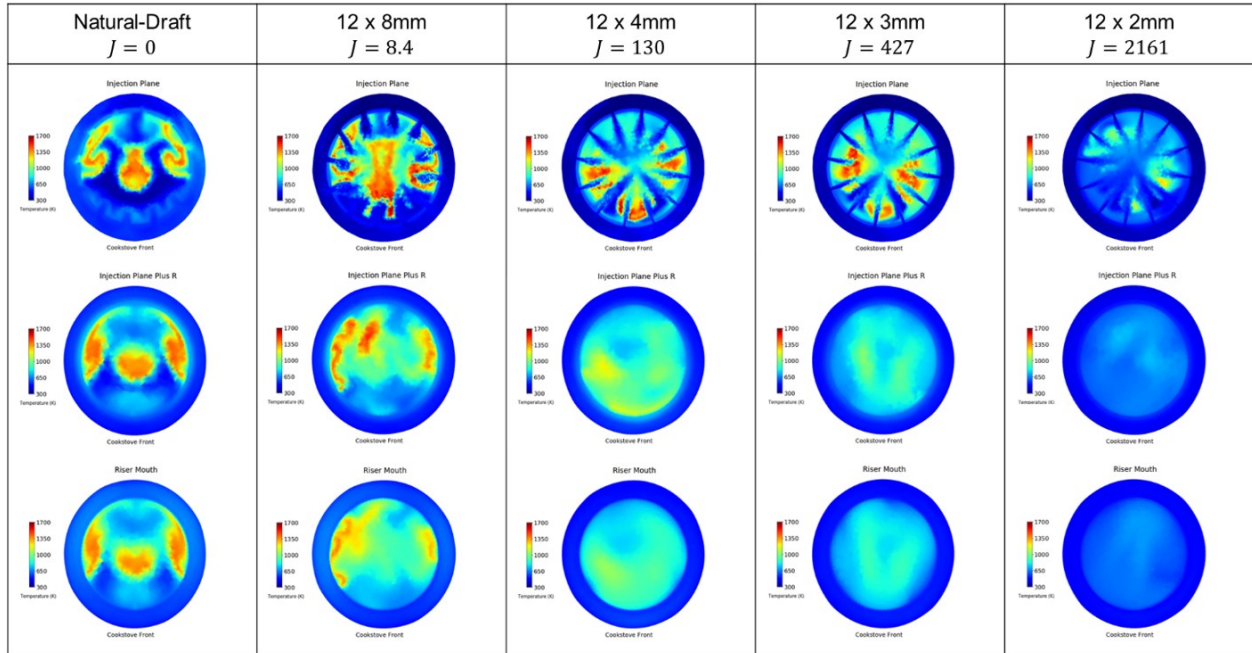


Figure 24: Riser temperature contours for the injection plane (top row), one radius downstream (second row), and riser outlet (bottom row) for all evaluated configurations. The contours are oriented so that the front of the stove corresponds to the bottom of each contour plot.

Figure 24 also provides an indication of the location of the reaction zone, or region of maximum heat release, which can be approximated by the high temperature structures (red/orange regions) in the riser temperature contours. The behavior we observed suggests that as J increases the reaction zone moves further towards the fuel-bed, or farther away from the riser outlet when comparing the natural-draft, 12 x 8mm, and 12 x 4mm contours. This behavior is consistent with the behavior observed in a previous investigation into air injection in pellet gasifier cookstove combustion systems.⁵⁵

Comparing the temperature contours of the 12 x 4mm, 12 x 3mm, and 12 x 2mm jet configurations provides little insight into the differences of riser temperature uniformity among these configurations, other than the observed reduction in overall riser flow temperature as J is increased, which is discussed later. To provide a more detailed comparison of temperature uniformity among these configurations (and the others), the temperature uniformity index, U_T , was

calculated from the inlet to the outlet of the riser using an interval of $Z = 5\text{mm}$, where Z is downstream distance. Figure 25 provides a comparison of U_T for each configuration as a function of Z/D_{xf} , where the left and right bounds of the x-axis correspond to the riser inlet and outlet, respectively, and a value of 0.1 corresponds to the injection plane. A decrease in U_T represents an increase in temperature uniformity. The general behavior of U_T for all configurations, including the natural-draft case, follows a similar trend as the temperature contours, with an increase in J resulting in an increase in downstream temperature uniformity. We also observed that for all cases, U_T decreases as the downstream distance increases, even for the natural-draft case.

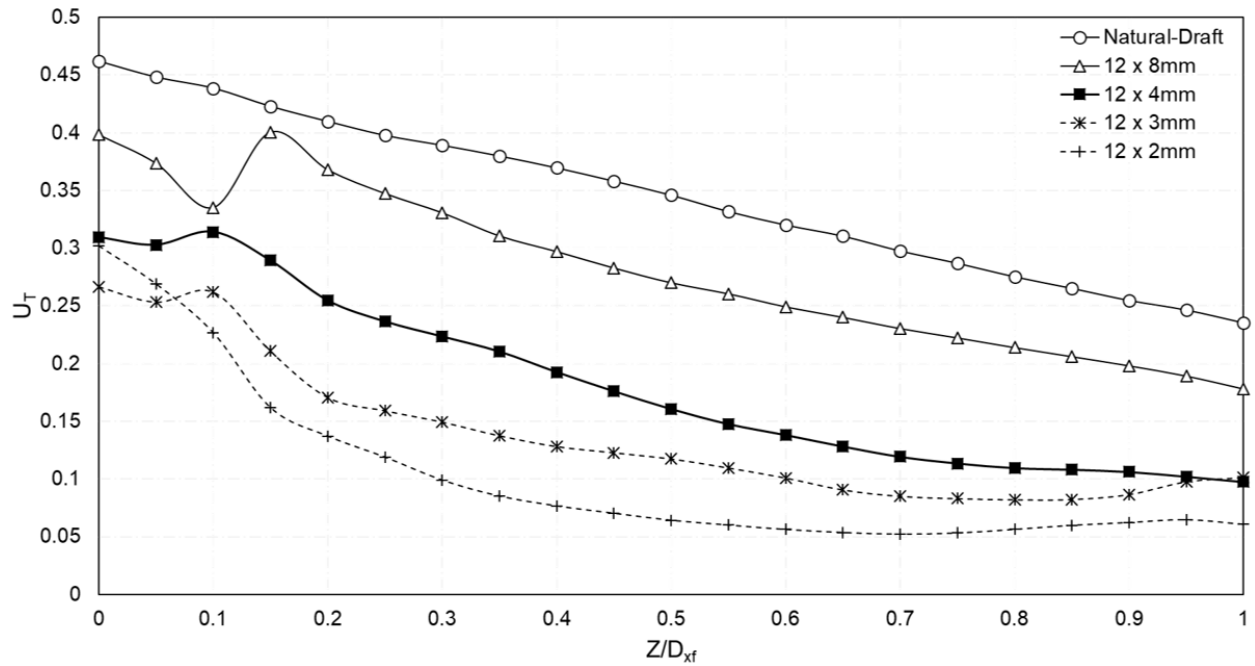


Figure 25: Riser cross-flow temperature uniformity index, U_T , defined for cross-sectional planes of the riser. The inlet and outlet of the riser correspond to an x-axis value of 0 and 1 respectively. The jet injection plane corresponds to an x-axis value of 0.1.

Figure 25 suggests that there is a dependency of downstream cross-flow temperature uniformity behavior on J , but the impact of J on U_T downstream of the injection plane has a diminishing effect as the jets start to over-penetrate the cross-flow, requiring progressively more energy to further improve U_T . The under-penetrating configuration (12 x 8mm), corresponding to a J value of just

8.4, results in an average increase in downstream temperature uniformity of 20% compared to the natural-draft case, and the predicted optimum (12 x 4mm - $J = 130$) provides an average increase of 50%. The 12 x 8mm and 12 x 4mm configurations provide the most efficient increases in cross-flow temperature uniformity, i.e., requiring relatively small jet injection energies (2.8 J/m³ and 45 J/m³, respectively) to achieve their respective increases in cross-flow temperature uniformity.

The high J value configurations, or the over-penetrating configurations (12 x 3mm - $J = 427$ and 12 x 2mm - $J = 2161$), represented by the dashed lines in Figure 25, result in significant increases in average temperature uniformity, 65% and 75%, respectively, but the additional increase in temperature uniformity compared to the predicted optimum case requires a disproportionate increase in J , analogous to an increase in jet injection energy. The 12 x 3mm configuration increases the average downstream temperature uniformity 15% more than the predicted optimum (12 x 4mm) but requires a 330% increase in J (also proportional to the increase in jet injection energy). This is even more pronounced when comparing the 12 x 2mm configuration which requires a 1600% increase in J to see an additional 25% increase in riser temperature uniformity compared to the predicted optimum configuration.

Interestingly, the predicted optimum configuration achieves near equivalent temperature uniformity as the high J value configurations at the riser outlet. When this behavior is considered along with the relative efficiency in increasing cross-flow temperature uniformity of the predicted optimum configuration it seems to suggest that the 12 x 4mm configuration provides a good compromise between jet injection energy and the effectiveness of the jets in increasing cross-flow temperature uniformity.

4.3.2 Cross-Flow Fuel Scalar Uniformity

The fuel scalar uniformity index, U_{FS} , was also calculated along the full length of the riser to attempt to quantify and compare the mixedness of the riser cross-flow, or more specifically the mixedness of wood volatile and reaction product species in the riser. U_{FS} is shown for each configuration evaluated as a function of downstream distance in Figure 26. The general behavior of U_{FS} , as J is increased, follows that of U_T , with an increase in U_{FS} corresponding to an increase in J , but again J having a diminishing impact on U_{FS} as J becomes larger.

This behavior follows what J. Vanormelingen and E. Van Den Bulck found in their investigation⁵², that is as jet penetration, Y_{max} , and therefore J increase, so does the effectiveness of the jet configurations in increasing cross-flow mixedness compared to the natural-draft behavior, or no air injection case. They also showed a diminishing effect as J is increased past a critical value, similar to the trend we observed. The U_{FS} results do not verify the behavior found by J. Vanormelingen and E. Van Den Bulck where a momentary decrease in mixedness is seen as J is increased past the predicted optimum point. Additional simulations with J values nearer to the predicted optimum ($J = 130$) would need to be performed to evaluate if this behavior is seen in cookstove riser cross-flow mixedness.

Contrary to the U_T results the predicted optimum configuration does not achieve the same U_{FS} as the over-penetrating configurations at the riser outlet, but still appears to provide the best compromise between jet injection energy and the effectiveness of the jets in increasing cross-flow mixedness.

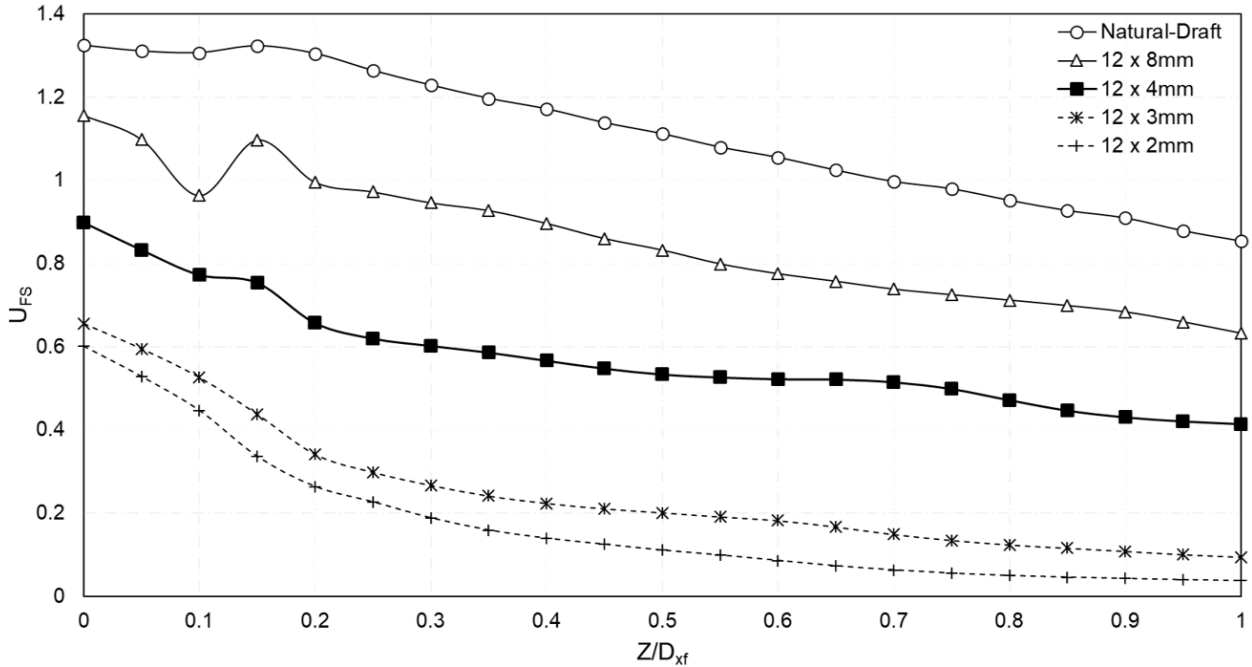


Figure 26: Riser cross-flow fuel scalar uniformity index, U_{FS} , defined for cross-sectional planes of the riser. The inlet and outlet of the riser correspond to an x -axis value of 0 and 1 respectively. The jet injection plane corresponds to an x -axis value of 0.1.

4.3.3 Flame Behavior

A decrease in U_{FS} , represents an increase in fuel and reaction product species mixing in the cross-flow, which should correspond to a reduction in the overall flame length of diffusion flames. The stoichiometric flame surfaces, shown in Figure 27, support this correlation, with a noticeable decrease in overall flame height as U_{FS} improves with an increase in J .

Not surprisingly, the natural-draft configuration has the longest flame length, extending from the fuel bed to the outer edges of the pot, and is relatively unperturbed due to the lack of turbulent/convective mixing in what is primarily laminar/transitional flow. The 12 x 8mm configuration results in a decrease in flame length, but not enough to prevent flame-to-pot interaction, which is a known contributor to $PM_{2.5}$ cookstove emissions. The predicted optimum configuration (12 x 4mm) appears to reduce flame height to the plane of injection, well below the cooking surface (bottom of the pot) and the outlet of the riser, preventing flame-to-pot interaction.

As J increases past the predicted optimum value into the over-penetration region the flame surface does not extend beyond the height of the combustion-chamber, which is unlikely to provide an additional benefit in emissions reductions compared to the optimum configuration, but suggests that there are jet mixing patterns inherent to over-penetrating jet configurations that extend upstream, into the combustion-chamber, and to the fuel-bed.

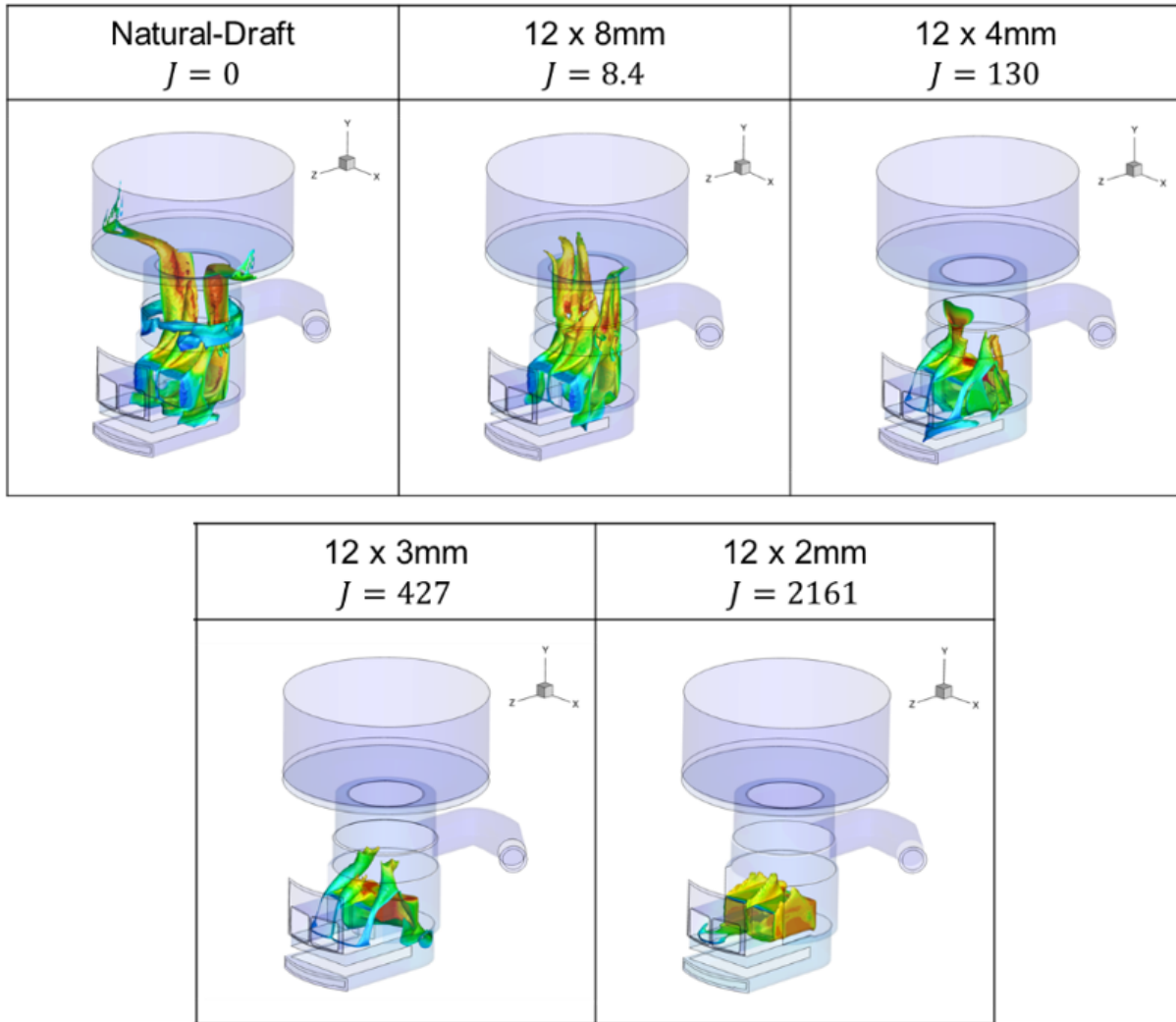


Figure 27: Stoichiometric flame surfaces for the natural-draft and jet configurations evaluated for a system firepower of 4kW.

4.3.4 Cross-Flow Velocity Contours

While all of the jet configurations improve upstream mixedness and temperature uniformity, apparent in Figure 25 and Figure 26, the increases seen in the over-penetrating configurations is attributed to the tendency of over-penetrating jets to create upstream recirculation zones near the walls of the cross-flow, which can provide very thorough upstream mixing patterns, but that are not always beneficial.⁵² The recirculation zones have a blockage effect on the flow near the walls of the cross-flow, which effectively reduces the cross-sectional area of the cross-flow, increasing the mainstream center-flow velocity (i.e., increasing the pressure-drop across the jet injection plane). The thorough upstream mixing patterns and localized increase of flow velocity where the jets converge in the center of the flow results in a reduction in mean gas residence time through the system, which has been found to negatively impact the ability for complete oxidation of fuel species, resulting in higher emissions and lower combustion efficiencies.⁵²

The velocity contours of a plane bisecting the riser and two opposing jets, shown in Figure 28, illustrates the increase in the center-flow velocity and upstream mixing patterns as J increases. We found that the 12 x 8mm configuration produces minimal increases in cross-flow velocity and no obvious upstream recirculation zones, but as J is increased, the center-flow velocity, the degree of jet impingement, and upstream recirculation patterns increase in magnitude and become more prominent. Even the predicted optimum configuration, which the model predicts to have a maximum jet penetration of 42% of the cross-flow diameter, shows signs of upstream mixing patterns, suggesting the analytical model's prediction of jet penetration is underestimated.

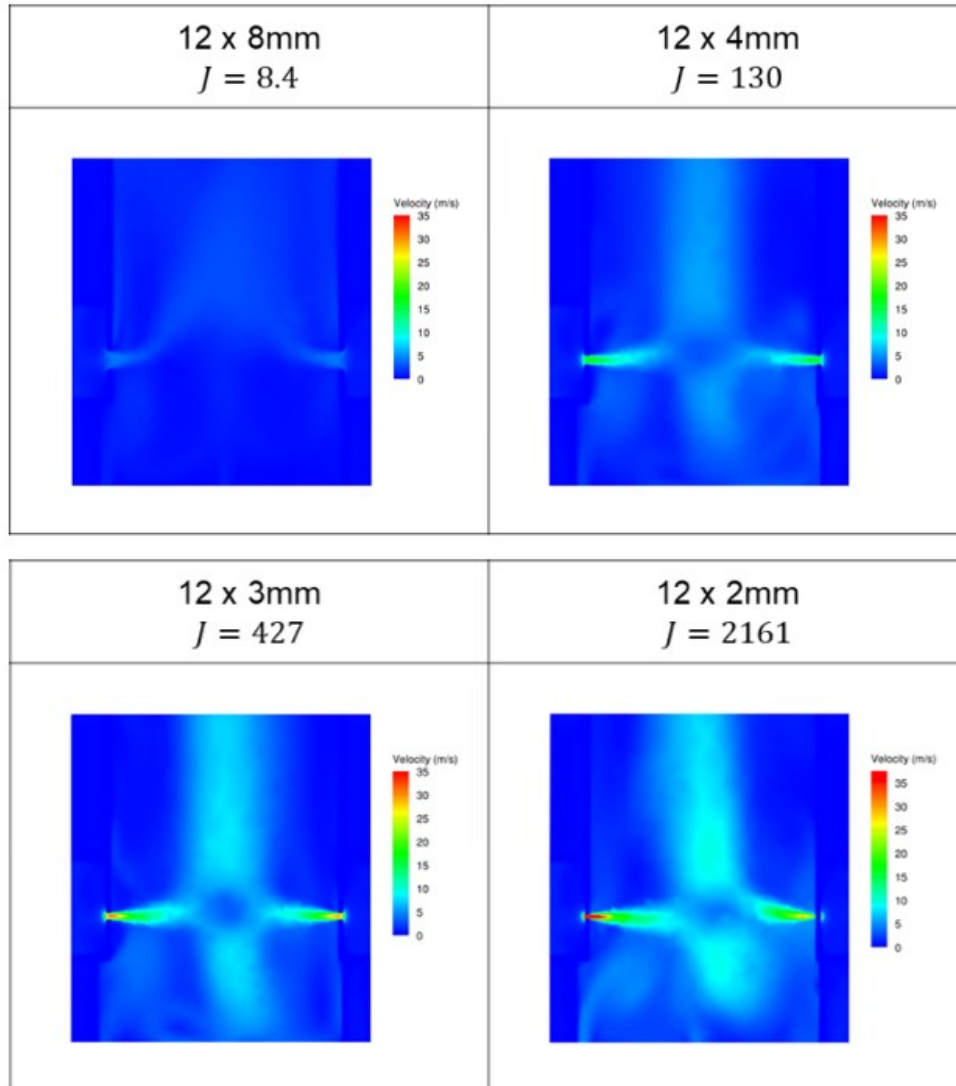


Figure 28: Riser velocity contours of a vertical plane bisecting the riser and two opposing jets. The bottom of the contour images correspond to the inlet of the riser and the top corresponds to the outlet.

4.3.5 $PM_{2.5}$ Emissions

The presence and magnitude of upstream recirculation zones and mixing patterns follows the flame height trend, but this continued reduction in flame height does not always correspond to a decrease in emissions. Figure 29 compares the experimentally measured $PM_{2.5}$ emission rate of the natural-draft case and three of the jet configurations determined from a modified FPS where the stove was operated at 4kW for an extended period of time using small-dry wood (2cm x 2cm

Douglas Fir sticks). Similar to the U_T and U_{FS} results we found that improvement in $PM_{2.5}$ emissions is much more sensitive to J leading up to the predicted optimum value. In natural-draft the stove was found to have a $PM_{2.5}$ emission rate of 20.3 mg/min (Tier 1), the 12 x 8mm configuration resulted in a $PM_{2.5}$ emission rate of 12.1 mg/min (Tier 2), and the optimum configuration (12 x 4mm) resulted in a $PM_{2.5}$ emission rate of 3.6 mg/min (Tier 3), an 82% reduction compared to the natural-draft case. As J is increased further, past the predicted optimum point, the $PM_{2.5}$ emission rate (8.4 mg/min, Tier 2) is improved when compared to the natural-draft and 12 x 8mm configuration, but is increased when compared to the predicted optimum case. This appears to confirm previous findings suggesting an increase in emissions at high J values due to the thorough upstream mixing patterns and reduction in gas residence time associated with over-penetrating jet configurations. This suggests that jet configurations that result in the most significant increases in cross-flow mixedness or temperature uniformity do not necessarily correspond to optimal performance.

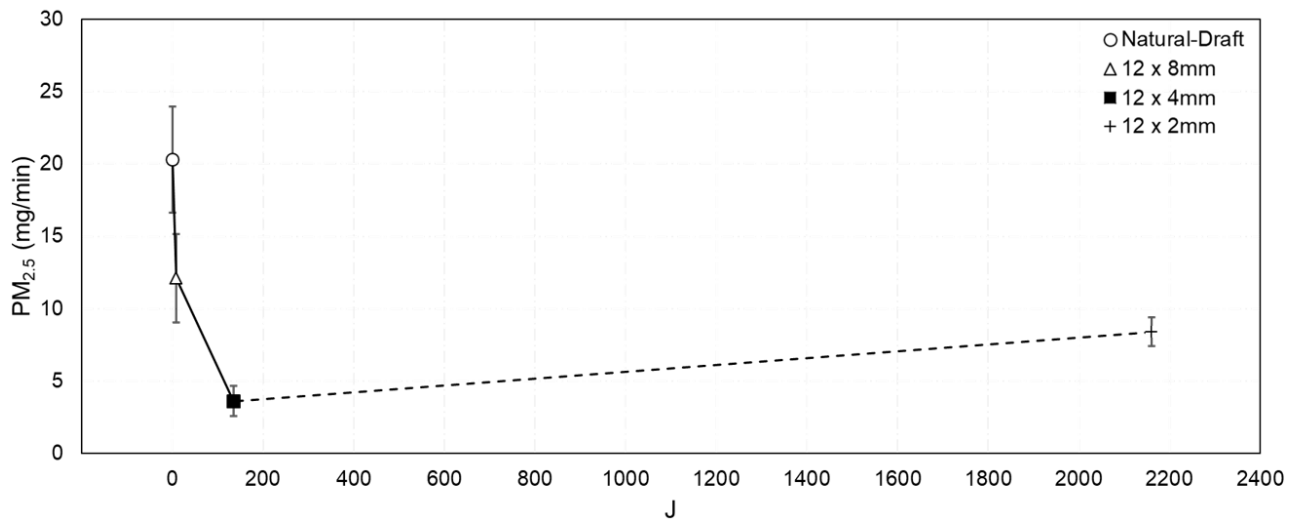


Figure 29: $PM_{2.5}$ emission rate (mg/min) as a function of momentum-flux ratio, J , at a firepower of 4kW. Note: Error bars represent a 90% CI.

4.3.6 Inlet Air Flow Ratio

Additionally, the increase in center-flow velocity as J increases was found to influence the total mass-flow of air through the cookstove. Figure 30 compares the primary-to-secondary air mass-flow ratio, λ , predicted by the CFD simulations for all the jet configurations. As J increases so does λ , suggesting an increase in primary air mass-flow as the center-flow velocity in the riser increases. The baseline natural-draft case operates using only primary air and the corresponding total air mass-flow rate is 2.9 g/s for a stove firepower of 4kW. The jet flow, which is constant for all the jet configurations, introduces 1.6 g/s of air into the system, but we see a varying amount of primary air for each jet configuration (2.1 g/s for 12 x 8mm, 2.4 g/s for 12 x 4mm, 2.6 g/s for the 12 x 3mm, and 2.9 g/s for the 12 x 2mm configurations) following the center-flow velocity trend in the velocity contours.

A drop in primary air mass-flow is seen for the 12 x 8mm configuration, compared to the natural-draft case, but this still corresponds to an overall increase in total mass-flow of air through the stove. The 12 x 2mm configuration is found to operate at the same primary air mass-flow rate as the natural-draft case, resulting in a 150% increase in total system air mass-flow.

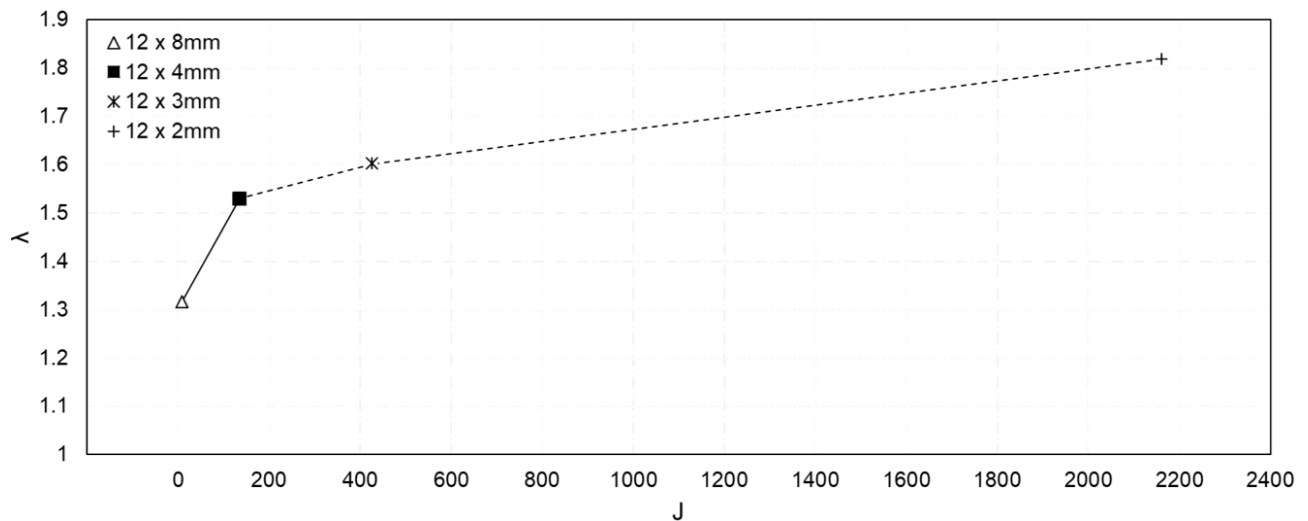


Figure 30: Primary to secondary air mass-flow ratio, λ , as a function of momentum-flux ratio, J , predicted by the CFD simulations.

Similar behavior is found in the experimental results from excess-air tests of the physical modular system, shown in Figure 31, throughout a wide-range of stove firepower's. The experimental results suggest an even more significant increase in primary air than the CFD simulations. For example, the CFD simulations predict $\lambda = 1.82$ at 4kW for the 12 x 2mm configuration, but the experimental results predict $\lambda = 4.3$ at an equivalent firepower. This is attributed to the different fuel size used in the laboratory experiments, which resulted in less of the fuel feed inlet (i.e., the main primary air inlet) being blocked with fuel than in the CFD simulations. The area of the primary air inlet(s) has been found to strongly impact total flow rate of air through a cookstove system in a previous investigation.⁵⁰

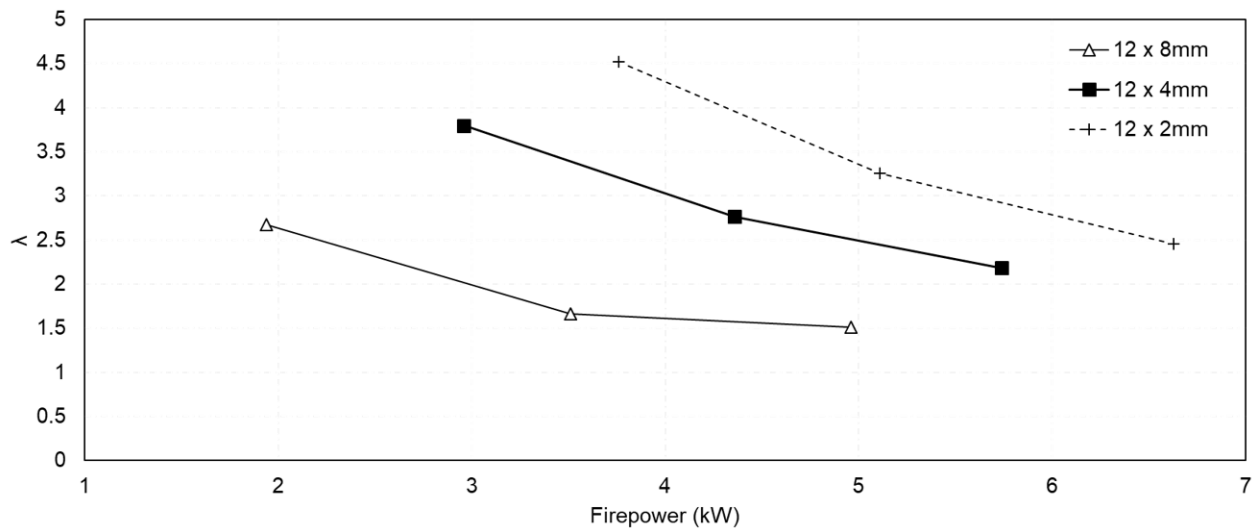


Figure 31: Primary to secondary air mass-flow ratio, λ , as a function of momentum-flux ratio, J , predicted by experimental excess-air tests.

An increase in total mass-flow of air results in a decrease in average flow temperature, if firepower, or total heat release remains constant, which was the case for the CFD simulations. This decrease in average flow temperature can be seen in the temperature contours shown in Figure 24. If the outlet temperature of the riser, T_{out} , is compared between all the jet configurations it is found that there is a near linear relationship between λ and T_{out} , shown in Figure 32.

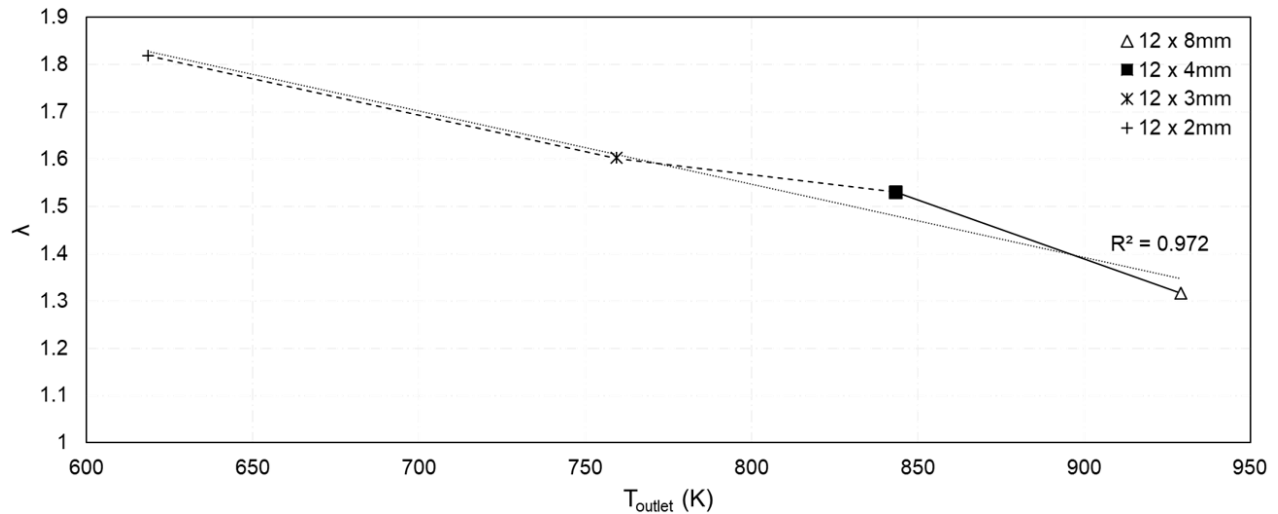


Figure 32: Primary to secondary air mass-flow ratio, λ , as a function of riser outlet temperature, T_{out} , predicted by CFD simulations.

4.3.7 Thermal-Efficiency

A reduction in riser outlet temperature can have negative impacts on thermal-efficiency and this is confirmed by both the CFD simulations and laboratory performance testing results, which are shown in Figure 33. As J increases, so does the total mass-flow rate of air through the stove, resulting in a decrease in T_{out} and a decrease in thermal-efficiency. The CFD simulations predict the decrease seen in thermal-efficiency to be in good agreement and proportional to the decreases in T_{out} .

This again suggests that jet configurations that result in the most significant increases in cross-flow mixedness or temperature uniformity do not necessarily correspond to optimal performance because they tend to correspond to increased λ emissions and significant decreases in thermal-efficiency when compared to the predicted optimum configuration. The predicted optimum configuration appears to provide a good compromise between jet injection energy, quality of cross-flow mixedness, flame-height reduction, particulate emissions reductions, and thermal-efficiency when compared to the natural-draft case and the other configurations evaluated.

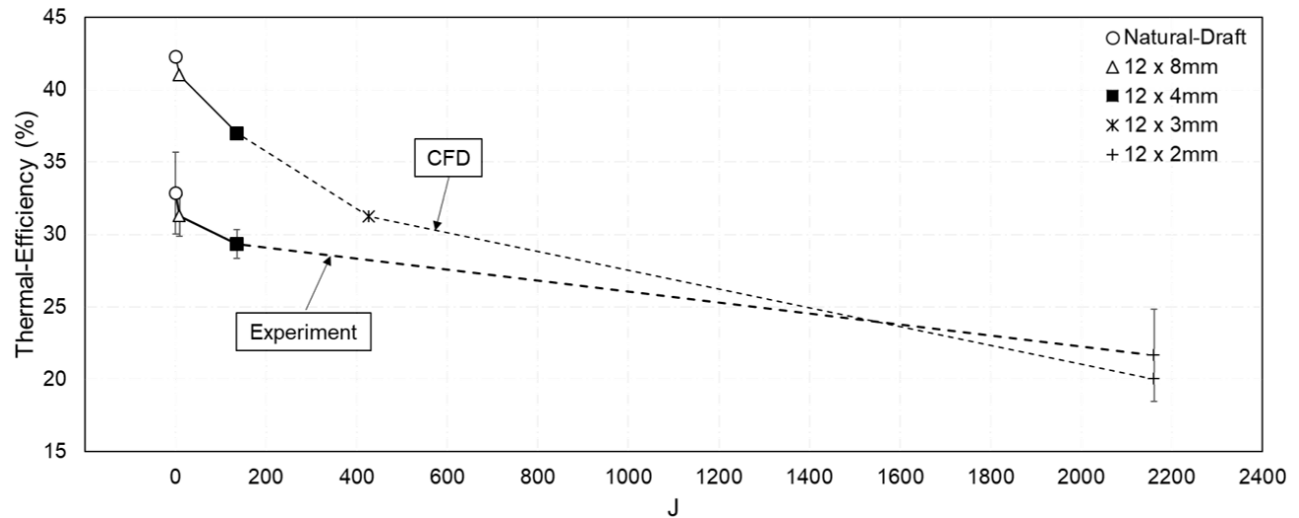


Figure 33: Thermal-efficiency (%) as a function of momentum-flux ratio, J , for both the CFD simulations and experimental results. Note: Error bars represent a 90% CI.

4.3.8 System Impedance

The modular secondary air systems were used to evaluate the accuracy of the analytical model's method of estimating system impedance. Figure 34 shows the comparison of the model predicted system impedance (solid lines) and the measured system impedance (data points) for the 12 x 2mm, 12 x 4mm, and 12 x 8mm configurations.

In general, Figure 34 suggests the model tends to overestimate system static-pressure when compared to the measured values. As the jet diameter decreases the agreement of the model with the measured values becomes worse with the model significantly overestimating the static pressure of the 12 x 2mm system as flow-rate is increased. The model uses a standard orifice discharge coefficient, C_d , of 0.6 which leads to a good approximation of system impedance for configurations with jet diameters less than 4mm, but significant overestimation for smaller jets. The estimation can be improved within the range of static-pressures capable by most small fans likely to be used in air injection systems (<1in-H₂O) by changing C_d to 0.78, 0.63, and 0.67 for the 12 x 2mm, 12 x 4mm, and 12 x 8mm configurations, respectively. The improved or corrected

predicted system impedances are shown in more detailed for static-pressure less than 1in-H₂O in Figure 35 represented by the dashed lines.

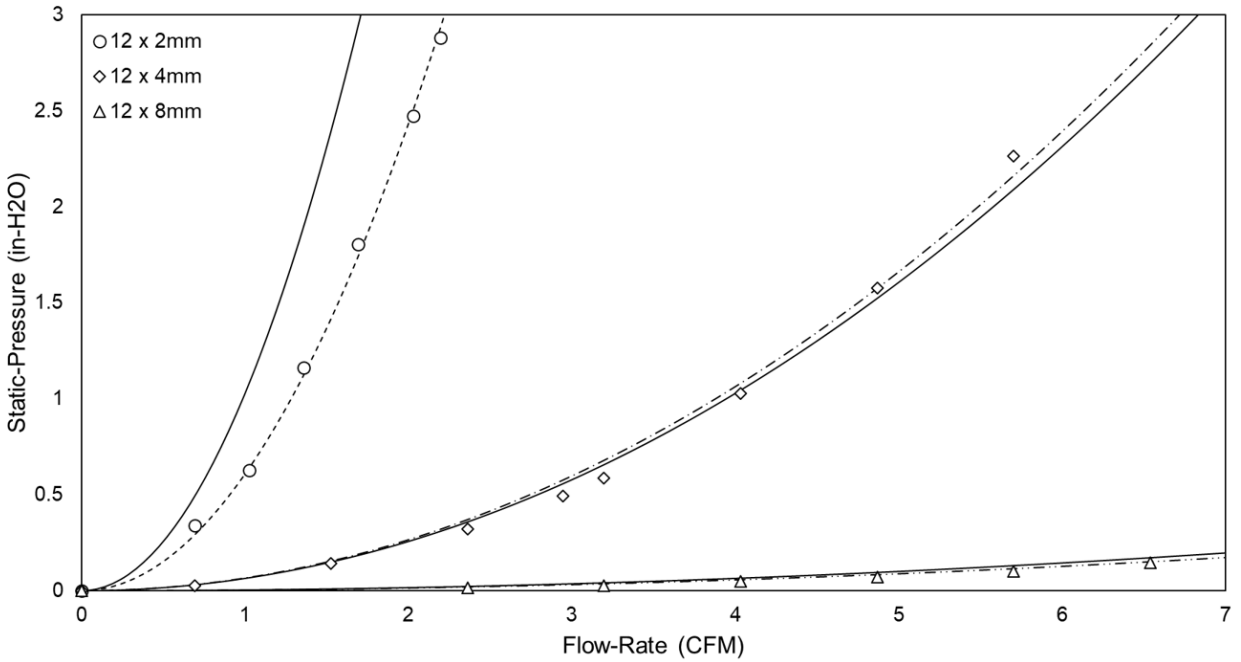


Figure 34: Jet system impedance comparison between the analytical model predictions (solid lines), measured values (points), and corrected model predictions (dashed lines).

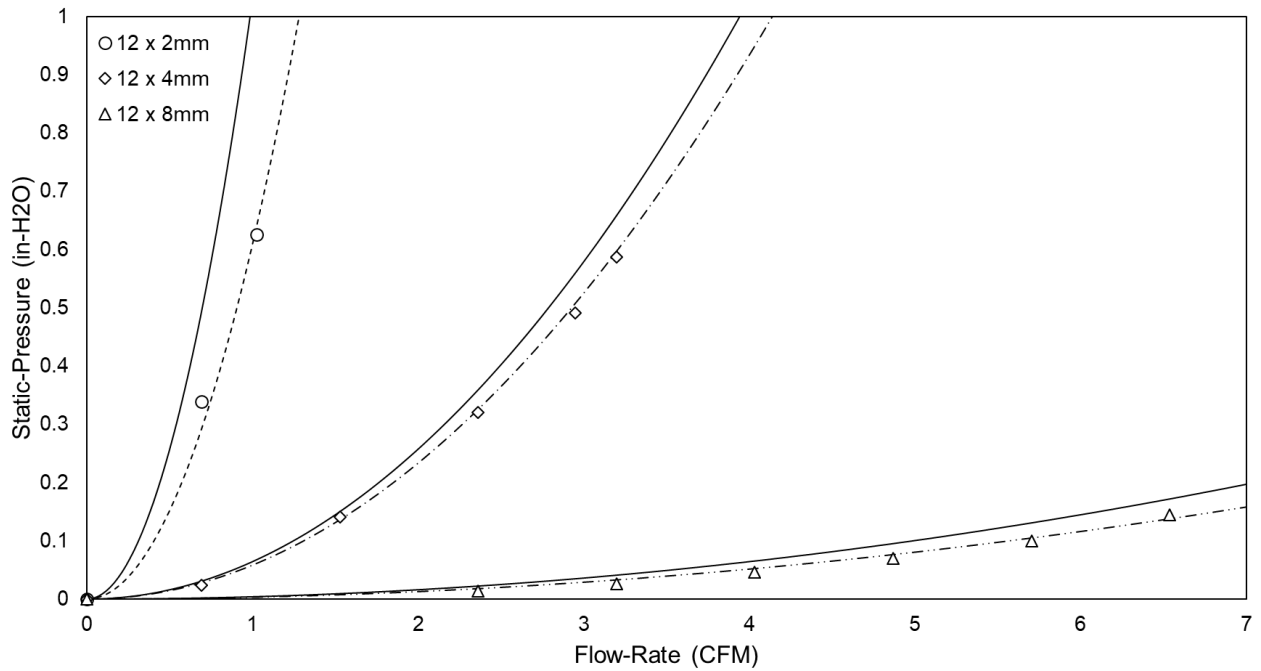


Figure 35: Model corrected jet system impedance (dashed lines) compared to the previous model predictions (solid lines) and measured values (points).

When using the model and a standard discharge coefficient ($C_d = 0.6$) the user should keep in mind that the predicted system static-pressures of jets less than 4mm is likely to be overestimated. A modified discharge coefficient and/or head-loss value or function should be used if the model is to provide the most accurate predictions of system impedance guiding the selection of optimum jet configurations within a projects fan design parameters and system characteristics.

4.4 Summary

Taking into account the CFD simulations and laboratory experimental evaluation of the natural-draft case and selected jet configurations, the results support the literatures suggested values of $Y_{max} = [0.4D_{xf} \dots 0.5D_{xf}]$ for calculating jet configurations with good cross-flow mixing characteristics and that require minimum jet injection energies. The analytical model's use of Y_{max} in calculating optimum jet configurations was found to provide a good estimation of secondary air jet configurations that successfully increase cross-flow mixedness and uniformity, reducing flame height, resulting in a maximum reduction in $PM_{2.5}$ emissions, and that provide a good compromise between jet injection energy, quality of cross-flow mixing, and thermal-efficiency.

The model tended to overestimate system impedance, especially for jet systems with jet diameters less than 4mm, so care should be taken in using the model for fan selection or when using the model to estimate optimum jet configurations within the fan design parameters of a specific stove project.

The model assumes the cross-flow variables remain constant regardless of jet configuration, contrary to what was observed in the CFD simulations and laboratory experiments. Table 14 displays the model's original jet characteristic predictions for the evaluated configurations and corrected values (shown in bold) calculated using the cross-flow average temperature and mass-flow predicted by the CFD simulations and the corrected estimations of system impedance.

Although the corrected values are in some instances significantly different than the original predictions, the overall trends remain the same.

Table 14: Corrected jet characteristics for the jet configurations evaluated. Corrected values are shown in bold.

Jet Configurations Selected for Evaluation (Corrected)				
	Under-Penetrating	Optimum	Over-Penetrating	
	(12 x 8mm)	(12 x 4mm)	(12 x 3mm)	(12 x 2mm)
Q (cfm)	2.8	2.8	2.8	2.8
\dot{m} (kg/s)	0.0016	0.0016	0.0016	0.0016
K	0.387 0.632	0.387 0.555	0.387 0.533	0.387 0.477
n_j	12	12	12	12
d_j (mm)	8	4	3	2
V_j (m/s)	2.2	8.6	15.6	35
J	8.4 22.2	130 281	427 873	2161 4536
Δp_{static} (in-H ₂ O)	0.03 0.027	0.49 0.50	1.54 n/a	7.8 4.75
Y_{max}/D_{xf}	0.21 0.29	0.42 0.54	0.56 0.72	0.84 1.1

CHAPTER 5: A SOLAR-POWERED FAN-DRIVEN SECONDARY AIR INJECTION SOLUTION FOR THE KUNIOKOA™

This chapter details the development of a solar-powered fan-driven secondary air injection system for the Kuniokoa™, a natural-draft, side-feed, wood-burning cookstove. The project's motivation is described in the context of current household electrification efforts and technologies in Sub-Saharan Africa, the performance deficiencies of the current natural-draft Kuniokoa™, and how the former can be used in combination with the cookstove air injection optimization design tool (detailed in Chapter 2) to overcome the latter. The project goals and design parameters are defined, and the final design prototype is detailed, known as the Kuniokoa-Turbo™. Finally, the laboratory performance of the Kuniokoa-Turbo™ is presented and compared to the performance of the baseline, or natural-draft Kuniokoa™, providing an example of how optimized air injection in the riser of a cookstove can be used to effectively improve the performance of intermediate cookstove designs.

5.1 Kuniokoa-Turbo™

In 2018 Intellectual Ventures (IV), through their Global Good Fund, partnered with the UWCCCL, Aprovecho Research Center (ARC), and BURN with the goal of developing a next generation wood-burning cookstove product for Sub-Saharan Africa. The goal was to develop a low-emissions and fuel-efficient wood-burning cookstove that leveraged the growing pay-as-you-go (PAYG) off-grid solar electrification efforts and household solar technologies market in rural Sub-Saharan Africa to power an innovative wood-burning cookstove design that improved upon the performance of the Kuniokoa™ by using air injection as a means to overcome existing performance limitations. The desired performance improvements included (1) reducing the performance variabilities of the Kuniokoa™ when subjected to in-home use, (2) effectively reducing HAP (specifically PM_{2.5} emissions), and (3) increasing the utility of the stove by widening the range of fuel characteristics that could be used with the design. The final product was to be

included as part of a complete household sustainable energy solution, along with solar powered lights and other appliances, which could be made affordable to some of the most rural and disadvantaged populations in the region through a PAYG financing structure.

The idea for the Kuniokoa-Turbo™ was conceived from the need to improve upon the in-home performance of the Kuniokoa™ and the increased accessibility to household electricity due to the growing off-grid solar system and device market in Sub-Saharan Africa. In Kenya and Tanzania approximately 50% of all off-grid and/or households with unreliable-grid access use a household solar system and/or device as of 2017, with over 6 million products distributed .⁵³ The global market for off-grid household solar solutions is experiencing immense growth and sales are expected to increase in regions like Sub-Saharan Africa by 30% annually, leading to an estimated 434 million sales worldwide by the year 2022 .⁵³ Many of these off-grid solar systems and devices operate using a PAYG business model that allows users to pay for a product via embedded consumer financing that provides the financial flexibility needed for poorer households, often in regions with limited grid access, to afford sustainable household energy solutions.

The presence of PAYG off-grid solar system and device companies in Sub-Saharan Africa is the highest in the world, with 98% of all PAYG business model companies operating in the region .⁵³ M-Kopa, Orb, Mobisol, and Greenlight Planet offer a diverse product line of PAYG solar systems and devices to households in Sub-Saharan Africa, with much of their focus in East-Africa in countries like Kenya and Tanzania. We are partnering with them with the goal of adding a clean-burning and fuel-efficient biomass household cooking solution to the PAYG household energy packages that they already offer. Packaging an improved cooking solution with PAYG off-grid solar systems and devices has two main advantages: (1) increased affordability and financial flexibility due to the PAYG financing structure and (2) the availability of a solar energy source that can be used to power a fan-driven air injection system to improve stove performance.

5.1.1 Project Goals and Design Parameters

Through previous work the UWCCCL did in developing the Kuniokoa™ and characterizing its performance (detailed in Chapter 1), combined with feedback BURN had received from consumers about the Kuniokoa™ since its launch, and current market data from PAYG off-grid solar companies in Sub-Saharan Africa, the design parameters and performance targets guiding the development of the Kuniokoa-Turbo™ were defined. We determined that the Kuniokoa-Turbo™ needs to be capable of firepower's upwards of 6kW, reduce the time-to-boil to less than 25 minutes, improve the stoves ability to burn large and/or high moisture content fuel, reduce in-home emissions throughout the stoves expected operating range to Tier 3 or better, and maintain the thermal-efficiency and durability performance of the Kuniokoa™.

The strategy to achieve these performance targets focused on the development of a fan-driven air injection system powered by the energy from the accompanying off-grid solar system. The solar companies we partnered with provided data showing that 98% of household off-grid solar systems have approximately 10 watt-hours of surplus energy per day after all other energy requirements have been met. This daily surplus energy represented the energy available to power an air injection system for the Kuniokoa-Turbo™, suggesting that any potential air injection system needed to operate on less than 2 watts of average peak power to provide a minimum of 5 hours of cooking per day if needed.

The air injection system and any additional changes to the Kuniokoa™ necessary to incorporate a system into the existing design needed to limit material and component cost (BOM) to less than \$5 USD to ensure that the Kuniokoa-Turbo™ could meet our retail cost targets. The BOM target suggests that the budget for the fan is approximately \$2 USD. Through contact with multiple fan manufacturers it was determined that the system needed to operate at a static-pressure under 0.6 in-H₂O to be capable of being driven by fans under \$2 USD. In addition, preliminary investigations into air injection in the riser of the Kuniokoa™ showed that the stove experienced

flame blowout at low-firepower's and backdraft at high-firepower (causing flames to exit out the fuel feed door of the stove) at system flow-rates greater than 3 CFM, so the flow-rate passing through the jets needed to be limited to below this value. BURN advised that their manufacturing techniques and the BOM would limit possible air jet configurations to jet diameters no smaller than 2mm diameter jets and no more than 12 jets. Finally, in the event an energy source is temporarily unavailable to power the air injection system the stove needed to allow for natural-draft operation without risking damage to the fan and/or associated electronic components after prolonged use.

5.1.2 Fan-Driven Secondary Air Injection System Design

Having already shown the performance benefits of optimized secondary air injection in the riser of the Kuniokoa™ during the evaluation of the analytical model in Chapter 4, we began by designing a manufacturable fan-driven riser air injection system for the Kuniokoa™. Unlike the fully-welded and compressed air powered modular secondary air systems built for the investigation detailed in Chapter 4, the system for the Kuniokoa-Turbo™ could not be welded due to manufacturing cost concerns and had to be driven by a fan. The strategy used to design the air injection system focused on developing a low-cost and easy to assemble ducting system that directed flow from an externally mounted fan to the air jets located in the riser.

The ducting assembly was built from 22-gauge 304 stainless-steel sheet and used a twist tab assembly technique to assemble and seal the ducting flow-path, which minimized manufacturing cost. The fan and associated control-board/electronics were mounted external to the stove body to thermally-isolate these relatively heat-sensitive components preventing damage while the stove is in operation in both fan-on (i.e., forced-draft) or fan-off (i.e., natural-draft) conditions. The fan was attached to the sheet-metal ducting assembly via a nozzle made from Nylon 12, which provided additional thermal-isolation from conductive heat-transfer from the stove-assembly. We found that the outer surface of the stove body and the portion of the ducting assembly external to

the stove body could reach temperatures upwards of 140°C during high-power natural-draft operation, well above the maximum operating temperature of fans. The fan control-board was contained in a plastic shroud, also made from Nylon 12, that wrapped around the fan, fan-nozzle, and ducting external to the stove body.

The fan used in the initial Kuniokoa-Turbo™ prototype was a Sunon PF40281B2-000U-A99 axial fan (Sunon Inc., Kaohsiung, Taiwan). The cost of this fan exceeded the \$2 USD allowed, but was readily available and provided performance flexibility if needed for initial design and testing purposes. Power was delivered to the fan via a custom control board that incorporated a potentiometer with variable set points to control fan voltage, power, and flow if needed. The air injection system and the Kuniokoa-Turbo™ are illustrated in Figures 36-38.

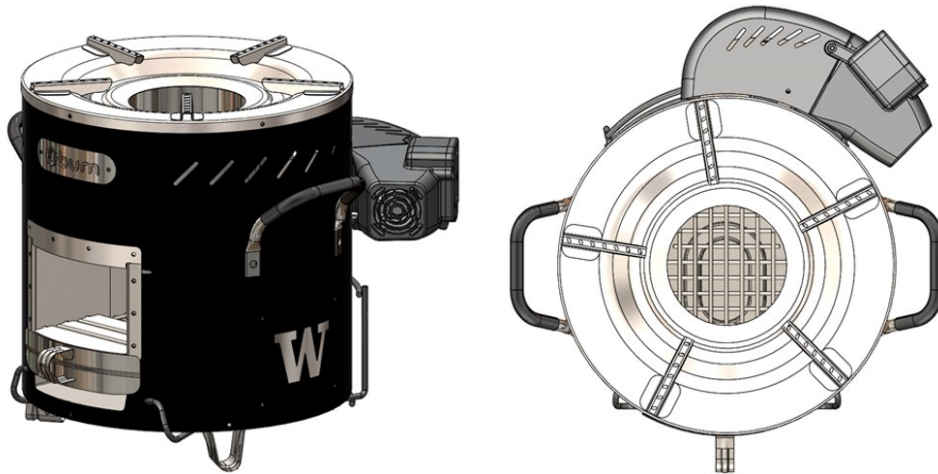


Figure 36: Kuniokoa-Turbo™ isometric and top view.

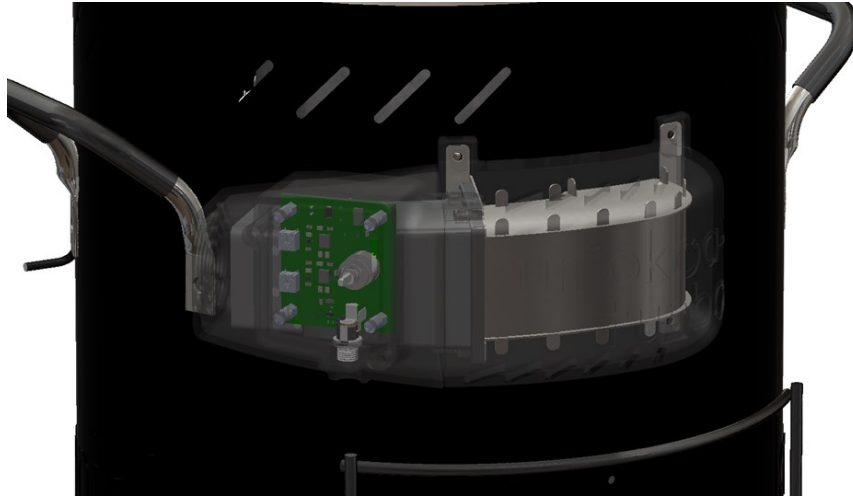


Figure 37: External duct, fan, fan nozzle, and control board assembly.

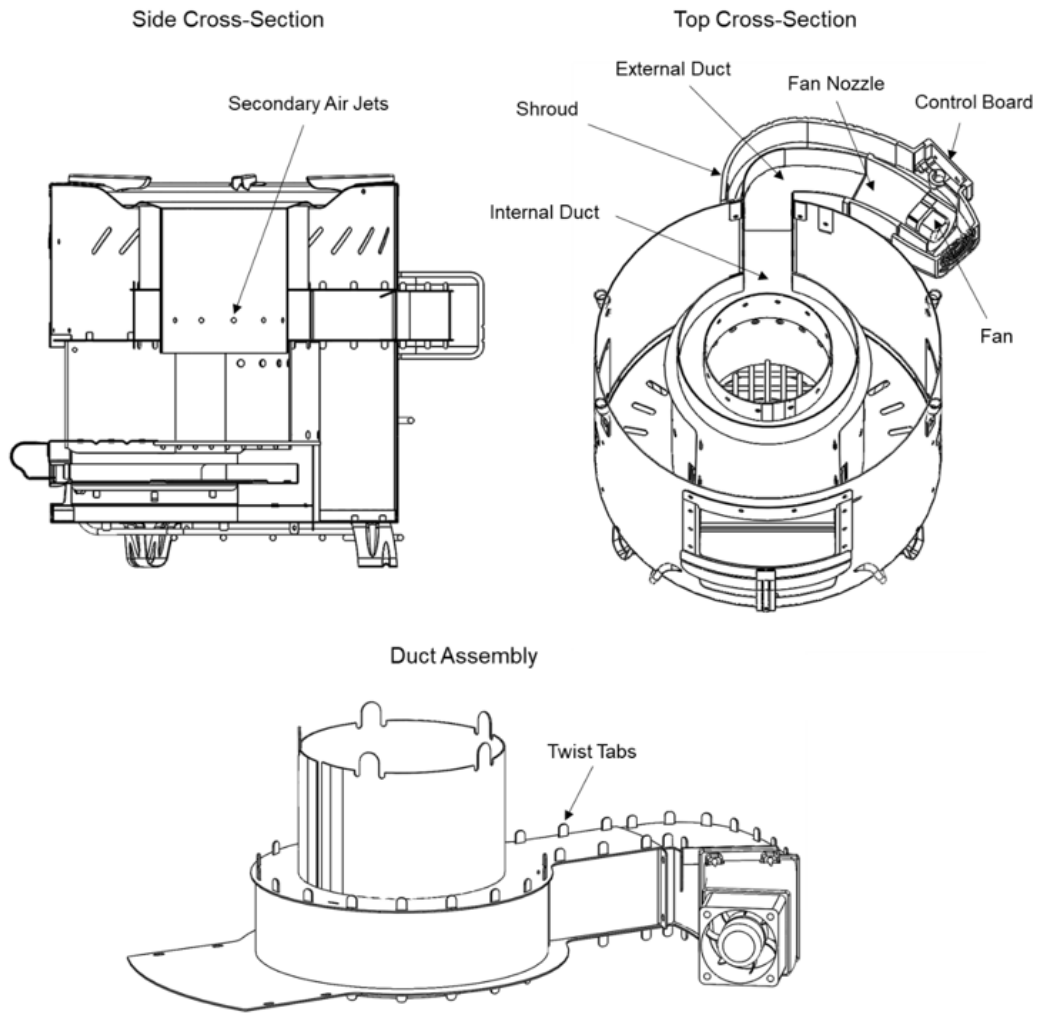


Figure 38: Kuniokoa-Turbo™ assembly cross-section and air injection system.

The twist-tab assembly technique of the secondary air injection ducting did not completely seal the assembly. We needed to account for system leakage when using the analytical model to calculate optimum jet configurations that our selected fan was capable of driving. System leakage will increase the fan flow-rate necessary to achieve the flow-rate corresponding to each optimum jet configuration predicted by the model and will generally lower the total system static-pressure, since a percentage of the flow will be lost through system leaks and the total equivalent jet area is increased due to leaks. We estimated the total system leakage area by inserting a riser with no secondary air jets into a fully assembled Kuniokoa-Turbo™ prototype. We then measured the static-pressure of the air injection system at a location 20mm downstream of the fan-to-fan-nozzle interface (i.e., the system inlet) as we passed known flow-rates of air through the system using the compressed air source and flow-meter used with the modular system detailed in Chapter 4. By using a riser with no secondary air jets, the only pathways for air to leave the system is through system leaks, so the resulting system impedance curve represented only the system leaks, or duct leakage. The resulting curve is shown in Figure 39.

With the system impedance of the duct leakage known, we were able to estimate the total area of the system leaks by matching the predicted system impedance of the model to the measured impedance of the leaks. We did this by assuming a negligible head-loss and a discharge coefficient of 0.63, and then manually iterated the total jet area variable, A_j , in the model until the model's predicted impedance aligned with the measured impedance (dashed line in Figure 39). Once this was accomplished the corresponding total jet area was taken as a representation of the cumulative area of all the system leaks, A_l , which was calculated to be 160mm².

The ratio of total jet area and total area of system leaks, A_j/A_l , is proportional to the ratio of total jet flow-rate and total flow-rate lost through system leaks, Q_j/Q_l , so by defining the total area of the system leaks we can then calculate the amount flow that will be lost through system leakage from Equation 32 by simply dividing the flow-rates of all the predicted optimum configurations by

A_j/A_l , where Q_j is the total jet flow rate for each optimum jet configuration corresponding to the user-defined parameter Q , and Q_l is the flow-rate lost through system leaks.

$$Q_j \left(\frac{A_j}{A_l} \right)^{-1} = Q_l \quad \text{Eq. 32}$$

The required fan flow-rate, Q_T , can then be calculated by taking the sum of Q_j and Q_l . The total open area of the system, A_T (i.e., the sum of the total jet area and the total area of system leaks), can be calculated similarly and used to calculate the actual system static-pressure using Equation 25.

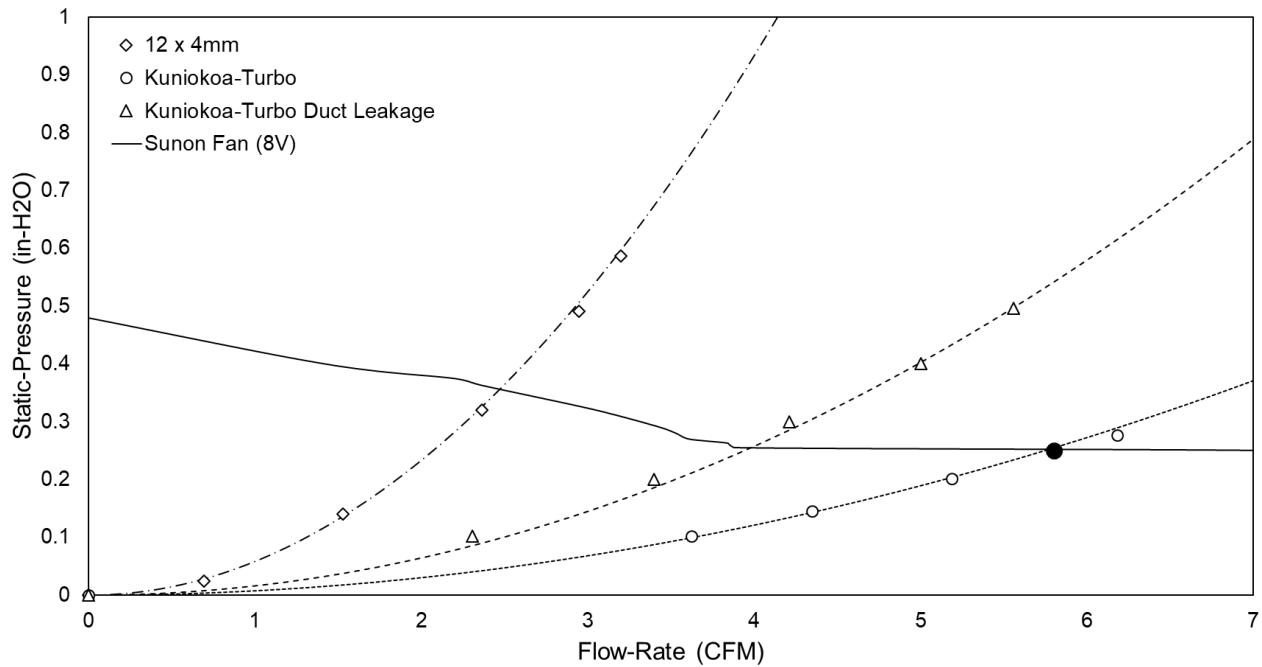


Figure 39: Comparison of the Kuniokoa-Turbo™ air injection system duct leakage impedance, system impedance of the 12 x 4mm modular system from Chapter 4, and the total system impedance and system operating point of the Kuniokoa-Turbo™ when using a 12 x 4mm jet configuration and the Sunon fan at 8V.

Using the analytical model detailed in Chapter 2 and the Kuniokoa-Turbo™ project design parameters and system characteristics, shown in Table 9, a selection of optimum jet configurations was calculated, shown in Table 10. Using the estimated system leakage area, the system flow-rates and static-pressures of the configurations listed in Table 10 were corrected for

system leakage. We selected the 12 x 4mm jet configuration, corresponding to a jet flow-rate of 2.8CFM, a total fan flow-rate of 5.8CFM (3CFM of system leakage), and a total system static-pressure of 0.25 in-H₂O, the corresponding system impedance and operating point are shown in Figure 39. The 12 x 4mm configuration was, in general, selected arbitrarily, any of the configurations listed in Table 10 would have been good choices. Although, the 12 x 4mm configuration did have the maximum number of jets (correlating to a higher quality of cross-flow mixing than the configurations with less jets), kept jet flow below 3CFM, and the leak corrected operating point aligned with the Sunon fan performance curve for a fan voltage of 8V, shown in Figure 39. The fan performance curve was determined using a fan testing apparatus built in accordance with Figure 12 in ANSI/AMCA 210-99. All other configurations required fan voltage to be reduced below 8V to achieve the proper system flow-rates, which limited the ability to test variable fan flow-rates during a subsequent field-study because the required fan voltage was too near the cut-off voltage of the fan.

When using the 12 x 4mm jet configuration and a fan voltage of 8V the Sunon fan consumed 1.1W of power, well below the 2W maximum peak power goal of the project, easily providing +9 hours of fan-on cooking per day based on the estimates of daily surplus energy. The jets were positioned in the same location in the riser (approximately 90mm below the riser outlet, or 10mm above the inlet of the riser) as in the modular system used in the evaluation of the analytical model detailed in Chapter 4, illustrated in Figure 38.

5.2 Kuniokoa-Turbo™ Laboratory Performance

The Kuniokoa-Turbo™ was subjected to the same performance tests as the Kuniokoa™, detailed in Chapter 1, to determine the impact the optimized secondary air injection system had on all aspects of cookstove performance throughout a wide range of operating conditions compared to the natural-draft stove. These tests were also used to evaluate if the Kuniokoa-Turbo™ met the performance requirements of the project.

An FPS was performed on the Kuniokoa-Turbo™ using small-dry and large-dry feedstocks covering firepower's ranging from 0.75 – 5.6kW and compared to the results for the natural-draft Kuniokoa™, shown in Figure 40. We observed that Kuniokoa-Turbo™ results in significant reductions in PM_{2.5} emissions at burn-rates above 2.8kW, with PM_{2.5} performance generally remaining Tier 3 throughout the entire range of firepower tested. When compared to the PM_{2.5} emissions of the Kuniokoa™ at a firepower of 4.5kW, corresponding to the upper-limit of the typical range of firepower's observed by BAMG in the field during the SFR 35B field study, we find that the Kuniokoa-Turbo™ reduces PM_{2.5} emissions by 91% compared to the Kuniokoa™. In general, the FPS results for the Kuniokoa-Turbo™ suggest that the 12 x 4mm jet configuration successfully reduces PM_{2.5} emissions to within the Tier 3 PM_{2.5} emissions performance target of the project for the complete range of firepower's expected to be seen in the field. The FPS results also suggest that the Kuniokoa-Turbo™ is capable of burn rates in excess of 5.5kW, nearly 1kW more than the Kuniokoa™ is capable of under similar conditions. This is attributed to the decreased char production in the Kuniokoa-Turbo™ due to the downstream mixing effects of the secondary air jets extending into the combustion-chamber of the stove that improve char combustion preventing a build-up of char that prevents high burn rates.

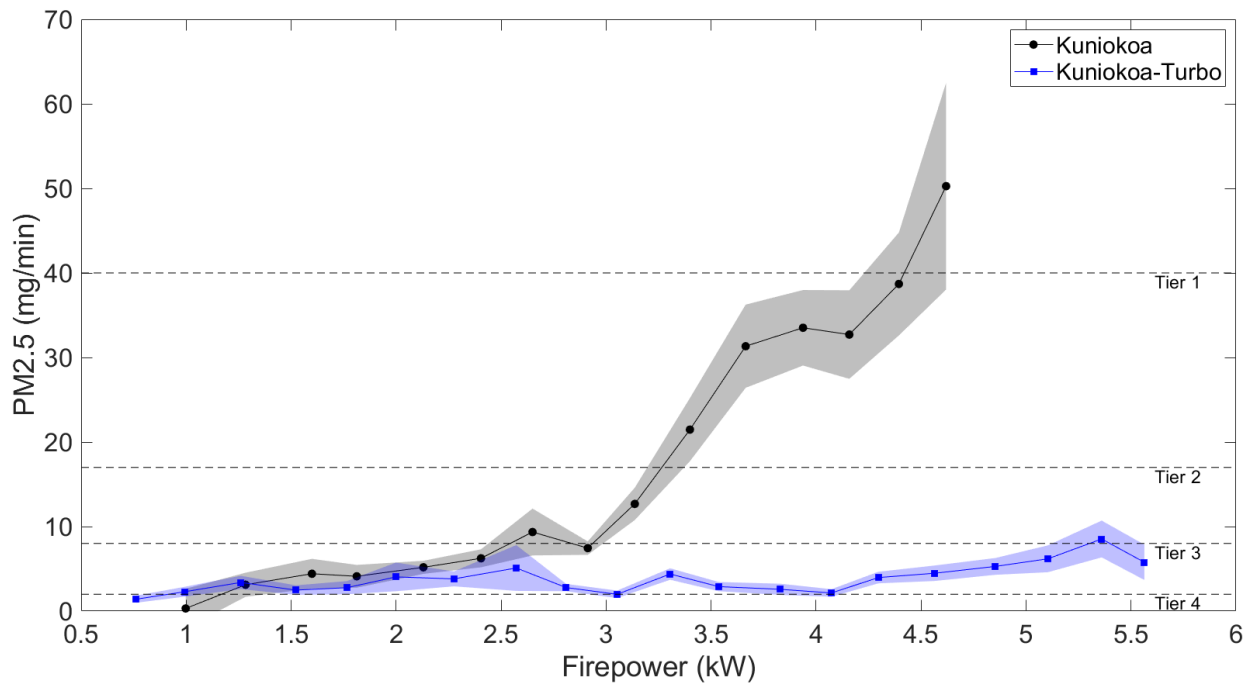


Figure 40: Kunioko-Turbo™ FPS results for small-dry and large-dry feedstocks compared to the results for the natural-draft Kunioko™. Note: Shaded region represents a 90% CI.

High-power WBT's were performed using small-dry, large-dry, and large-wet feedstocks. The corresponding WBT performance metrics and tiers are reported in Table 15 and Figure 41. The results for the Kunioko-Turbo™ suggest an improvement in all emissions metrics for all fuel feedstocks when compared to the corresponding results for the Kunioko™. The Kunioko-Turbo™ maintains Tier 3, or near Tier 3 performance regardless of fuel type. The wet-wood WBT results suggest that the Kunioko-Turbo™ has an improved ability in burning wet-wood, increasing wet-wood heat output by 36% compared to the Kunioko™. We also find that the thermal-efficiency of the Kunioko-Turbo™ is not significantly different than the natural-draft stove with the simulated field-typical performance average efficiency matching the efficiency of the Kunioko™ (36%). This suggests that duct flow leakage does not significantly impact thermal-efficiency, a concern we had with the use of an imperfectly sealed assembly.

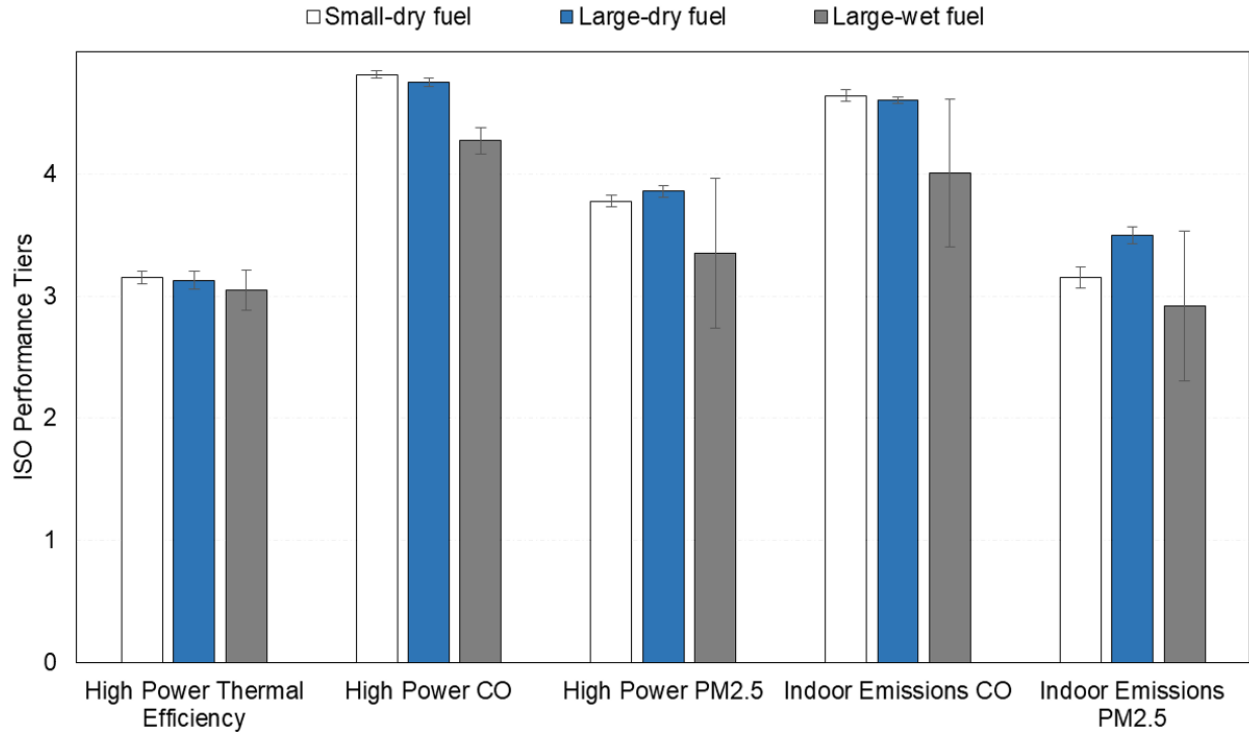


Figure 41: Kuniokoa-Turbo™ high-power WBT ISO performance tiers for small-dry, large-dry, and large-wet feedstocks. Note: error bars represent a 90% CI.

Table 15: Kenya TSF baseline values and Kuniokoa-Turbo™ high-power WBT ISO performance values for small-dry, large-dry, and large-wet feedstocks. Simulated field-typical performance metrics are averaged across all fuel-types and shown for comparison.

	Firepower (kW)	Time-to-Boil (min)	High Power Thermal-Efficiency (%)	High Power CO (g/MJd)	High Power PM _{2.5} (mg/MJd)	Indoor Emissions CO (g/min)	Indoor Emissions PM _{2.5} (mg/min)
Kenyan TSF	7.1 ± 2	N/A	N/A	4.2 ± 1.7	542 ± 212	1.7 ± 0.7	217.9 ± 71
Small-dry fuel (n = 6)	4.7 ± 0.2	18 ± 0.5	36.5 ± 0.6	1.47 ± 0.3	69.2 ± 7.4	0.15 ± 0.02	7.1 ± 0.7
Large-dry fuel (n = 6)	3.9 ± 0.4	23.5 ± 2.3	36.3 ± 0.9	1.96 ± 0.3	58.9 ± 7.2	0.16 ± 0.01	5.0 ± 0.5
Large-wet fuel (n = 3)	3.4 ± 0.2	31.8 ± 2.4	35.5 ± 1	5.80 ± 0.5	123 ± 49	0.42 ± 0.04	8.7 ± 2.9

Simulated Field- Typical	4 ± 0.7	24.4 ± 7	36 ± 0.5	3.1 ± 2.4	83.8 ± 35	0.24 ± 0.15	6.9 ± 1.9
--------------------------------	---------	----------	----------	-----------	-----------	-------------	-----------

Note: variabilities represent one standard-deviation.

The simulated field-typical performance of the Kuniokoa-Turbo™ results in a 65% reduction in high-power CO emissions, a 76% reduction in high-power PM_{2.5} emissions, and a 66% and 77% reduction in CO and PM_{2.5} indoor emissions, respectively, when compared to the simulated field-typical performance of the Kuniokoa™. When compared to the TSF data collected by BAMG during the SFR 35B field-study, the Kuniokoa-Turbo™ results in a 27% reduction in high-power CO emissions, an 85% reduction in high-power PM_{2.5} emissions, and an 86% and 97% reduction in CO and PM_{2.5} indoor emissions, respectively. A summary of the tiered performance metrics comparing the simulated field-typical performance of the Kuniokoa™ and Kuniokoa-Turbo™ is shown in Table 16. On average the Kuniokoa-Turbo™ improves the simulated field-typical performance to Tier 3 or above for all high-power performance metrics at an equivalent firepower to the Kuniokoa™ but does not appear to provide significant reductions in cooking time.

Table 16: High-power WBT tiered performance summary for the Kuniokoa-Turbo™ comparing the simulated field-typical performance to the corresponding results for the Kuniokoa™.

	Firepower (kW)	Time-to- Boil (min)	High Power Thermal- Efficiency	High Power CO	High Power PM _{2.5}	Indoor Emissions CO	Indoor Emissions PM _{2.5}
Kuniko™ <i>Simulated Field-Typical</i>	3.8 ± 1	26 ± 8.9	3	3	2	1	1
Kuniokoa- Turbo™ <i>Simulated Field-Typical</i>	4 ± 0.7	24.4 ± 7	3	4	3	4	3

Note: variabilities represent one standard-deviation.

5.3 Summary

The Kuniokoa-Turbo™ is still in the early stages of development as of writing, with many questions about the viability of the design and product left unanswered, but the initial prototype our team

developed does support the benefits of using the secondary air injection optimization design tool in designing secondary air injection systems to reduce emissions and improve stove performance throughout a wide range of operating characteristics. Using the design tool, we were able to design a secondary air injection system that met the jet design parameters defined by the manufacturer and the fan design parameters defined by the fan budget. We found that the Kuniokoa-Turbo™ is capable of firepower's upwards of 5.5kW when using small-dry wood (determined from FPS results), has an improved ability to burn high moisture content fuel, reduces in-home emissions throughout the stoves expected operating range to Tier 3 or better for all fuel-types, and maintains thermal-efficiency performance. The laboratory performance tests do fail to provide evidence that the Kuniokoa-Turbo™ results in a significant reduction in time-to-boil and the impact of air injection on stove durability is still an unanswered question.

In early 2019, eight Kuniokoa-Turbo™ prototypes were sent to Kenya for field-evaluation, which included user focus-groups, controlled cooking tests, in-home placements, and extended durability testing to gain a better understanding of the perception of local cooks to a fan-powered rocket-stove and to answer some of the performance questions that were left unanswered by the laboratory performance testing. As of writing the field-evaluation is on-going, but preliminary feedback has indicated that local cooks prefer the Kuniokoa-Turbo™ over the natural-draft stove, due to a perceived reduction in emissions, higher heat output resulting in faster time-to-cook, and an increased ability to burn a wide range of moisture content and size wood. Figures 42-44 are images from some of the Kuniokoa-Turbo™ focus-groups.



Figure 42: Kuniokoa-Turbo™ user focus-group.



Figure 43: Kuniokoa-Turbo™ user focus-group.



Figure 44: Kuniokoa-Turbo™ user focus-group.

CHAPTER 6: CONCLUSIONS AND FUTURE WORK

Innovative cookstove design tools and strategies are needed to help define, understand, and overcome the technical issues preventing the successful development and implementation of improved cookstoves that: (1) burn locally available biomass fuels, (2) are clean-burning and fuel-efficient, (3) result in meaningful improvements in personal health, quality of life, and financial-stability, and (4) result in meaningful reductions in environmental damage.

In this thesis, an innovative secondary air injection system design tool for fan-driven systems in side-feed wood-burning cookstoves (i.e., rocket-stoves) is developed, evaluated, and discussed. The design tool presented optimizes the mixing characteristics of a single-row of equal-diameter circular air jets located symmetrically around the perimeter of a cylindrical cross-flow (i.e., the cylindrical riser of a cookstove). Using optimum values of maximum jet radial penetration length suggested in literature for furnace and gas turbine combustion-chamber applications, and user-defined design parameters and system characteristics, optimum jet configurations are predicted that result in: (1) good cross-flow mixing characteristics, (2) minimum jet injection energies, (3) reduced flame-height, (4) maximum reductions in $PM_{2.5}$ emissions, and (5) minimum impact on thermal-efficiency. The cookstove performance trade-offs of different secondary air jet characteristics are discussed, and the method used to predict optimum jet configurations is validated by evaluating a range of jet penetrations and jet-to-cross flow momentum-flux ratio's using a 3-dimensional CFD model and a stove prototype with a modular secondary air injection system. We find that the jet mixing optimization parameter and values suggested in literature (i.e., maximum jet radial penetration lengths that approach the mid-line of the cross-flow) can be used to approximate secondary air jet configurations in the riser of wood-burning cookstoves that provide optimum cross-flow mixing characteristics.

The design tool is applied to the development of the Kuniokoa-Turbo™, a side-feed, wood-burning cookstove with a solar-powered secondary air injection system used to reduce emissions and

improve stove utility. We determine that the design tool can be successfully used to design a fan-driven secondary air injection system for a wood-burning cookstove that results in comprehensive reductions in emissions throughout a wide-range of stove operating conditions typical of in-home use.

As the design tool does not optimize secondary air injection location, further investigation is needed to determine the optimum location of the injection plane within a cookstove design. In addition, previous investigations have shown a dependence of PM size distribution on secondary air jet characteristics.⁴⁸ Investigating the size distribution of the PM produced by stoves using the optimum jet configurations predicted by the design tool will ensure that air injection systems reduce PM emissions throughout the entire particle size range.

With the development of innovative cookstove design tools, like the one presented in this thesis, we can help improve current improved cooking technologies and guide the development of future technologies that are more effective in reducing HAP, reducing household fuel-consumption, and meeting household cooking and/or heating needs; all contributing to the successful adoption of clean-burning and fuel-efficient cooking products that have the potential to save lives, save the environment, and improve the livelihoods of billions of people around the globe.

References

1. Landrigan PJ, Fuller R, Acosta NJR et al. *The Lancet Commission on pollution and health*. Lancet. 2017; (published online Oct 19.)
2. World Health Organization. (2018, May 2). *9 out of 10 people worldwide breathe polluted air, but more countries are taking action* [Press release]. Retrieved from <https://www.who.int/news-room/detail/02-05-2018-9-out-of-10-people-worldwide-breathe-polluted-air-but-more-countries-are-taking-action>
3. World Health Organization. *WHO Guidelines for Indoor Air Quality: Household Fuel Combustion*. 2014.
4. Hutton, G.; Rehfuss, E.; Tediosi, F. *Energy for Sustainable Development*. 2007, 11 (4), 34–43
5. Bonjour, S.; Adair-Rohani, H.; Wolf, J.; Bruce, N. G.; Mehta, S.; Prüss-Ustün, A.; Lahiff, M.; Rehfuss, E. A.; Mishra, V.; Smith, K. R. *Solid Fuel Use For Household Cooking: Country and Regional Estimates for 1980–2010*. *Environ. Health Perspect. Environmental Health Perspectives*. 2013, 121, 784–790.
6. World Health Organization. *Preventing Disease Through Healthy Environments: A global assessment of the burden of disease from environmental risks*. 2016.
7. Liu, Li; Johnson, H.; Cousens, S.; Perin, J.; Scott, S.; Lawn, J. et al. *Global, regional, and national causes of child mortality: an updated systematic analysis for 2010 with time trends since 2000*. Lancet. 2012.
8. Bond, T. C.; Streets, D. G.; Yarber, K. F.; Nelson, S. M.; Woo, J.; Klimont, Z. *A technology-based global inventory of black and organic carbon emissions from combustion*. J. Geophys. Res. 2004, 109, D14203.

9. Bond, T. C.; Sun, H. *Can Reducing Black Carbon Emissions Counteract Global Warming?* Environmental Science & Technology Environ. Sci. Technol. 2005, 39, 5921–5926.
10. Center for Climate and Energy Solutions. *What is Black Carbon?* [Fact sheet]. 2010. Retrieved from <https://www.c2es.org/site/assets/uploads/2010/04/what-is-black-carbon.pdf>
11. Jetter, J.; Zhao, Y.; Smith, K. R.; Khan, B.; Yelverton, T.; Decarlo, P.; Hays, M. D. *Pollutant Emissions And Energy Efficiency under Controlled Conditions for Household Biomass Cookstoves and Implications for Metrics Useful in Setting International Test Standards.* Environmental Science & Technology Environ. Sci. Technol. 2012, 46, 10827–10834.
12. World Health Organization. *Burning Opportunity: Clean Household Energy for Health, Sustainable Development, and Wellbeing of Women and Children.* 2016.
13. International Energy Agency. *World Energy Outlook.* 2006. Retrieved from <https://www.iea.org/publications/freepublications/publication/weo2006.pdf>
14. Clean Cooking Alliance. *About Us.* 2019. Retrieved from <http://cleancookingalliance.org/about/our-mission/>
15. Africa Renewable Energy Access Program (AFREA). *Wood-Based Biomass Energy Development for Sub-Saharan Africa: Issues and Approaches.* 2011.
16. The Organization for Economic Co-operation and Development (OECD) Development Centre. Roy, R. *The Cost of Air Pollution in Africa.* 2016.
17. Hanna, R.; Duflo, E.; Greenstone, M. *Up in Smoke: The Influence of Household Behavior on the Long-Run Impact of Improved Cooking Stoves.* 2012.
18. Rysankova, D., Putti, V. R., Hyseni, B., Kammila, S. and Kappen, J. F., 2014. Clean and Improved Cooking in Sub-Saharan Africa: A Landscape Report. Report No. 98664. Africa Clean Cooking Solutions Initiative. The World Bank, Washington, DC. Available

- at: <http://documents.worldbank.org/curated/en/2015/07/24853349/clean-improved-cooking-sub-saharan-africa-landscape-report>
19. Yip, F.; Christensen, B.; Sircar, K.; et al. *Traditional and Improved Stove Use on Household Air Pollution and Personal Exposures in Rural Western Kenya*. 2016. Available at: <https://www.ncbi.nlm.nih.gov/pmc/articles/PMC5538771/>
 20. Lozier M, Sircar K, Christensen B, Pillarisetti A, Pennise D, Bruce N, et al. Objective Assessment of Stove Use with Temperature Sensors in a Multi-Stove Study — Kenya, 2012–2013. *Environ Sci Tech*. 2016;50(8):4564–71.
 21. Clean Cooking Alliance. *2017 Progress Report: Driving Demand. Delivering Impact*. 2017. Available at: <http://cleancookingalliance.org/binary-data/RESOURCE/file/000/000/536-1.pdf>
 22. US Department of Energy (DOE). *Energy Department Announces \$2.5 Million to Advance Technologies for Clean-Burning, Efficient Biomass Cookstoves* [Press release]. 2012. Available at: <https://www.energy.gov/articles/energy-department-announces-25-million-advance-technologies-clean-burning-efficient-biomass>
 23. Bacon, R; Bhattacharya, S; Masami, K. The World Bank. *Expenditure of Low-Income Households on Energy: Evidence from Africa and Asia*. 2010. Available at: http://siteresources.worldbank.org/EXTOGMC/Resources/336929-1266963339030/eifd16_expenditure.pdf
 24. UNFCCC. *Investment and financial flows to address climate change*. 2007. Available at: https://unfccc.int/resource/docs/publications/financial_flows.pdf
 25. International Institute for Applied System Analysis (IIASA). *Energy Inequality*. 2014. Available at: <http://www.iiasa.ac.at/web/home/research/alg/energy-inequality.html>
 26. International Organization for Standardization (ISO). *International Workshop Agreement (IWA) 11:2012: Guidelines for evaluating cookstove performance*. 2012. Available at: <https://www.iso.org/standard/61975.html>

27. Clean Cooking Alliance. *The Water Boiling Test (Version 4.2.3): Cookstove Emissions and Efficiency in a Controlled Laboratory Setting*. 2014. Available at: <http://cleancookingalliance.org/binary-data/DOCUMENT/file/000/000/399-1.pdf>
28. International Organization for Standardization (ISO). *Clean cookstoves and clean cooking solutions – Harmonized laboratory test protocols – Part 1: Standard test sequence for emissions and performance, safety and durability*. 2018. Available at: <https://www.iso.org/standard/66519.html>
29. International Organization for Standardization (ISO). *Clean cookstoves and clean cooking solutions – Harmonized laboratory test protocols – Part 3: Voluntary performance targets for cookstoves based on laboratory testing*. 2018. Available at: <https://www.iso.org/standard/73935.html>
30. US Department of Energy (DOE). *Energy Department Announces \$2.5 Million to Advance Technologies for Clean-Burning, Efficient Biomass Cookstoves* [Press release]. 2012. Available at: <https://www.energy.gov/articles/energy-department-announces-25-million-advance-technologies-clean-burning-efficient-biomass>
31. Pundle, A; Sullivan, B; Allawatt, G; Posner, J; Kramlich, J. 2016. *Two Dimensional Axisymmetric CFD Model of a Natural Draft Wood Fueled Rocket Cookstove*, paper presented to Western States Section of the Combustion Institute, Seattle, Washington, March 21-22, 2016.
32. Allawatt, G; Pundle, A; Sullivan, B; Posner, J; Kramlich. 2016 *A Transient State-Space Heat Transfer Model of a Natural Draft Wood Fueled Rocket Stove Used to Guide Stove Design*, paper presented to Western States Section of the Combustion Institute, Seattle, Washington, March 21-22, 2016.
33. Pundle, A; Sullivan, B; Allawatt, G; Posner, J; Kramlich, J. 2017. *Predicting the Performance of a Natural Draft Cookstove for the Developing World using*

- Computational Fluid Dynamics*, paper presented to 10th U.S. National Combustion Meeting, College Park, Maryland, April 23-26, 2017.
34. Allawatt, G; Pundle, A; Sullivan, B; Posner, J; Kramlich. 2017. *A Transient State-Space Heat Transfer Model of Natural Draft Biomass Fueled Rocket Stove*, paper presented to 10th U.S. National Combustion Meeting, College Park, Maryland, April 23-26, 2017.
35. Allawatt, G; Udesen, D; Pundle, A; Sullivan, B; Posner, J; Kramlich; et al. 2017. *Reducing Pollutant Emissions in a Wood Burning, Natural Draft Cookstove Using Laboratory-Based Fire Power Sweep Measurements*, paper presented to 10th U.S. National Combustion Meeting, College Park, Maryland, April 23-26, 2017.
36. I. Glassman and R.A. Yetter, *Combustion*, 4th ed. Amsterdam; Boston: Academic Press, 2008.
37. Lamberg, H.; Sippula, O.; Tissari, J.; Jokiniemi, J. *Effects of Air Staging and Load on Fine-Particle and Gaseous Emissions from a Small-Scale Pellet Boiler*. *Energy Fuels* 2011, 25 (11), 4952–4960.
38. Lyngfelt, A.; Leckner, B. *Combustion of wood-chips in circulating fluidized bed boilers — NO and CO emissions as functions of temperature and air-staging*. *Fuel* 1999, No. 78, 1065–1072.
39. Carroll, J. P.; Finnan, J. M.; Biedermann, F.; Brunner, T.; Obernberger, I. *Air staging to reduce emissions from energy crop combustion in small scale applications*. *Fuel* 2015, 155, 37–43.
40. Nuutinen, K.; Jokiniemi, J.; Sippula, O.; Lamberg, H.; Sutinen, J.; Horttanainen, P.; Tissari, J. *Effect of air staging on fine particle, dust and gaseous emissions from masonry heaters*. *Biomass and Bioenergy* 2014, 67, 167–178.
41. Sutar, K. B.; Kohli, S.; Ravi, M. R.; Ray, A. *Biomass cookstoves: A review of technical aspects*. *Renewable and Sustainable Energy Reviews* 2015, 41, 1128–1166.

42. Still, D.; Bentson, S.; Li, H. *Results of Laboratory Testing of 15 Cookstove Designs in Accordance with the ISO/IWA Tiers of Performance*. *EcoHealth* 2015, 12, 12–24.
43. Okasha, F. *Staged combustion of rice straw in a fluidized bed*. *Experimental Thermal and Fluid Science* 2007, 32 (1), 52–59.
44. Tryner, J.; Tillotson, J. W.; Baumgardner, M. E.; Mohr, J. T.; DeFoort, M. W.; Marchese, A. J. *The Effects of Air Flow Rates, Secondary Air Inlet Geometry, Fuel Type, and Operating Mode on the Performance of Gasifier Cookstoves*. *Environ. Sci. Technol.* 2016, 50 (17), 9754–9763.
45. Pettersson, E.; Lindmark, F.; Öhman, M.; Nordin, A.; Westerholm, R.; Boman, C. *Design Changes in a Fixed-Bed Pellet Combustion Device: Effects of Temperature and Residence Time on Emission Performance*. *Energy Fuels* 2010, 24 (2), 1333–1340.
46. Rapp, V. H.; Caubel, J. J.; Wilson, D. L.; Gadgil, A. J. *Reducing Ultrafine Particle Emissions Using Air Injection in Wood-Burning Cookstoves*. *Environ. Sci. Technol.* 2016, 50 (15), 8368–8374.
47. Wiinikka, H.; Gebart, R. *Critical Parameters for Particle Emissions in Small-Scale Fixed-Bed Combustion of Wood Pellets*. *Energy Fuels* 2004, 18 (4), 897–907.
48. Caubel et al. 2018. *Optimization of Secondary Air Injection in a Wood-Burning Cookstove: An Experimental Study*. *Environ. Sci. Technol.* 2018, 52 (17), 449–4456.
49. Lefebvre, A. H., & Ballal, D. R. (2010) Chapter 4: Aerodynamics. In *Gas Turbine Combustion: Alternative Fuels and Emissions* (pp. 113-149). Boca Raton, FL: Taylor & Francis.
50. Sullivan, B (2016). *Development of Cookstove Emissions and Performance Testing Suite with Time-resolved Particulate Matter Analysis and Excess Air Estimation* (Master's thesis). University of Washington, Department of Mechanical Engineering. 2016. Retrieved from:

https://digital.lib.washington.edu/researchworks/bitstream/handle/1773/36764/Sullivan_washington_0250O_16167.pdf?sequence=1

51. Kobayashi N.; Okada N.; Hirakawa, A.; Sato, T.; Kobayashi, J.; Hatano, S.; Itaya, Y.; Mori, S.: *Characteristics of solid residues obtained from hot-compresses-water treatment of woody biomass*. Industrial & Engineering Chemistry Research. 2009, 48, 373-379.
52. Vanormelingen, J.; Van Den Bulck, E. *Optimization of Overfire Air Systems of Cylindrical Combustion Chambers*. Environmental Engineering Science 1999, 16 (5), 353-373.
53. Pundle, A.; Sullivan, B.; Means, P.; Posner, J. D.; Kramlich, J. C.; *Predicting and Analyzing the Performance of Biomass-Burning Natural Draft Cookstoves for the Developing World Using Computational Fluid Dynamics*. Unpublished manuscript. University of Washington, Department of Mechanical Engineering. 2019.
54. The World Bank Group. *Off-Grid Solar Market Trends Report 2018*. January 2018. Retrieved from: https://www.lightingafrica.org/wp-content/uploads/2018/02/2018_Off_Grid_Solar_Market_Trends_Report_Full.pdf
55. Tryner, J (2016). *Combustion Phenomena in Biomass Gasifier Cookstoves* (PhD dissertation). Colorado State University, Department of Mechanical Engineering. 2016 Retrieved from: https://mountainscholar.org/bitstream/handle/10217/176745/Tryner_colostate_0053A_13787.pdf?sequence=1

Appendix

A1: Analytical Model Code

The following is the MATLAB script used in calculating optimum secondary air jet configurations using the methods detailed in Chapter 2. This does not include the necessary code to calculate optimum jet configurations for specific fan designs based off user-defined fan performance curves due to the more complex nature of that scripts structure. Although, this functionality can be accomplished via a simple excel sheet or a few additional lines of code if fan performance curves are known.

The attached MATLAB script also includes a module for optimizing single-sided air injection in a cylindrical cross-flow, as opposed to radial air injection discussed in this thesis.

```
%% Enter Variables
%% Jet Configuration Optimization Parameters

%Minimum Number of Jets Allowed
nj_min = 6;
%Maximum Number of Jets Allowed
nj_max = 12;
%Minimum Diameter of Jets Allowed
dj_min = 0.002; %m
%Maximum Diameter of Jets Allowed
dj_max = 0.01; %m
%Minimum System Flow-Rate Allowed
Q_min = 0.2; %CFM
%Maximum System Flow-Rate Allowed
Q_max = 2.8; %CFM
%Maximum System Static Pressure Allowed
dPj_max = 10; %in-H2O

%% Jet System Characteristics

% Discharge Coefficient
Cd = 0.6;
%Jet Plate Area
A1 = 0.01257; %m^2
%Preheat Temperature
T = 300; %K

%% Fuel/Combustion Characteristics
```

```

%Firepower
FP = 4; %[kW]
%Excess Air
ExAir = 3; %[*100%]
%Fuel Species - Douglas-Fir
Carbon = 0.0419; %moles/g-fuel
Hydrogen = 0.0635; %moles/g-fuel
Oxygen = 0.0269; %moles/g-fuel
%Fuel Heating Value
LHV = 19314; %[kJ/kg-fuel]

%% Cross-Flow Characteristics

%Diameter
D_xf = 0.1; %m
Dh_xf = 0.092; %m
%Gas Temperature
T_xf = 900; %K
%Kinematic Viscosity
v_xf = 99.35e-6; %m^2/s (900K and 1 atm)
%Gas Constant
R_xf = 287.058; %J/kg*K
%Pressure
P_xf = 101325; %Pa

%% Optimization Code

%% Cross-Flow Calculations

% Calculate stoichiometric air flow rate for specified firepower
A_to_F = 138.25*(Carbon + 0.25*Hydrogen - 0.5*Oxygen)/(12.01*Carbon + 1.01*Hydrogen +
16*Oxygen); %[kg-Air/kg-Fuel]
m_fuel = (FP/LHV); %kg-fuel/s
m_SA = m_fuel*A_to_F; %kg-air/s
% Cross-Flow
m_xf = (ExAir*m_SA) + m_fuel; %kg-air+fuel/s
A_xf = (pi()/4)*(D_xf^2); %m^2
rho_xf = P_xf/(R_xf*T_xf); %kg-air/m^3
Q_xf = (m_xf/rho_xf); %m^3/s
V_xf = Q_xf/A_xf; %m/s
Re_xf = V_xf*D_xf/v_xf; %Reynolds number of cross-flow

%% Jet System Variables

R_j = R_xf; %J/kg*K
P_j = P_xf; %Pa
rho = P_j/(R_j*T); %kg/m^3

%% Find Matrix of Optimum Jet Configurations (Q,nj,dj,Vj,J,dPj,zeta)

```

```

%Radial Air Injection
zeta_max = 0.4:0.01:0.5; %Optimum jet max penetration factor (fraction of duct diameter)
Q = Q_min:0.2:Q_max; %CFM total jet volumetric flow-rate
m_j = 0.0004719474*rho.*Q; %kg/s total jet mass flow-rate
Kj = m_j./m_xf; %mass flow-rate ratio (jets/cross-flow)
nj = nj_min:2:nj_max; %# of jets vector
for i = 1:length(Kj)
    for k = 1:length(nj)
        for h = 1:length(zeta_max)
            Jj =
(0.8*zeta_max(h)*sqrt(nj(k))*((rho/rho_xf)^0.25)*(1+Kj(i))/sqrt(Kj(i)))^4; %Momentum flux ratio
(single-jet/cross-flow)
            Vj = sqrt(Jj*rho_xf*(V_xf^2)/rho); %m/s Jet velocity
            dj = sqrt(4*m_j(i)/(nj(k)*Vj*pi()*rho)); %m Jet diameter
            dPj = 0.00401865*((Vj*pi()*(dj^2)/4)^2)*0.5*rho*(1-
((pi()*(dj^2)/4)/A1)^4)*((1/(Cd*pi()*(dj^2)/4))^2); %in-H2O System static-pressure
            Config_data{i,k,h} = [Q(i) ; nj(k) ; dj ; Vj ; Jj ; dPj ; zeta_max(h)]; %All configurations that
satisfy zeta_max for nj and Q
        end
    end
    Config_data_comp{i} = [Config_data{i,,:}];
end
for i = 1:length(Kj)
    Opt_data_mat = Config_data_comp{i};
    indices_dj = find(Opt_data_mat(3,:) < dj_min | Opt_data_mat(3,:) > dj_max); %eliminate
configurations that are not within djmin and djmax
    Opt_data_mat(:,indices_dj) = [];
    indices_dPj = find(Opt_data_mat(6,:) > dPj_max); %eliminate configurations >dPjmax
    Opt_data_mat(:,indices_dPj) = [];
    indices_nj = find(Opt_data_mat(2,:) < max(Opt_data_mat(2,:))); %eliminate all configurations
but those with maximum number of jets
    Opt_data_mat(:,indices_nj) = [];
    Opt_data_mat = mean(Opt_data_mat,2); %if more than one configuration with maximum
number of jets, take average of all to define optimum
    Opt_data{i} = Opt_data_mat;
end
Opt_data = cell2mat(Opt_data); %Optimum configurations that satisfy all user-defined design
parameters (Qmin,Qmax,njmin,njmax,djmin,djmax,dPjmax)

% Single-Sided Air Injection
S = Dh_xf./(nj+1); %Jet Spacing
Jjss = ((2.5*Dh_xf)^2)./(S.^2);
for i = 1:length(Q)
    for k = 1:length(nj)
        djss = sqrt((0.0004719474*Q(i))/(nj(k)*(pi()/4)*sqrt(rho_xf/rho)*sqrt(Jjss(k))*V_xf));
        Vjss = sqrt(Jjss(k)*rho_xf*(V_xf^2)/rho);
        dPjss = 0.00401865*((Vjss*pi()*(djss^2)/4)^2)*0.5*rho*(1-
((pi()*(djss^2)/4)/A1)^4)*((1/(Cd*pi()*(djss^2)/4))^2);
        Config_datass{i,k} = [Q(i) ; nj(k) ; djss ; Vjss ; Jjss(k) ; dPjss];
    end
    Config_data_comp_ss{i} = [Config_datass{i,,:}];
end

```

```

end
for i = 1:length(Q)
    Opt_data_mat_ss = Config_data_comp_ss{i};
    indices_dj = find(Opt_data_mat_ss(3,:) < dj_min | Opt_data_mat_ss(3,:) > dj_max); %eliminate
configurations that are not within djmin and djmax
    Opt_data_mat_ss(:,indices_dj) = [];
    indices_dPj = find(Opt_data_mat_ss(6,:) > dPj_max); %eliminate configurations > dPjmax
    Opt_data_mat_ss(:,indices_dPj) = [];
    indices_nj = find(Opt_data_mat_ss(2,:) < max(Opt_data_mat_ss(2,:))); %eliminate all
configurations but those with maximum number of jets
    Opt_data_mat_ss(:,indices_nj) = [];
    Opt_data_mat_ss = mean(Opt_data_mat_ss,2); %if more than one configuration with
maximum number of jets, take average of all to define optimum
    Opt_data_ss{i} = Opt_data_mat_ss;
end
Opt_data_ss = cell2mat(Opt_data_ss); %Optimum configurations that satisfy all user-defined
design parameters (Qmin,Qmax,njmin,njmax,djmin,djmax,dPjmax)

```

A2: Kuniokoa™ Modular Air Injection Prototype Diagram

